Mapping indigenous vegetation health in the Luvuvhu River Catchment using Sentinel-2 data

By

Tshishonga Unarine Emmanuel

(15011444)

Supervisor: Dr OE Malahlela

Co-supervisor: Mr F Dondofema

A thesis submitted in partial fulfilment of the requirements for the degree of Master of Environmental Sciences in the Department of Geography and Environmental Sciences at the University of Venda, South Africa

September 2022

Declaration

I, **Tshishonga Unarine Emmanuel**, student number 15011444, hereby declare that this thesis submitted to the Department of Geography and Environmental Sciences at the University of Venda for the degree of Master of Environmental Sciences is my own original work except for the quotations and references which are attributed to their sources, and it has never been submitted to any other university. The work has been done under the direction of the supervisor and co-supervisor listed below:

……

Mr. Unarine Emmanuel Tshishonga

(Student)

Dedication

I dedicate this study to my loving mother, Mukwevho Lufuno and my late father, Tshishonga Mbengeni Joseph. I also dedicate this work to my siblings, Dakalo, Azwindini, and Phathutshedzo, my partner, Thato as well as our beautiful daughter, Anzani. This dedication is owed to their out-of-ordinary support.

Acknowledgement

I would like to thank the Almighty God for giving me the wisdom, strength, and the ability to successfully carry out this research. I acknowledge my supervisor, Dr OE Malahlela for his endless academic support during the course of this study. His input, guidance and sacrifices are highly appreciated. I would also like to acknowledge my co-supervisor, Mr F Dondofema for his constructive input for the success of this study. Mr N Musumuvhi Ms R Novela, your assistance is much appreciated as well. I acknowledge Dr JN Steyn for giving us permission to collect some of the leaf samples from his farm.

I would like to extend my gratitude to the University of Venda for the financial support and the opportunity to carry out this study, otherwise, this research would not have made it thus far. All in all, I appreciate everyone who contributed to the success of this study in any way. Thank you!

Contents

List of figures

List of tables

Acronyms

C	– Carbon
Chl	– Chlorophyll
CO_2	– Carbon dioxide
DN	– Digital Number
ESA	– European Space Agency
GPS	– Ground Positioning System
Ha	– Hectare
KNP	– Kruger National Park
LAI	– Leaf Area Index
LRC	– Luvuvhu River Catchment
MLC	– Maximum Likelihood Classifier
MSI	– Moisture stress index
MSI	– Multi-Spectral Imager
N	– Nitrogen
NDII	– Enhanced difference infrared index
NDMI	– Normalised difference moisture index
NDVI	– Normalised Difference Vegetation Index
NDVIRededge	– Enhanced difference red edge vegetation index
NDWI	– Normalised difference water index
NDWSwir	– Enhanced difference water index
RF	– Random Forest
SIWSI	– Shortwave infrared water stress index
SRWI	– Simple ratio water index
SVM	– Support Vector Machine

SWIR – Shortwave infrared ratio

Abstract

Natural vegetation plays a significant role in global climate since it is involved in fluxes of solar radiation, CO_2 sequestration, hydrological cycle. However, over the past few decades, there has been massive changes when it comes to both natural vegetation and cropland cover at regional and continental scales under the global changing which makes it very crucial to map and assess vegetation conditions across landscapes. Nevertheless, vegetation mapping using remotely sensed data comprises of many procedures, and approaches. Fortunately, there has been swift improvements in remote sensing technology as well as increased data availability which increases the accessible pool of data. Different sources of remotely sensed data are distinguished by their unique spectral, spatial, and temporal characteristics which can be utilized to serve the purpose of vegetation mapping such as vegetation health. This study aimed to map the health of indigenous vegetation within Luvuvhu River Catchment (LRC). This was achieved through (i) discrimination of croplands from natural vegetation across Luvuvhu River Catchment; (ii) the estimation of natural vegetation leaf water content, and (iii) the prediction of foliar nitrogen concentration using Sentinel-2 imagery. The study the used the normalized difference vegetation (NDVI) to map all vegetation in the study area using a threshold of > 0.2. The maximum likelihood classifier was then used to classify between two vegetation types which are croplands and natural vegetation. The maximum-likelihood classification results (n = 164) showed that about 331 602, 477 hectares (ha) of the catchment is covered with vegetation. The study achieved an overall accuracy of 98.41% and a KHAT of 0.949. Additionally, the study compared the capability of narrowband (red-edge centred), broadband and the combination of both broadband and narrowband derived vegetation indices to estimate vegetation leaf moisture content across Luvuvhu River Catchment (LRC). A stepwise linear regression model was used for modelling of vegetation leaf moisture content. The results showed that the combined vegetation indices model outperformed other models with $R^2 = 0.54$ and RMSE = 0.085 g/cm^2 while the narrowband achieved $R^2 = 0.48$ and RMSE = 0.097 g/cm^2, and finally, the broadband vegetation indices achieved $R^2 = 0.24$ and RMSE = 0.096 g/cm^2. Through stepwise regression, the study concluded that the combined vegetation indices outperformed the other pair of models. As a result, its coefficients were utilized to produce thematic maps showing the distribution of vegetation leaf moisture content across the study area using multiple linear regression in ArcGIS. Finally, the study made use of three different categories of spectral indices to fulfil its objectives. Narrowband, broadband, and combined spectral indices based on Sentinel-2 data were subjected to stepwise regression on R studio software to determine which category of spectral indices is more efficient in estimating plant nitrogen concentration. Results have shown that combined spectral indices performed better with R^2 = 0,69, RMSE = 0,47% and MAE = 0,38%, followed by broadband spectral indices with R^2 = 0,44, RMSE = 0.65% and MAE = 0,48%, and the last category is narrowband spectral indices with R^2 = 0,35, RMSE = 0.81% and MAE = 0,65%. The coefficients of the

best performing model obtained from stepwise regression were used to compute multiple linear regression on QGIS to produce a map showing the concentration of plant nitrogen across the study area. The findings of this study suggest that the use of remotely sensed data effectively discriminated the afore-mentioned classes and allow automated extraction of features as well as being effective when it comes to data processing, cost reduction, and accuracy assessment. Thematic maps such as the ones produced in this study are fit for land cover change and large-scale modelling and can be utilized as reference point for further exploration.

Keywords: Vegetation cover, Sentinel-2, spectral indices, maximum likelihood classifier, Vegetation leaf water content, broadband, narrowband, stepwise multiple regression, plant nitrogen.

CHAPTER ONE: INTRODUCTION

1.1 Background of the study

Terrestrial vegetation is the main element of the Earth's climate system, as it influences fluxes of solar radiation, water, and occurrence of gases and their processes in the atmosphere (Hikosaka *et al.*, 2016). It also holds a prominent place in the biosphere, not only by producing biomass, but also by the role it plays in assisting to understand global climatic change (Lemaire *et al.,* 2005). Vegetation is one of the major sources of raw material for industrial use, fuel, and other ecosystem services (Schneider-Binder, 2017). Vegetation biochemistry and biophysical variables are used to assess the health of vegetation including vegetation stress that may be triggered by drought and other climatic factors. They are also vital in monitoring how vegetation responds to fluctuations associated with climate change as well as assisting in the construction of climate and ecological models (Croft *et al.*, 2014). These natural and anthropogenic activities influence perpetual changes in vegetation cover across the world.

Over the past few decades, there has been a massive change in vegetation cover in the study area (Dagada, 2017). These changes are observed on both indigenous vegetation and cropland cover due to population growth, climate change and since natural vegetation have been converted subsistence, commercial farmlands, cleared for firewood and settlements (Griscom *et al.*, 2010). Deforestation negatively affects the hydrological cycle which leads to soil erosion, high rate of baseflows if the capacity of the soil to infiltrate water persists (Brooks *et al.,* 2009). Another issue of great concern is the report that different parts of the world are frequently experiencing extreme heat stress events (Wang *et al.*, 2008). Luvuvhu River Catchment is also one of those areas that are greatly affected by extremely high daily temperatures (Dagada, 2017). Such record-breaking high temperatures are reported that they will significantly have influence on ecosystem processes and carbon (C) cycling (Cox *et al.*, 2000). Therefore, it is vital for us to develop programs that conserve and restore vegetation since they will provide us with up-to-date vegetation cover status (He *et al.*, 2014). It is also critical to have methods that assist with the early detection of plant water stress to understand forest fires, vegetation diseases as well as defoliation as a result of leaf water and nutrient deficiency (Meentemeyer *et al.*, 2008).

There is a large pool of studies on the estimation and mapping of vegetation biophysical and biochemical parameters (Zhang *et al.*, 2021; Zhou *et al.*, 2022; Dimitrov *et al*., 2019). Conventional approaches to monitor and assess vegetation cover, vegetation health and other aspects have been employed in the past. However, they are not effective when it comes to readily data provision at a large scale because they are labor-intensive and often too costly. The need to understand the state and how vegetation functions has resulted in the advancement of many different earth observational instruments and modelling methods (Hikosaka *et al.,* 2016). Over the past decades, remote sensing has been a central

part of efforts to address many environmental problems since satellite and airborne instruments have a larger spatiotemporal scale (Hikosaka *et al.*, 2016). The developments of remote sensing have gone through many changes in terms of instrument design, accuracy, consistency, and the ability to process complex datasets (Lynch, 2008). Satellite-based remote sensing platforms have a number of advantages such as high spatial resolution which offer an ability to obtain long-time data series which are consistent and comparable at a lower cost (Foley *et al.*, 2006). Furthermore, sensors such as Landsat 7-8 and Sentinel-2 satellites offer free access to remotely sensed data. However, Landsat and MODIS have problems related to mixed pixels, which are 30 m^2 for Landsat and 500 m^2 for MODIS. The other problem has something to do with their obit period which is 16 days for Landsat and 26 days for SPOT (Cheng *et al.*, 2016). More recently, satellites with higher resolution and short orbit period such as Sentinel-2, WorldView-2 and 3 have been developed (Hikosaka *et al.*, 2016).

Remote sensing of vegetation is mainly performed by obtaining the reflectance information from canopies using passive sensors. It is well known that the reflectance from plants changes with plant type, water content within the leaf tissues, and other intrinsic factors (Chang *et al.*, 2016). The reflectance from vegetation to the electromagnetic spectrum (spectral reflectance or emission characteristics of vegetation) is determined by chemical and morphological characteristics of the surface of leaves (Zhang et al., 2012). Vegetation emissivity of plant canopies has been well studied using the near and mid infrared regions (Foley *et al.*, 2006). Many plant characteristics besides growth and vigour quantification such as water content, pigments, sugar and carbohydrate content, and protein content among others can be easily extracted using indices from the near and mid infrared (Batten, 1998). Many studies have formulated various spectral indices for vegetation monitoring such as Normalised difference vegetation index (NDVI), crop water stress index (CWSI), normalized difference water index (NDWI), ratio index (Jiang et al., 2010). However, in light of recently launched sensors such as Sentinel-2, there has been new VI's due to additional red-edge bands (Hoffmann et al., 2015). The use of red-edge section in a spectral index (i.e., NDRE, or normalized difference red edge index) instead of red band normally displays changes in plant pigment (Gitelson and Mezalyak, 1994). There are a number of considerations when formulating simple spectral indices, however, they remain the simplest and most effective way to assess vegetation health status (Hikosaka et al., 2016).

In light of this background, the study aims to map indigenous vegetation health in the Luvuvhu River Catchment using Sentinel-2 data. To achieve this main objective, the study has the following specific objectives:

i. Map the area covered by vegetation in Luvuvhu Catchment Area, and
ii. Distinguish between the area covered with indigenous vegetation and croplands.
iii. Mapping of indigenous vegetation leaf water content using Sentinel-2 data
iv. Mapping of the indigenous plant nitrogen concentration through Sentinel-2 data

1.2 Research outline

This thesis consists of five chapters. These chapters are General Introduction, three analysis chapters and the synthesis chapter. In each analysis chapter, the research objectives (i - iv) have been addressed. Chapter two discriminated indigenous vegetation from agricultural vegetation in Luvuvhu River Catchment using Sentinel-2 imagery. Chapter three evaluated vegetation moisture within the study area. Chapter four estimated and mapped plant N for the indigenous vegetation within the Luvuvhu River Catchment. This thesis was concluded with Chapter five (synthesis) where the findings of each research objective are presented and summarized. Chapter five ends with an outlook and suggestions for future research.

1.3 General methodology

The study used Sentinel-2 imagery to map the area covered by vegetation in Luvuvhu River Catchment using the < 0.2 threshold for NDVI, and the results were used to discriminate croplands and natural vegetation by the use of maximum likelihood classifier. The study then used data collected from the field with remotely sensed data to estimate vegetation leaf water content by employing different sets of vegetation indices and the use of stepwise regression to find the best model suitable for the task. Lastly, this study estimated plant nitrogen (N) concentration across the study area using the same Sentinel-2 data and another set of vegetation indices and stepwise regression to find the model fit for the task.

CHAPTER TWO: DESCRIMININATING CROPLANDS AND INDIGENOUS VEGETATION WITHIN LUVUVHU RIVER CATCHMENT USING SENTINEL-2 IMAGERY

Abstract

Luvuvhu River Catchment (LRC) consists of a variety of vegetation types ranging from natural vegetation to croplands. Over time, there has been enormous change in the catchment due to increased human population growth, built-up areas and clearing up of natural vegetation for agricultural purposes. Quantifying the proportion of natural vegetation to the total vegetation in the Luvuvhu catchment is important for understanding hydrological and nutrient flows. This study aimed to quantify the extent of natural vegetation cover using remote sensing techniques in the Luvuvhu catchment. We used the normalized difference vegetation (NDVI) to map all vegetation in the study area using a threshold of NDVI >0.2. The maximum likelihood classifier was then used to classify between two vegetation types which are croplands and natural vegetation. The maximum-likelihood classification results (n = 164) showed that about 331 602, 477 hectares of the catchment is covered with vegetation. Land cover maps of LRC containing two classes were created with the aid of Sentinel-2 imagery using the maximum-likelihood classifier supervised classification. The study achieved an overall accuracy of 98.41% and a KHAT of 0.949. The use of remotely sensed data effectively discriminated the afore-mentioned classes and allow automated extraction of features as well as being effective when it comes to data processing, cost reduction, and accuracy assessment. Thematic maps such as the ones produced in this study are suitable for land cover change detection and largescale modelling and can be utilized as a reference point for future research.

Keywords: vegetation cover, NDVI, Maximum likelihood classifier, Sentinel-2

2.1. Introduction

Vegetation covers almost one-third of the terrestrial surface of the Earth (Chu, 2020) and plays an essential role in the connections between the earth's atmosphere, hydrosphere, and continental surface (Lemaire et al., 2005). It is mostly considered as a vital indicator that has a significant impact on biodiversity, ecological processes as well as a critical medium in water and energy balance, carbon cycling and so on (Fan et al., 2009). It holds a prominent place in the biosphere, not only by producing biomass, but also by the role it plays in assisting to understand global climatic change (Lemaire *et al.* 2005). Vegetation is one of the major sources of raw material for industrial use, fuel, and other ecosystem services (Schneider-Binder, 2017).

On the other hand, vegetation biochemistry and biophysical variables are important in indicating the health of vegetation as well as vegetation stress that may be triggered by drought and other climatic factors. It is also vital to monitor how vegetation responds to fluctuations associated with climate change as well assisting in the construction of climate and ecological models (Croft et al., 2014). Considering the variety of vegetation parameters which include leaf nitrogen (N), chlorophyll (Chl) content and leaf area index (LAI) are of prime importance (Darvishzadeh, 2008; Houborg et al., 2007). For example, N_2 is one of the most crucial elements which has an enormous influence on how plants survive and the extent to which crops yield (Zhou and Mmelink, 2016). Appropriate nitrogen ratios are crucial to both biochemistry and biophysical characteristics of plants which influence vegetation health (Zhou et al, 2016; Clevers and Kooistra, 2012). There is a distinct relationship between leaf Chl and N (Jia et al., 2018). Chl content has long been utilized as a supplementary means to understand leaf N content and served as a guide on how much fertiliser should be applied as well as in estimating crop yields (Jia et al., 2018). Physiologically, leaf Chl can be used as a vegetational health indicator because it is sensitive to various environmental stress and interferences such as drought and heat (Zhu et al., 2019; Houborg et al., 2012). LAI has been used to validate vegetation physiological status and health, and has been long-established for vegetation biomass accumulation, and the extent to which a plant can photosynthesize, and its production rate (Mingzhu et al., 2019; Boegh et al., 2002).

However, over the past few decades, there has a been massive change in both natural vegetation and cropland spatial coverage at regional and continental scales (Schneider-Binder, 2017. Consequently, due to population growth, areas that were covered by natural vegetation have been converted to places of residence, some cleared for firewood, agricultural fields (commercial and/or subsistence farming as well as grazing land). Exponential population growth leads to increased crop production to avoid malnutrition and starvation which brings about drastic reduction in natural vegetation cover (Mishra et al., 2021). Many scholars have indicated that massive vegetation clearing which is associated with expansion of croplands to cater the perpetual increase in human population is of concern (Koning et al.,

2011). However, this socio-environmental problem is yet to be solved (Koning et al., 2011). Literature reports that if farmers can maximize the potential of the land which is already converted to croplands they can still produce more while conserving the virgin land (Estel et al., 2016). Deforestation can also lead to high rate of baseflows if the capacity of the soil to infiltrate water persists (Brooks et al., 2009). However, if land-use practices that take place after vegetation clearing leads to reduced infiltration and influence soil erosion will result in low groundwater recharge (Griscom et al., 2010). Therefore, for us to develop programs that conserve and restore vegetation it is of utmost importance to acquire up-to-date vegetation cover status (Yichun et al., 2008; He et al., 2005).

Hence, comprehensive studies of vegetation cover change are very critical since it serves many purposes such as assisting in understanding spatial and temporal distinction that forms part of terrestrial ecosystem (Forkour, 2014). Vegetation mapping and classification is a very crucial task that ecologists are faced with for the reason that vegetation supports all living organisms and takes a very critical part in regulating climate change and influencing global CO_2 sequestration (Xie et al., 2008). Therefore, it is very important that we understand the present state of vegetation cover, so that vegetation protection and restoration may be initiated (He et al., 2005). Studies have advised that vegetation cover maps should be updated continuously to improve environmental assessment (Yichun et al., 2008; Knight et al., 2006). Conventional approaches were often employed in the past to assess and monitor vegetation cover and vegetation health; however, they are not effective when it comes to readily data provision at a large scale because they are labor-intensive and often too costly.

The progress made in satellite remote sensing technologies brought complete change to approaches that were previously used to assess natural (forest, water bodies, etc) and human resources. This development enables the feasibility to assess landscapes more frequently, more accurately (Jucker et al., 2017). The freely available remotely sensed data from Sentinel-2, have since its launch and provision, played a significant part in assessing natural resources and several ecosystem processes (Phiri et al., 2020). The great impact of freely accessible data is seen more in developing and underdeveloped countries where it is still difficult to access the remote sensing data (Phiri et al., 2020). Sentinel-2 data has been used to distinguish different types of crops and indigenous vegetation species (Immitzer et al., 2016) and recognition of water bodies (Du et al., 2016). In regions where vegetation is vastly influenced by seasons like the subtropical regions with distinct rainy and dry seasons, it is crucial to use intra-seasonal reflectance (Sedano et al., 2019).

However, there are uncertainties associated with land cover classifications based on remote sensing data when it comes to the extent and spatial distribution of cropland in most rural areas across the world due to small-scale subsistence farming which overlaps with natural vegetation (Cord et al., 2010). Nevertheless, over the years, there has been remarkable improvement when it comes to the depiction of farmlands in West Africa by means of the newly established and moderate resolution sensors such as

PROBA-V and Sentinel-2 (Larmbert et al., 2016). Whereas other scholars have used different active sensors that have multi-temporal optical reflectance which can detect and distinguish land cover over the landscape such as Synthetic Aperture Radar (SAR) (Schulz et al., 2021).

There are a number of classifiers that have been established and utilized to create land use and land cover maps. These classifiers have distinct performance which is influenced by their unique response to input data, definition of reference classes and conditions of the environment (Schulz et al., 2021). Furthermore, depending on geographic location, a classifier that worked in a particular environment may not produce desired results if used at another geographic location. Hackman et al. (2017) tested various classifiers such as Maximum Likelihood Classifier (MLC), Random Forest (RF), Support Vector Machine (SVM) and Decision Tree classification in Ghana for land cover classification and found that MLC outperformed other classifiers within that environment with 82.6% overall accuracy. A study by Yesuph and Dagnew (2019) indicates that MLC also reported high accuracies while other researchers found that SVM or RF performed better compared to MLC (Talukdar et al., 2020), particularly with several input datasets used together (Schulz et al., 2021). Classification error can be reduced by taking advantage of different classifiers depending on their strength and/or merging various classifiers to create a collective map with better results (Bullock et al., 2020). A study by Nzabarinda et al. (2021) reported that there are persistent significant changes that have taken place over the past few decades when it comes to land cover and land use. These changes have a negative effect on vegetation cover and on the sustainable development associated with natural resources such as indigenous vegetation. Therefore, in this chapter, this study sought to achieve the objectives below:

i) Map the area covered by vegetation in Luvuvhu Catchment Area, and

ii) Distinguish indigenous vegetation from croplands.

2.2. Material and methods

2.2.1 Description of the study area

The Luvuvhu River Catchment is located in the northeastern region of Limpopo province, South Africa as shown in Figure 2.1. The catchment is situated between the latitudes 22^0 17' 33'' S and 23^0 17' 57'' S and longitudes 29^0 49' 46'' E and 31^0 23' 32'' E. The Luvuvhu Catchment Area covers an area of approximately 331 602, 447 hectares with an elevation in the catchment ranging between 200 to 1,700 m resulting in shallow storage dams that are exposed to excess evaporation due to large water surfaces (Odiyo et al., 2012). The catchment is also characterized by topographic features such as the Soutpansberg mountain range on the eastern side of the catchment. This topographic feature rises to a height of approximately 1 700 m above mean sea level prior to reaching the low-lying surface of the Limpopo River Valley (Kundu et al., 2013). The landscape in other parts of the catchment has a mean ridge height of about 800 - 1 200 m while some places within the catchment whereas other parts of the catchment reach a peak above 1 500 m (Singo et al., 2012; Kundu et al., 2013).

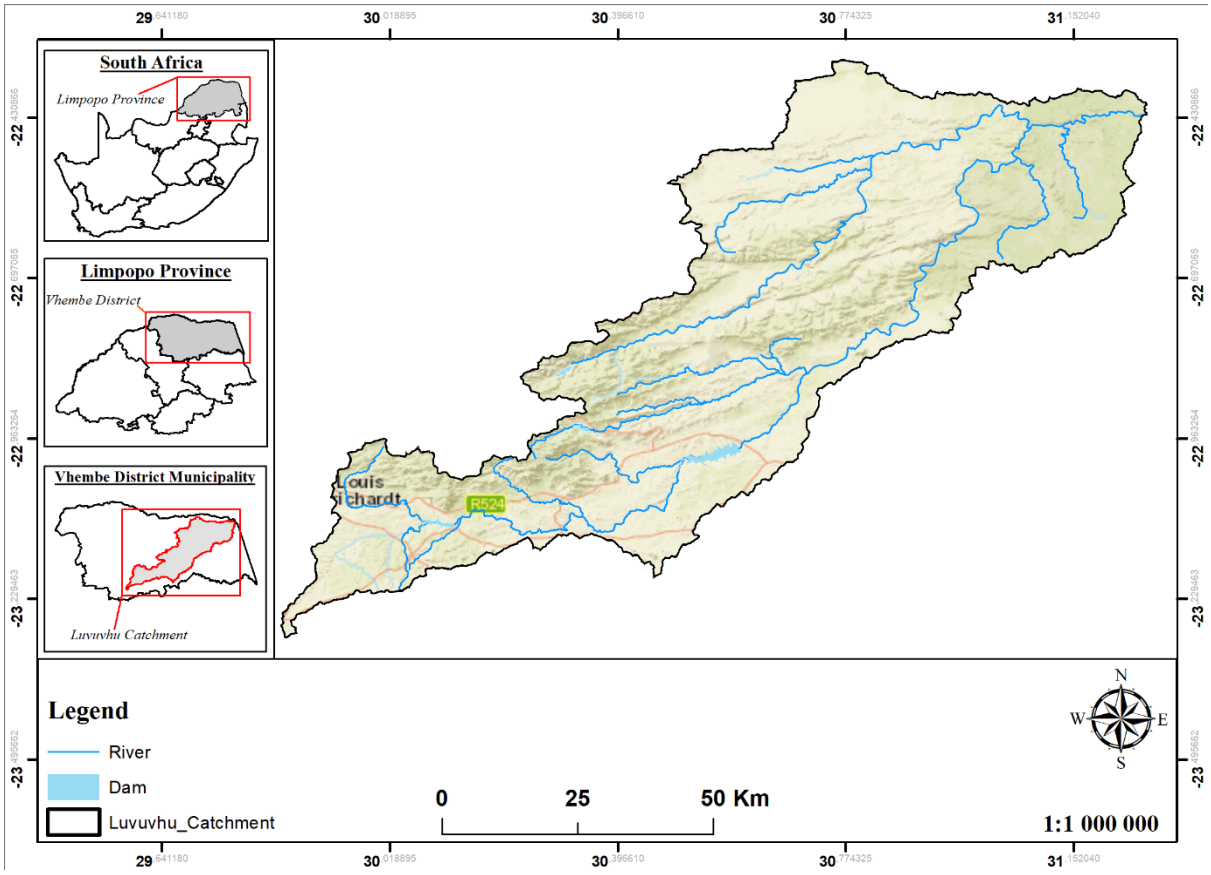

Figure 2.1 Location of the Luvuvhu River Catchment within Vhembe district municipality in South Africa.

Precipitation in the catchment is influenced by orographic uplift due to the east-west orientation of the Soutpansberg mountain range, where warm moisture is blown from the Indian Ocean and result into precipitation of about 1 200 mm to 1 500 mm/year in the forested mountain headwaters (Shongwe, 2007). The slope gradient then drops rapidly into semi-arid forest and bushland which receives only 200 mm to 600 mm/year (Singo et al., 2012). Within the catchment, the Soutpansberg mountain range influences massive differences in topography, and height fluctuations over short distances resulting in dramatic climatic variance within the LRC (Volenzo and Odiyo, 2018). LRC has a subtropical climate with distinct wet summers with regular and severe rainfall. From November to March, the area receives rainstorms followed by a dry winter with little precipitation from April to October.

High temperatures influence the gradual increase in evaporation rates within the study area ranging between 1400 mm and 1900 mm/year (Nethononda, 2018). Climates have a significant impact on the vegetation type of a particular area, especially the length of wet seasons (Dagada, 2017). An estimated area of 168 km^2 within the LRC is covered by vegetation of which the upper reaches of the catchment are dominated by alien vegetation (Nare et al., 2011).

Land use within the study area is comprised of conservation areas, commercial forestry, rangeland, urban and rural settlement, commercial dryland agriculture as well as commercial irrigation agriculture (Hope et al., 2003). Kruger National Park (KNP) is South Africa's foremost eco-tourism attraction which dominates the eastern part of the LRC (Griscom et al., 2010). The north-eastern part of the catchment is dominated with rural settlements; however, the north-eastern part of the catchment is the driest (Griscom et al., 2010). Irrigation farming practices within the LRC are the biggest consumer of Luvuvhu freshwater.

2.2.2 Field data collection

Fieldwork was conducted during summer early December 2021 between the 2nd and the 11th using stratified random sampling. The study region had both broadleaf and needle leaf plant species and their distribution differed throughout the study area. To integrate various plant species and canopy structures, dominating species within the sampled points only, were considered in this study. However, other plant species around the sampled points were also taken into consideration to supplement plant data collected. A total of 168 sampling points were generated and spread out within the study area with at least 2 km between the points to minimize pixel overlapping on satellite imagery. 82 points accounted for indigenous vegetation while 82 points account for cropland data, the latter collected randomly from Sentinel-2 10 m spatial resolution image composite. A total of 60% ($n = 98$) of data was randomly

selected as training data and 40% ($n = 66$) was used for validation, this rational discrepancy between the output values and the validation set will improve the integrity of the model while a large difference may nullify the model. The calibration data set was used for training the maximum likelihood classifier. The classification technique was assessed using the validation data set. Leica GPS 1200 (Leica Geosystems AG, Iteerbrugg, Switzerland) was used to record coordinates at the center of each plot an accuracy of approximately 3m. At each sampled point, depending on its heterogeneity, one dominating overstory plant species was selected for sampling. Each sample composed of five leaflets was collected from the sunlit branches of the exact sampled trees.

2.2.3 Satellite data collection

Satellite images from Sentinel-2 were downloaded from (https://scihub.copernicus.eu/) between 02 December and 09 December 2021 for image classification. In 2015 and 2017, a pair of Sentinel-2 satellites were launched. The launch of Sentinel-2A in 2015 and Sentinel-2B in 2017 has improved the remote monitoring of land surfaces and assessment of vegetation variables (Gitelson et al., 2014). Sentinel-2 provides data at an unprecedented spatial and temporal resolution (Frampton et al., 2013). Both Sentinel-2A and Sentinel-2B satellites have Multi-Spectral Imager (MSI) with a swath width of 290 km and offer remotely sensed data in 13 spectral bands from the visible and near-infrared region to the shortwave infrared region, of which four bands are at 10 m, six bands at 20 m and the remaining three bands at 60 m spatial resolution (Xie et al., 2019; Richter et al., 2019).

2.2.4 Image differencing and thresholding

The NDVI was computed using the sentinel-2 data. The thresholding and differencing were done through Esri, ArcGIS ArcMap, the tool which was employed is the raster calculator, as stated above that the best value for identifying healthy vegetation starts from 0.2 hence (NDVI=>0.2) (Badamasi and Yelwa, 2010). The study used the NDVI threshold of 0.2 because any threshold below that does not indicate the presence of healthy vegetation if there is vegetation at all. In the raster calculator, the following formulae was used to extract the DN value of the selected threshold value **Con ("NDVI_img" >= threshold, "NDVI_img")**. After the results have been obtained from the formula, the raster was then reclassified into two main classes which are non-vegetation and those which are Vegetation. The reclass raster was then converted to a polygon shapefile where it was renamed as “VEG ALL.shp”. The converted “VEG ALL.shp” file was then again altered in ArcGIS feature class tool editor, removing all the non-vegetation, in which the non-Vegetation were having the NDVI values of less than 0.2, were removed from the shapefile. The remaining was then used as the main vegetation

shapefile layer. A Tool in ArcMap called the composite band tool was then used to compile or stack the images together to form one single major band image of the entire sentinel bands, and the composite band raster was then renamed to image.tif, after the "VEG ALL" shapefile was then used to crop or extract the composite band image, to produce results which were renamed to S2Image_VEG.tif.

2.2.5 Vegetation cover mapping and validation

Vegetation cover mapping was executed using a maximum likelihood classifier. The MLC is based on the Bayes' theorem which has assumptions that cell values of each reference class are normally distributed (Schultz et al., 2021). Mean values and covariance matrix are used to describe each reference class and each reference class is allocated by reducing a covariance-weighted gap among the reference cluster and the chosen pixel value (Schultz et al., 2021). In this study, we used MLC implemented in ESRI ArcGIS 10.7. Remote sensing applications have high computational performance, classification accuracy as well as the capacity to operate at largescale characterized by diverse feature spaces using fairly few training samples (Muller et al., 2015; Rogan, Rodriguez-Galiano et al., 2012). In this study, 98 (60%) of sampling points generated during the field work were randomly selected for model calibration. A very high-resolution Sentinel-2 imagery was used to classify training points. In cases where there was confusion, the labelling was conducted in favor of natural vegetation since it was the dominant and mixed vegetation class in the catchment. 2 km was set as a minimum distance criterion to reduce spatial clustering of training points and related autocorrelation. The remaining ($n = 66$) points (40%) were used to validate the accuracy of the model as shown on Table 2.1.

Table 2.1 A number of training and validation samples for each land cover class

Class	Training samples	Validation samples
Indigenous vegetation	49	33
Croplands	49	33
Total	98	66

2.3. Results

Figure 2.2 shows the occurrence of indigenous vegetation across sampled points.

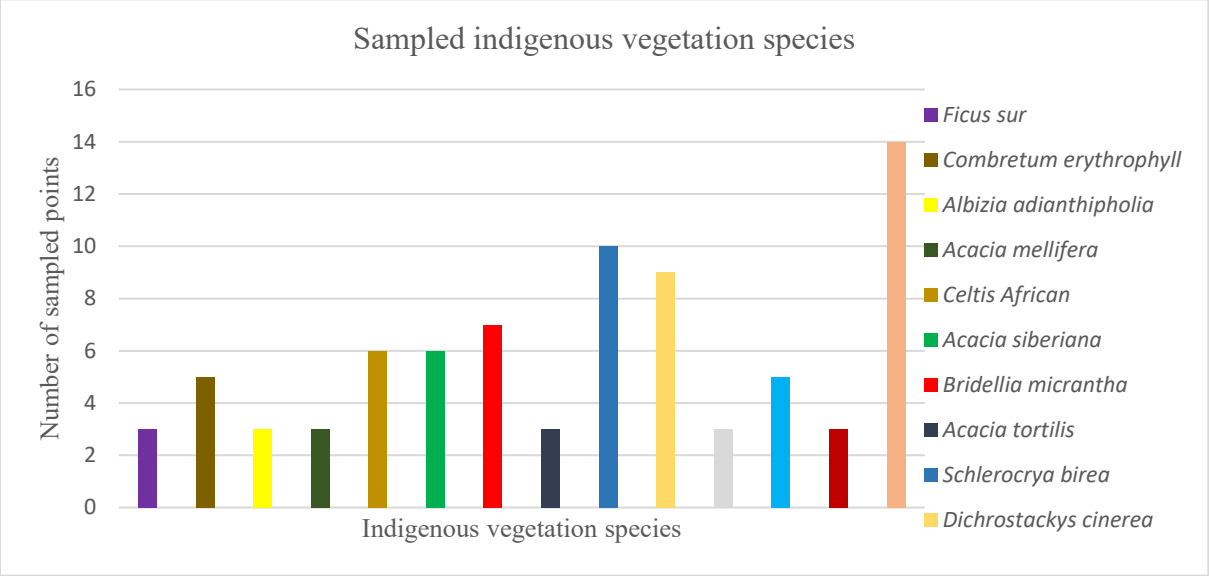

Figure 2.2 The occurrence of sampled indigenous vegetation species

2.3.1 Vegetation cover

Vegetation mapping using optical remote sensing is very common and NDVI is the most broadly utilized approach (deFries et al. 1995; Xie et al., 2008). NDVI is one of the most used spectral indices in vegetation mapping due to the high reflectance of vegetation in the near-infrared and high reflectance in the visible red (Xie et al., 2008). The distinction between near-infrared and visible red can be used to assess vegetation cover and health status. Moreover, NDVI provides a good indication of the vegetation 'greenness" since it correlates well with photosynthetic activity (Wang et al., 2007). The range of NDVI is between -1 to 1. Therefore, areas that have high vegetation cover have the value to 1 while non-vegetated areas are close to 0 (and negative for within water bodies) (Bdamasi and Yelwa, 2010). Areas of barren rocks and water could be represented by NDVI values of 0.1 or lower while the NDVI values between 0.2 and 0.5 indicate sparse vegetation covers. Areas with dense forest typically have high NDVI reflectance with values ranging between 0.6 to 1 (Turner et al., 2013). This study used

Sentinel-2 imagery to apply the NDVI algorithm in mapping the area covered with vegetation within the LRC.

Near-infrared and visible red reflects in band 8 and band 4, respectively in the Sentinel-2 sensor. Therefore, we determined the NDVI values using the formula (1) below:

$$NDVI = \frac{(IR - R)}{(IR + R)} \quad (1)$$

where IR is near-infrared band and R is red band.

The use of NDVI over the area of interest, LRC has depicted the results shown in Figure 2.3

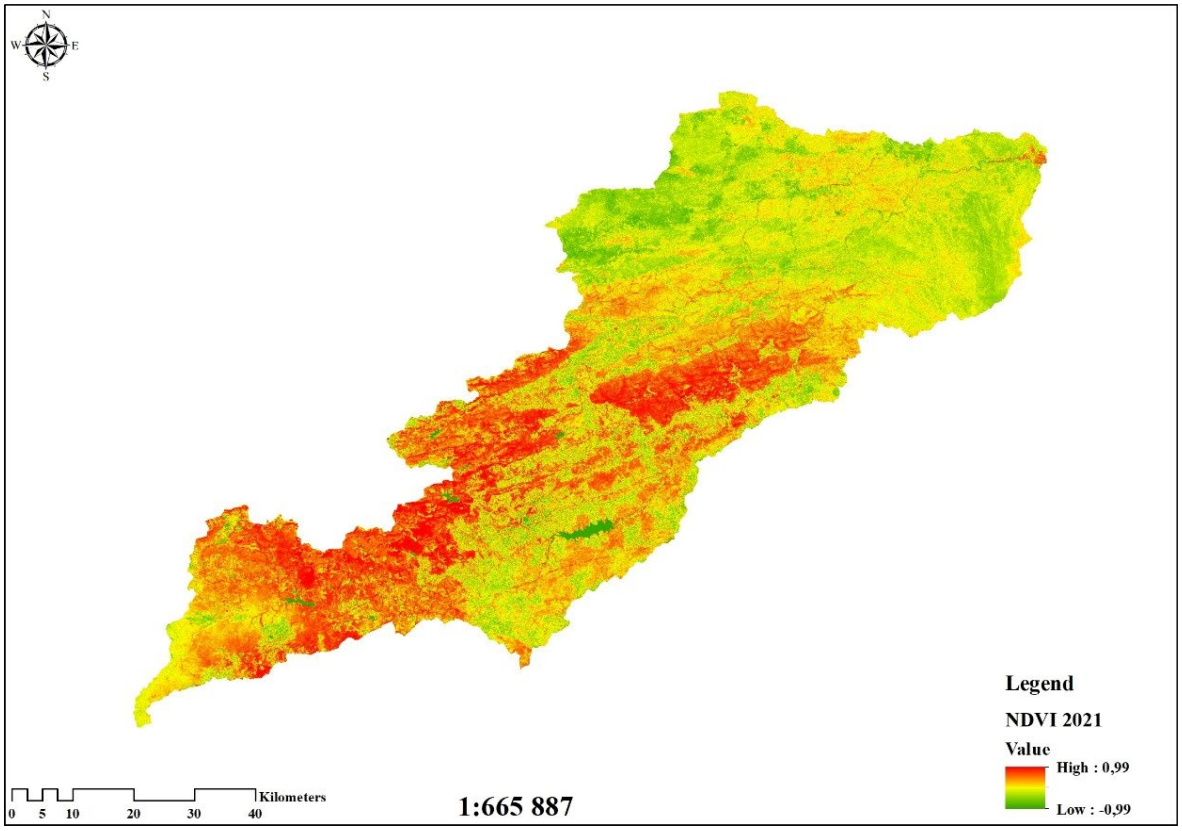

Figure 2.3 The NDVI distribution across the LRC.

2.3.2 Vegetation classification

Figure 2.4 displays the vegetation cover map created for the LRC using Sentinel-2 imagery and shows that the most abundant vegetation cover across the catchment is classified as natural vegetation while the other portion of vegetation cover is classified as croplands. Grassland woodland, bushland and thickets dominate indigenous vegetation cover in LRC (Griscom et al., 2010). It is noted with great concern that the area covered with natural vegetation within the study areas has been decreasing over the years in the catchment. This is greatly owed to land conversion into agricultural land to suit the need of the growing population.

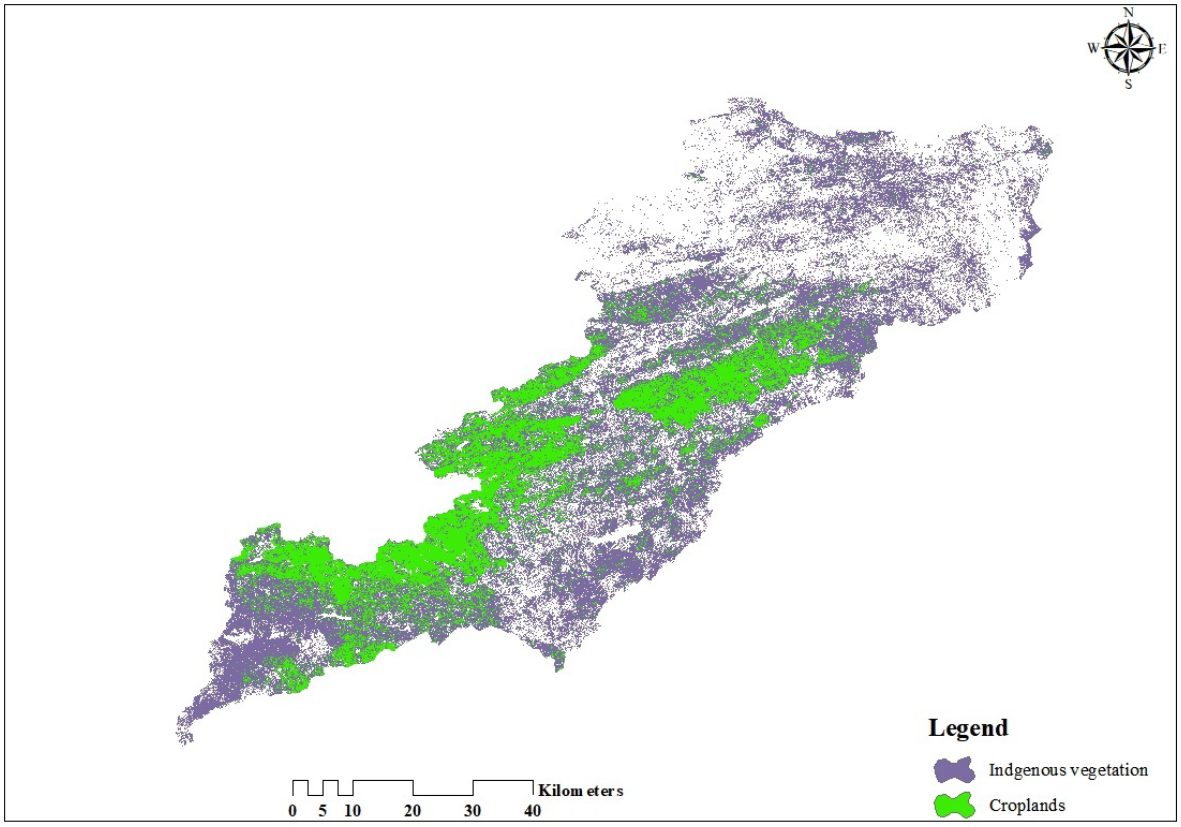

Figure 2.4 Vegetation type distribution

Table 2.3 Pixel count error matrix

Class name	Indigenous Vegetation	Croplands	Total
Indigenous vegetation	3 595	30	3 624
Croplands	276	15 275	15 551
Total	3 870	15 305	19 175
User's accuracy (%)	99.17		

Producer's accuracy (%)	99.23
Overall accuracy (%)	98.41
Kappa hat classification	0.949

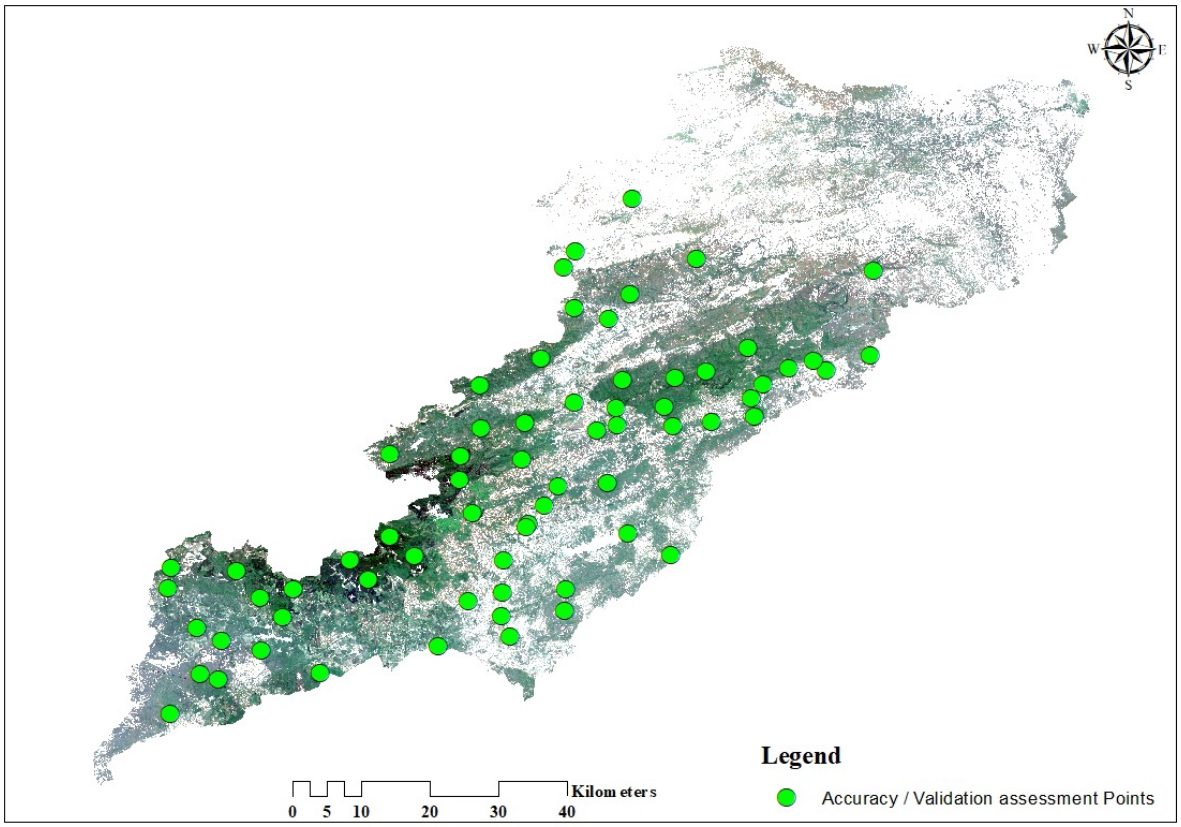

Figure 2.5 The distribution of validation points across the LRC.

2.4 Discussion

The aim of the current study was to map the areas covered with vegetation within the LRC in the Limpopo province, thereafter, distinguish agricultural vegetation from indigenous vegetation. This study obtained an overall accuracy of 98.41% for vegetation cover mapping. This accuracy is within the range reported for subtropical environments which forms part of our study area, and these results are similar to the observations by Griscom et al. (2010). As recorded by Landis and Koch (1977), the study recorded KHAT of 0.949 which is almost "perfect". The KHAT value makes the vegetation cover map satisfactory for the determination of inputs to vegetation cover classification, vegetation cover change analyses, ecological management, and coarse-scale hydrological modelling. Vegetation cover maps play a crucial role for variety of application, however, mapping vegetation at a large scale within heterogeneous ecosystem such as LRC in Limpopo province still comes with a number of challenges

since there is still a huge inconsistency when it comes to vegetation cover maps. Nonetheless, improvement in remote sensing, increased free access to satellite imageries and means to compute remotely sensed data have made it feasible to generate high-resolution vegetation cover products of large geographic areas. Information obtained from remotely sensed data can be utilized for monitoring terrestrial variations and trends which are influenced by climate variation, global climate change, environmental phenomenon, and human activities that influence the way that the ecosystem functions (Griscom et al., 2010).

This study used data from Sentinel-2 imagery to map vegetation cover in the LRC. Sentinel-2 products have been widely used with remarkable results when it comes to vegetation health assessment as it can be applied to a variety of applications including mapping of the vegetated area, establishing boundaries between variety of vegetation types such as croplands and natural vegetation (Adjognon et al., 2019; Phiri et al., 2020). Sentinel-2 imagery can also be used to monitor the production of crops, nutrient content as well as the health status of vegetation (Phiri et al., 2020). A study on a global project by Fan et al., (2020) that involved a number of African countries such as Burkina Faso, South Africa, Morocco, and Madagascar reported on the effectiveness of using Sentinel-2 data for both small and large-scale farming. These studies range from small scale monitoring (i.e., field-level) to continental level. Sentinel-2 data has been widely used for real-time agricultural monitoring since there is a high demand for information for agriculture production.

There are a number of spectral indices derived from remote sensing which are used to detect areas covered with vegetation and their health status, and amongst them, NDVI remains the one that is often used by researchers. NDVI is one of the most used spectral indices for vegetation mapping due to high reflectance of vegetation in the near-infrared and high reflectance in the visible red (Xie et al., 2008). The distinction between near-infrared and visible red can be used to assess vegetation cover and health status. NDVI provides a good indication of the vegetation ‘greenness” since it correlates well with photosynthetic activity (Wang et al., 2007). As shown in Figure 2, northern-eastern and southern central parts of the catchment recorded lower NDVI values compared with the rest of the catchment (Turner et al., 2013). Across those areas, large proportion of land has been converted from natural vegetation to several land-use activities which influence the values of NDVI across the catchment. There has been exponential growth in population within the catchment which resulted in large areas being converted to places of settlements and other infrastructural developments. Moreover, communities within the LRC are among the most disadvantaged communities in the country, where most people are still heavily relying on nature for service provision such as fuelwood for energy. There is a persistent propensity of cutting firewood for sale to upmarket areas. This is one of the extensive human activities behind the high rate of conversion from vegetated land to sparsely vegetated or bare land observed across the catchment, followed by land conversions to croplands and small-scale mining (sand and gravel).

In disparity, the north-western and south-western parts of the catchment are heavily characterised by dense natural vegetation, subsistence farming crops and commercial cultivation land uses recorded higher NDVI compared to the north-eastern and southern parts of the catchment. Good vegetation health found in the northern parts of the catchment is influenced by slope and nutrient-rich soil as well as deep rooting which enables plants to draw underground water. Croplands in the south-eastern part of the catchment have contributed to higher NDVI values recorded in the areas since there is supplementary water supply within the farms (Turner et al., 2013). Commercial farming is dominant near Albasini dam and along the Levubu farming district and some parts of Tshakhuma while small-scale farming is also spread out across the catchment especially along the riverbanks where the soil is fertile. Low-lying areas along the riverbanks within the catchment are utilized for agricultural activities due to flat fertile land easier access to water resources. A variety of fruits such as avocadoes, mangoes, bananas, and macadamia are intensively produced along the Soutpansberg mountain range, this is influenced by high rainfall recorded in the area. There has been devasting land clearing for agricultural activities, settlements as well as firewood harvest in areas that are not protected, this also affect the state of rivers within the catchment (Hope et al., 2004). Human impact on the landcover is observed with synchronous changes on vegetation cover and use. Some areas within the catchment area experience poor land use where natural vegetation is being cleared or it has been removed, thus increasing soil erosion.

NDVI on its own cannot efficiently distinguish the entire collection of plant communities. This was realised during the use of NDVI to map vegetation since some of the croplands were giving similar NDVI values as natural vegetation within the same landscape making it impossible to separate them on a spectral basis (Turner et al., 2013). Therefore, optical data from Sentinel-2 was classified using the MLC implemented in ESRI ArcGIS 10.7 for land cover classification of the LRC heterogeneous landscape. The MLC is based on the Bayes' theorem which has assumptions that cell values of each reference class are normally distributed (Schultz et al., 2021). Mean values and covariance matrix are used to describe each reference class and each reference class is allocated by reducing a covariance-weighted gap among the reference cluster and the chosen pixel value (Schultz et al., 2021). The classified Sentinel-2 images show that in LRC, 331 602.477 ha is covered with vegetation of which natural vegetation covers 232 168, 773 ha while cropland covers 99 433.697 ha, this exhibits a decrease in natural vegetation cover in the catchment. This may be a result of increased agricultural practice, both commercial and subsistence farming, uncontrolled grazing, and cutting down of natural vegetation for firewood. Population growth within the catchment is also playing a significant role in reducing the vegetation cover within the study area since many parts of the catchment are being converted to settlement areas and shopping complexes among other infrastructural development.

2.5. Conclusion

There are various classification techniques in remote observation studies. In this study, Sentinel-2 images were used to map the area covered with vegetation using NDVI technique since it is one of the significant methods in mapping vegetation cover. Since NDVI cannot be used to differentiate between different types of vegetation, this study used MLC, which indicated that croplands have covered greater area compared to indigenous vegetation. The study achieved an overall accuracy of 98.14% and a KHAT of 0.949 which is almost perfect for classification. This substantiates that Sentinel-2 imagery can be utilized to map vegetation cover over at a landscape scale for vegetation health monitoring. However, vegetation cover on its own cannot be used to assess vegetation health, hence there are other vegetation parameters that can be assessed to conclude on vegetation health such as vegetation water content, nutrients, and others.

CHAPTER THREE: ESTIMATING LEAF MOISTURE CONTENT OF INDIGENOUS VEGETATION WITHIN LUVUVHU RIVER CATCHMENT USING SENTINEL-2 IMAGERY

Abstract

Global climate change continues to exert pressure on the hydrological cycle especially in the arid and semi-arid environments of the world. Interestingly, healthy vegetation contributes to water balances thus helping in regulating global hydrological fluxes. The vegetation water content is one of the most important parameters of vegetation health. Remote estimation can be utilized for real-time monitoring of vegetation water stress. This study aims to estimate the leaf moisture content of natural vegetation using field data, and high spatial and temporal resolution Sentinel-2 imagery. The study compared the capability of narrowband (red-edge centred), broadband and the combination of both broadband and narrowband derived vegetation indices in estimating vegetation leaf moisture content across Luvuvhu River Catchment (LRC). A stepwise linear regression model was used in modelling vegetation leaf moisture content. The results have shown that the combined vegetation indices model outperformed other models with $R^2 = 0.54$ and RMSE = 0.085 g/cm^2 while the narrowband achieved $R^2 = 0.48$ and RMSE = 0.097 g/cm^2, and finally, the broadband vegetation indices achieved $R^2 = 0.24$ and RMSE = 0.096 g/cm^2. Through stepwise regression, the study concluded that the combined vegetation indices outperformed the other pair of models. As a result, its coefficients were utilized to produce thematic map showing the distribution of vegetation leaf moisture content across the study area using multiple linear regression in ArcGIS. It is also established that vegetation leaf moisture content across the study area is unevenly distributed, with the mountain range receiving relatively higher rainfall and resulting in higher vegetation leaf moisture content. Vegetation leaf moisture appears to be very low on the north-eastern part of the study area. This study demonstrated that with the right spectral indices for moisture content estimation, Sentinel-2 data can efficiently estimate water content across the landscape. This study provides reference for estimating vegetation moisture content in LRC using data from the Sentinel-2 satellite.

Keywords: Sentinel-2, vegetation water content, red-edge, spectral indices.

3.1 Introduction

Vegetation leaf moisture content is a crucial parameter in natural vegetation and agricultural applications (Danson and Bowyer, 2004). Leaf moisture content is often determined as Equivalent Water Thickness (EWT) and it serves as an important primary indicator of vegetation water stress, vegetation diseases and act as principal input when vegetation models are created (Gaulton et al., 2013). Vegetation leaf moisture content also serves as an indicator of infection by tree diseases (Danson & Bowyer, 2004) and as an indication for fire risks across different ecosystems (Peterson et al., 2008). Most physiological processes of plants such as transpiration and photosynthesis cannot take place when there is no water involvement (Chapin et al., 2011). Water stress affects vegetation directly when it comes to growth and development, the rate of photosynthesis dry mass production as well as production of seeds (Zhou et al., 2013). However, when plants are stressed, they tend to maintain the leaf moisture content of the living leaves to maintain physiological processes of plants, this happens at an expense of losing old leaves so that the demand for water may decrease (BassiriRad et al., 2003). It is critical to have methods that assist with the early detection of plant water stress to avoid forest fires, vegetation diseases as well as defoliation as a result of leaf water deficiency (Meentemeyer et al., 2008).

Traditionally, vegetation leaf water content is estimated manually by calculating the weight of fresh leaves and the weight of dry leaves of sampled plants (Wang and Liu, 2013). This method is accurate; however, it requires a lot of time, laborious and costly to carry out at a landscape scale (Zhang et al., 2010). Remote sensing has gained popularity when it comes to multi-scale and real-time leaf content monitoring as an alternative to the use of laboratory estimates (Zhang and Zhou, 2019). The fast-growing remote sensing technology is associated with large amount of literature on how remote estimations of vegetation leaf content is accurately estimated at a large scale within a very short space of time (Gao et al., 2015). Remote sensing techniques which are used to estimate vegetation moisture content over a large area includes the use of the radar, thermal optics, and optical remote sensing. Vegetation health, productivity, water deficiency and other physiological status of vegetation can be effectively monitored by the use of remote sensing techniques and immediately adopt necessary measures to protect the vegetation (Easterday et al., 2019; Gao et al., 2015; Zhang and Zhou, 2019).

In the 1970s, the first Landsat satellite was launched, and with the use of this generation of sensors for vegetation monitoring such as estimation of leaf pigment content, one has to use the visible part of the spectrum while short-wave infrared (SWIR) is explored for leaf water estimation (Boren and Boschetti, 2020). This is often achieved by developing simple ratio spectral vegetation indices such as the normalized difference vegetation index (NDVI) (Easterday et al., 2019). Many spectral vegetation indices have been formulated over the years after Jordan introduced the concept of vegetation index in 1969 (Zhang et al., 2018). Spectral indices that are used to estimate vegetation leaf water content are

mostly based on NIR and SWIR bands since they are sensitive (Dong et al., 2019). Combining NIR and SWIR plays a crucial role in retrieving canopy water content at leaf level (Cecato et al., 2001). However, NDVI is one of the most commonly used spectral indices that serves as an indicator of plants' photosynthetic capacity (Byrd et al., 2014). It correlates well with leaf chlorophyll, green colour, and plant vigour (Jensen et al., 2011) and is frequently utilized to estimate vegetation cover, health, and growth (Tuxen et al., 2011; Easterday et al., 2019) and to quantify evapotranspiration (Nouri et al., 2014).

The launch of new a generation of satellite sensors such as WorldView-3, Sentinel-2, and RapidEye which have narrowband red-edge band(s) (in the region between 680 nm to 730 nm) have opened new paths for assessing leaf water content (Jiao et al., 2021; Easterday et al., 2019). Unlike the broadband sensors, narrowband instruments are capable of measuring individual spectral features such as composition of plant pigments (Bryd et al., 2014), vegetation leaf water content (Wang et al. 2018), canopy dry plant litter and/or wood, or other aspects of foliar chemistry (Zhang and Zhou, 2018). The impact of water stress on plant biochemical elements such as plant chlorophyll a/b has been well studied using the red-edge band; since the leaf chlorophyll make-up changes when the plants are experiencing a water stress, resulting in a shift of red-edge reflectance towards shorter wavelengths (Virnodkar et al., 2020). Using reg-edge band instead of the red band when formulating spectral indices normally displays changes in plant pigment (Gitelson and Mezalyak, 1994) and has been connected with drought-induced distinction in leaf photosynthetic rates (Sims and Gamon, 2002). In most cases where optical instruments have been compared, narrowband imaging instruments provide more detailed information about vegetation features than multispectral instruments (Serrano et al., 2000).

Optical-based estimation of water content typically involves empirical methods, relying on statistical relationships between field-measured vegetation water and water sensitive spectral indices. Over the years, many spectral indices have been formulated to estimate vegetation parameters such as crop water stress index (CWSI) normalized difference water index (NDWI) (Jiang et al., 2010), ratio index (Idso et al., 1981). Leaf water content estimation has been achieved with ease and good accuracy by the use of remotely sensed data to calculate spectral indices (Chen et al., 2016; Li et al., 2020; Junttila et al., 2018). The use of remotely sensed data to calculate spectral indices is affected by the relationship between vegetation leaf water content and spectral indices which depend heavily on sampling methods in the field, image pre-processing and the statistical model to be used (Chen et al., 2006). However, despite these limitations, the use of vegetation indices is still recommended for the analysis of vegetation biophysical and biochemical parameters including moisture content (Wang et al., 2021), nutrient status (Ramoelo and Cho, 2018), photosynthesis (Bryd et al., 2014) and net primary production among others (Vina et al., 2011). This is especially true when the spectral configuration of optical satellites is focused on new spectral regions that are otherwise not present in conventional satellites.

The aim of this study was to estimate natural vegetation leaf moisture content using Sentinel-2 data using regression models and various vegetation indices. The study was guided by the following objectives:

(i) Comparing the performance of narrow-band spectral indices vs broadband spectral indices in estimating leaf water content of natural vegetation

(ii) Mapping of the leaf water content through the best model

3.2 Materials and methods

3.2.1 Description of the study area

The Luvuvhu River Catchment is located in the northeastern region of Limpopo province, South Africa as shown in Figure 3.1. The catchment is situated between the latitudes 22^0 17' 33'' S and 23^0 17' 57'' S and longitudes 29^0 49' 46'' E and 31^0 23' 32'' E. The Luvuvhu Catchment Area covers an area of approximately 331 602, 447 hectares and the elevation in the catchment ranges from 200 to 1,700 m which gives rise to shallow storage dams which are exposed to excess evaporation due to large water surfaces (Odiyo et al., 2012). The catchment is also characterized by topographic features such as the Soutpansberg mountain range in the east of the catchment, which reaches about 1 700 m above mean sea level before dropping off into Limpopo River Valley (Kundu et al., 2013). The general terrain of mean ridge height is approximately 800 - 1 200 m is common in some places within the catchment while other places reach a peak above 1 500 m (Kundu et al., 2013).

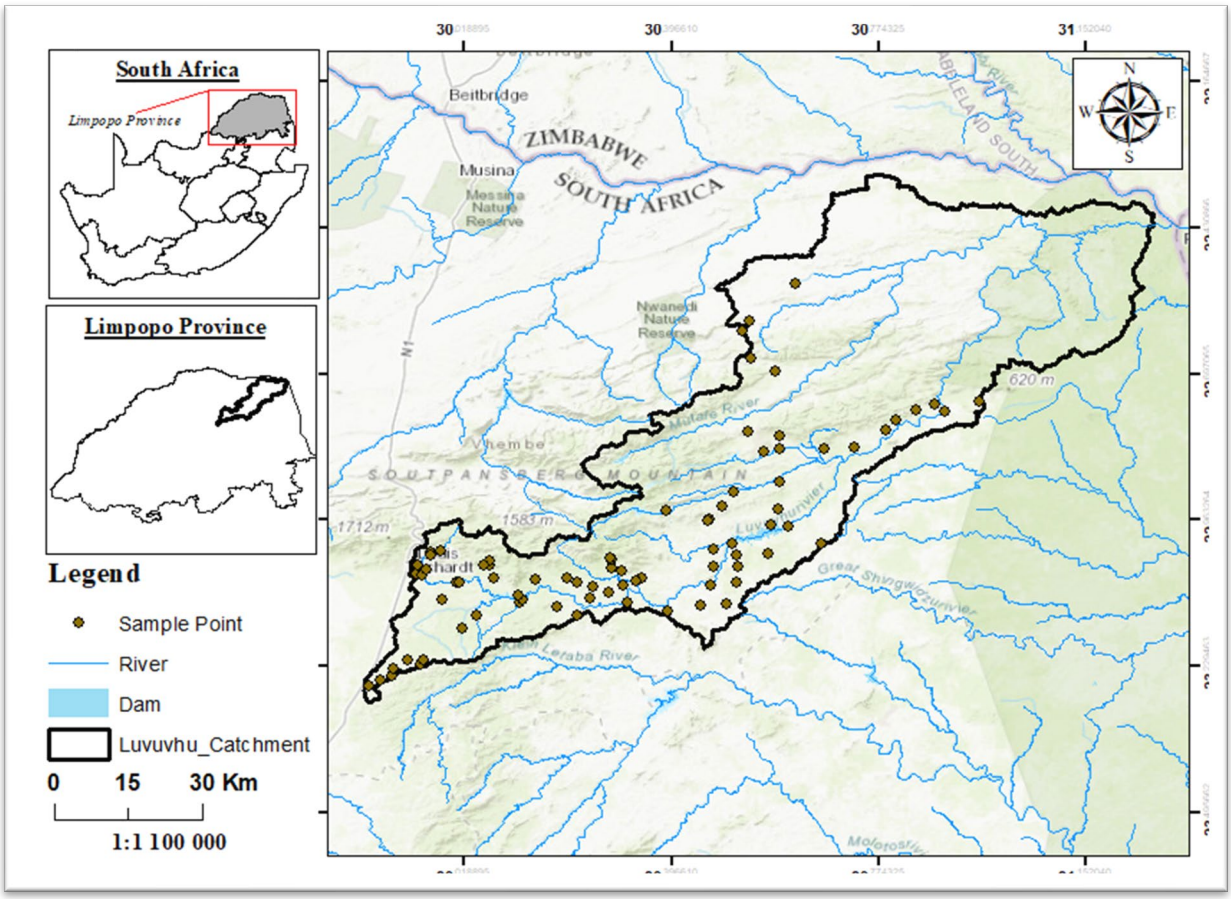

Figure 3.1 The location of the study area

Precipitation in some parts of the catchment is influenced by orographic uplift due to east-west orientation of the Soutpansberg mountain range where the western movement of moisture from the Indian Ocean results in 1 200 mm to 1 500 mm/year in the forested mountain headwaters (Shongwe, 2007). Semi-arid forest and bushland receive only 200 mm to 600 mm/year as the terrain drops across the study area. Extreme topographic diversity and altitude changes over short distances within the Soutpansberg result in dramatic climatic variance within the LRC (Volenzo and Odiyo, 2018). Luvuvhu River catchment is characterized by subtropical climate with rainy days during November to March, and little rainfall from April to October. High temperatures in the study area influence the gradual increase in evaporation rates ranging between 1 400 mm and 1 900 mm/year (Nethononda, 2018).

Climates have a significant impact on the vegetation type of a particular area, especially the length of wet seasons (Dagada, 2017). Luvuvhu River, Dzondo River, Dzindi River, and other perennial rivers, as well as wetlands influence vegetation health conditions within the catchment. Vegetation found along riverbanks or beside wetlands is mostly greener throughout the year and they also help to reduce the impacts of floods. However, deforestation of riparian vegetation has taken place in most parts of the catchment to make land available for both commercial and subsistence farming.

3.2.2 Field data collection

Fieldwork was conducted from the 2nd of December 2021 to the 11th of December 2021 using simple random sampling. In contrast to typical methods used in plot investigations (Zhao et al 2019), a recently developed method for the collection of data from all species in the sampling sites was adopted (Zhang et al 2020). The typical method represents a quadrat survey focusing on the dominant species. The study region had both broadleaf and needle leaf plant species and their distribution varied across the study area. To incorporate various plant species and canopy structures, dominant species within the sampled location were considered for this study. A total of 82 samples were collected within the study area. Data was randomly split into 60% training (n = 49) and 40% validation (n = 32) data sets. This reasonable difference between the values and the validation sets will usually improve the credibility of the model while a large difference may invalidate the model (Croft et al., 2014). The validation data set was used to assess the accuracy of the models. Standard Garmin eTrex 10 Handheld GPS with the maximum spatial accuracy of approximately of 3 meters was used to record coordinates at the center of each plot. A total number of five-leaf samples per tree from the sunlit branches of an individual trees were harvested for laboratory analysis. The leaves were weighed on-site using Digital Portable Kitchen Scale of accuracy 0.1g to obtain vegetation leaf wet weight and dry weight after being subjected to oven-drying for 24hrs at 70°C.

The vegetation leaf water content was calculated based on the difference of wet weight and dry weight of the leaves using the equation (1):

$$wc = \frac{Q1 - Q2}{Q1} \quad (2)$$

Where wc is water content, $Q1$ is the wet weight, and $Q2$ is the dry weight.

3.2.3 Satellite data collection

Satellite images from Sentinel-2 were downloaded from (https://scihub.copernicus.eu/) between 02 December and 09 December 2021 for this study. When compared to other satellites such as Landsat that have low to medium spatial resolution Sentinel-2 offers better-quality data especially in temporal and spatial resolution (Novelli et al., 2019). Sentinel-2 images have 13 bands with spatial resolutions ranging from 10 to 60 m, with visible and near-infrared having the spatial resolution of 10 m, while infrared bands have spatial resolution of 20 m and lastly, other bands have spatial resolution of 60 m (Immitzer et al., 2016; Chastain et al., 2019). The Sentinel-2 potential for detailed Earth's surface exploration (Natural vegetation and croplands) is owed to the 10 m spatial resolution. Moreover, the effectiveness of Sentinel-2 data when it comes to Earth's surface exploration and monitoring is influenced by wide swath and freely available data. Monitoring of the Earth's surface more effective includes the wide swath and the free access data policy (Phiri et al., 2019). Large areas are processed much easier and with higher accuracy due to the 290 km wide swath of 290 km which requires less need for normalisation and merging of data (Hansen and Loveland, 2012). The free open access to Sentinel-2 data offers a great alternative for high spatial resolution for many countries that are economically disadvantaged and struggle to access high-resolution satellite images (Turner et al., 2015). Sentinel-2 high spatial resolution images have already contributed to the 20 m land cover maps for Africa (Xu et al., 2019) and other regional land cover maps based on Sentinel-2 images, especially that most of the regional land cover/use maps have a spatial resolution of 30 m (Chen et al., 2015).

3.3 Spectral variables

To achieve the objectives of this chapter which was to compare the performance of narrowband and broadband spectral indices in estimating vegetation leaf water content, a list of narrowband and broadband-based indices was created based on literature review (Roumenina et al., 2020). For this study, three datasets were prepared, and stepwise regression was repeated for all of them. The first dataset included the narrow bands-based spectral indices (with focus given to the red-edge centred bands), the second dataset involved broadband-based spectral indices, and the third dataset included

spectral indices from both narrow and broad bands part of the electromagnetic spectrum. Vegetation leaf moisture was calculated using formulas in Table 3.1 and 3.2.

Table 3.1 Summary of selected optical red-edge based vegetation indices used in this study based on Sentinel-2.

Vegetation index	**Formulas**	**Reference**
Enhanced difference red edge vegetation index (NDVIRed edge)	$NDVI1 = \frac{(B08 - B05)}{(B08 + 505)}$ $NDVI2 = \frac{(B08 - B06)}{B08 + B06}$ $NDVI3 = \frac{B08 - B07}{B08 + B07}$	Han et al., 2019
Simple ratio (SR)	$SR2 = \frac{B07}{B04}$ $SR3 = \frac{B07}{B06}$ $SR4 = \frac{B07}{B05}$	Jordan, 1969
Normalised difference red edge (NDRE)	$NDRE = \frac{B06 - B05}{B06 + B05}$ $NDRE1 = \frac{B07 - B05}{B07 + B05}$	Sims and Gamon, 2002
Normalized Difference Vegetation Index with band B07 (NDVI7)	$NDVI7 = \frac{B07 - B04}{B07 + B04}$	Fern et al., 2018
Red Model	$Red\_Model = B08 - B06$	Vina and Gitelson, 2005

Table 3.2 Summary of selected optical broadband spectral indices used in this study based on Sentinel-2.

Vegetation index	**Formulas**	**Reference**
Normalised difference water index (NDWI)	$\mathrm{NDWI} = \frac{\mathrm{B03} - \mathrm{B08}}{\mathrm{B03} + \mathrm{B08}}$	Gao, 1996
Normalised difference vegetation water index (NDVI)	$\mathrm{NDVI} = \frac{\mathrm{B08} - \mathrm{B04}}{\mathrm{B08} + \mathrm{B04}}$	DeFries et al., 1995
Enhanced multi-band drought index (NMDI)	$\mathrm{NMDI1} = \frac{\mathrm{B4} - (\mathrm{B10} - \mathrm{B11})}{\mathrm{B4} + (\mathrm{B10} + \mathrm{B11})}$ $\mathrm{NMDI2} = \frac{\mathrm{B4} - (\mathrm{B10} - \mathrm{B12})}{\mathrm{B4} + (\mathrm{B10} + \mathrm{B12})}$ $\mathrm{NMDI3} = \frac{\mathrm{B4} - (\mathrm{B11} - \mathrm{B12})}{\mathrm{B4} + (\mathrm{B11} + \mathrm{B12})}$	Wang et al., 2008
Enhanced difference infrared index (NDII)	$\mathrm{NDII1} = \frac{\mathrm{B10} - \mathrm{B04}}{\mathrm{B10} + \mathrm{B04}}$ $\mathrm{NDII2} = \frac{\mathrm{B11} - \mathrm{B04}}{\mathrm{B11} + \mathrm{B04}}$ $\mathrm{NDII3} = \frac{\mathrm{B12} - \mathrm{B04}}{\mathrm{B12} + \mathrm{B04}}$	Wang et al., 2015
Moisture stress index (MSI)	$\mathrm{MSI1} = \frac{\mathrm{B10}}{\mathrm{B08}}$ $\mathrm{MSI2} = \frac{\mathrm{B11}}{\mathrm{B08}}$ $\mathrm{MSI3} = \frac{\mathrm{B12}}{\mathrm{B08}}$	Meng et al., 2016
Enhanced difference water index ($\mathrm{NDWI_{Swir}}$)	$\mathrm{NDWI1} = \frac{\mathrm{B03} - \mathrm{B10}}{\mathrm{B03} + \mathrm{B10}}$ $\mathrm{NDWI2} = \frac{\mathrm{B03} - \mathrm{B11}}{\mathrm{B03} + \mathrm{B11}}$ $\mathrm{NDWI3} = \frac{\mathrm{B03} - \mathrm{B12}}{\mathrm{B03} + \mathrm{B12}}$	Han et al., 2019

Shortwave infrared ratio (SIWSI)	$SIWSI1 = \frac{B08 - B10}{B08 + B11}$ $SIWSI2 = \frac{B08 - B10}{B08 + B12}$ $SIWSI4 = \frac{B08 - B11}{B08 + B12}$ $SIWSI5 = \frac{B08 - B12}{B08 + B10}$ $SIWSI6 = \frac{B08 - B12}{B08 + B11}$	Olesen et al., 2015

For this study, 29 spectral indices which are directly sensitive to leaf water content and others that are not directly sensitive to leaf water content were selected for vegetation leaf water content. Spectral indices that were obtained from the combination of NIR (NDWI, NDVI), SWIR (SIWSI1, SIWSI2, SIWSI3, etc.) and other bands (NDVIrededge, Red_Model, etc.) were also considered for this study since NIR and SWIR bands since they are water sensitive bands (Dong et al., 2019). This study also made use of spectral indices which are red-edge centred (NDVIredege, SR1, SR2, SR3, Red_Model, etc.) since the impact of water stress on plant physiology such as plant chlorophyll a/b has been well studied using the red-edge band; since the leaf chlorophyll make-up changes when the plants are experiencing a water stress, resulting in a shift of red-edge reflectance towards shorter wavelengths (Filazzola et al., 2020).

3.3.1 Statistical analysis

3.3.1.1 Spatial interpolation

For this study, Kriging interpolation method was used. Kriging is a geostatistical interpolation with multistep technique that considers both the distance and the degree of variation between known points when estimating the unknown points (Paramasivam and Venkatramanan, 2019). In Kriging, interpolated values are modelled by a Gaussian process governed by prior covariance and it is used to forecast geographic area. This method of interpolation was considered for this study to gain a general overview of how vegetation leaf moisture content is distributed across the entire catchment since sampled points are not spread throughout the study area. Kriging is expressed by equation (3)

$$\hat{Z}(s_0) = \Sigma_{i=1}^{N} \lambda_i Z(s_i) \quad (3)$$

Where $Z(s)$ = the measured value at the ith location, λ = an unknown weight for the measured value at the ith location, s = prediction location and N = the number of measured values.

3.3.1.2 Stepwise regression

Field data were randomly split into training and validation data sets. 60% ($n = 49$) was used to construct a stepwise multiple regression for vegetation leaf water content, and 40% ($n = 33$) was used to validate the models. This study had three data sets and stepwise regression was repeated for each of them. The calibration of models was first done for (i) narrowband, then (ii) broadband, and finally (iii) combined vegetation indices using 60% of field data. Stepwise regression was done using R software (version 3.0.2), (R development Core Team 2014) packages 'rgdal' (Michael, 2015; Bivand et al., 2015). The best model was selected automatically using 'both directions' stepwise regression with the 'step lm' in R which selects the higher coefficient of determination (R^2) and lower RMSE. The estimates (coefficients) of the best model from stepwise regression were used to compute a multiple linear regression using a raster calculator in QGIS and the map showing vegetation leaf moisture content was created in QGIS. Multiple linear regression was computed using equation (4)

$$y = \beta_0 + \beta_1 X_1 + \cdots B_n X_n + \varepsilon \quad (4)$$

Where y = the predicted value of the dependent variable, β_0 = the y-intercept, $\beta_1 X_1$ = the regression coefficient (β_1) of the first independent variable (X_1) and ε is a random error component.

3.3.2 Model validation

Validation data set that accounted for 40% ($n = 39$) of field data was used to validate the models. The three calibrated models were validated by predicting the outcome of the validation data set using remotely sensed data and compare with the observed data. The Root Mean Squared Error (RMSE) and Mean Absolute Error (MAE) were used as indicators of model validity using formulas that follow:

$$RMSE = \sqrt{\frac{\Sigma_{t=1}^{T}(x_t - y_t)^2}{T}} \quad (5)$$

$$MAE = \frac{\Sigma_{i=1}^{n}|y_i - x_i|}{n} \quad (6)$$

Where y_t is the observed leaf water content, x_t is the predicted leaf water content, x_i is values at each sampled point, m(X) is the average value of the data set and n is the number of samples.

3.4 Results

Table 3.3 Leaf moisture content of dominant species

Species	Leaf moisture content (g/cm^2)			
	Min	**Max**	**Mean**	**Range**
Ficus sur	0.33	0.38	0.36	0.05
Combretum erythrophyll	0.11	0.31	0.20	0.20
Albizia adianthipholia	0.11	0.51	0.36	0.40
Acacia mellifera	0.11	1.00	0.41	0.89
Celtis Africana	0.11	0.42	0.28	0.31
Acacia siberiana	0.00	0.38	0.22	0.38
Bridellia micrantha	0.18	0.31	0.22	0.18
Acacia tortilis	0.13	0.33	0.25	0.20
Schlerocrya birea	0.13	1.00	0.47	0.87
Dichrostackys cinerea	0.13	0.45	0.20	0.32
Combretum molle	0.11	0.40	0.27	0.29
Ficus sycamore	0.31	0.41	0.37	0.10
Terminalla sericea	0.27	0.50	0.35	0.23
Other	0.11	1.00	0.41	0.89

n = 82

This study used 28 optical vegetation indices based on Sentinel-2 data. Indices were separated into three categories (narrowband, broadband, and combined indices), and stepwise regression was repeated in R studio software for each one of them using common training data set. In both three sets of data, indices that were not fit for the model of vegetation leaf water content were eliminated. Table 4 shows the results that were obtained from stepwise regression. Stepwise multiple linear regression model was constructed using equation (3) for the data set containing both narrow and broadband indices (RedEdgeNDVI2, RedEdgeNDVI3, NMDI1, Red_Model, NDII3, SWIR3, NDWI2 and NDWI3, SR1, SR2, SR3). The coefficients from these respective indices were used to map vegetation leaf moisture content across the catchment.

Table 3.4 Results of stepwise regression

	Source	Estimate	Std. Error	T value	Pr(>|t|)
Narrowband indices	Intercept	-0.8551	0.4858	-1.760	0.091141
	RedEdgeNDVI2	-3.1610	1.1172	-2.829	0.009274 **
	NDRE1	6.1678	2.0012	3.082	0.005102**
	RedEdgeNDVI3	6.35113	1.6133	3.937	0.000618***
	Red_Model	-1.9441	0.4758	-4.086	0.000424***
	SR3	-1.1855	0.3338	-3.551	0.001623**
	SR4	1.2479	0.3618	3.449	0.002089**
	RedEdgeNDVI1	1.0029	0.3206	3.129	0.004561**
Broadband indices	Intercept	6.677e+01	4.320e+01	1.546	0.138
	NDVI	-1.925e+00	1.807e+00	-1.066	0.299
	NDII1	-8.305e+00	2.614e+01	-0.318	0.754
	NDII3	2.271e+00	2.370e+00	0.958	0.349
	NDWI1	-7.408e+01	5.902e+01	-1.255	0.244
	NDWI3	2.696e+00	2.362e+00	1.141	0.267
	MSI1	-3.230e+02	1.929e+02	-1.675	0.110
	MSI2	3.110e-01	6.476e-01	0.048	0.636
	NMDI1	3.250e-02	6.249e-01	0.052	0.959
	NMDI2	-1.198e-01	2.130e-01	-0.562	0.580
	RVIgreen	-7.724e-04	1.029e-01	-0.008	0.994
	GNDVI	-6.924e-02	7.738e-01	-0.089	0.930
Combined indices	Intercept	2.7444	0.09072	3.025	0.00668 **
	RedEdgeNDVI2	1.4813	0.6307	2.349	0.02923 *
	RedEdgeNDVI3	2.4481	1.1943	2.050	0.05372
	NMDI1	-1.2311	0.4320	-2.850	0.00990 **
	Red_Model	0.6272	0.2293	2.736	0.01274 *
	NDII3	-2.8276	1.1217	-2.521	0.02031 *
	NDWI2	-0.5639	0.2022	-2.789	0.01134 *
	NDWI3	0.7844	0.6039	1.299	0.20873
	SWIR3	-0.9407	0.3263	-2.883	0.00920 **
	SR1	-0.6774	0.3530	-1.919	0.06940
	SR2	0.4637	0.2627	1.765	0.09283
	SR3	-1.3854	0.6198	-2.235	0.03698 *

Note: ***Model significant at the probability level 0.001 ($p < 0.001$); **Model significant at the 0.01 probability level ($p < 0.01$); * Model significant at the 0.05 probability level ($p < 0.05$).

3.4.1 Vegetation leaf water content estimation

Figures 3.2 – 3.4 show the results of natural vegetation leaf moisture content models which were constructed based on Sentinel-2 data. These models randomly selected 49 training points to train the model and used 33 as verification points, and the narrowband model produced an accuracy of $R^2 = 0.48$, RMSE = 0.097 g/cm^2, MAE = 0.080%, broadband model produced an accuracy of $R^2 = 0.25$, RMSE = 0.097 g/cm^2, MAE = 0.075%, and the model containing both narrowband and broadband produced an accuracy of $R^2 = 0.54$, RMSE = 0.085 g/cm^2, MAE = 0.065%. Based on these results, the study has selected the model with both narrowband and broadband indices to estimate vegetation leaf water content across the study area.

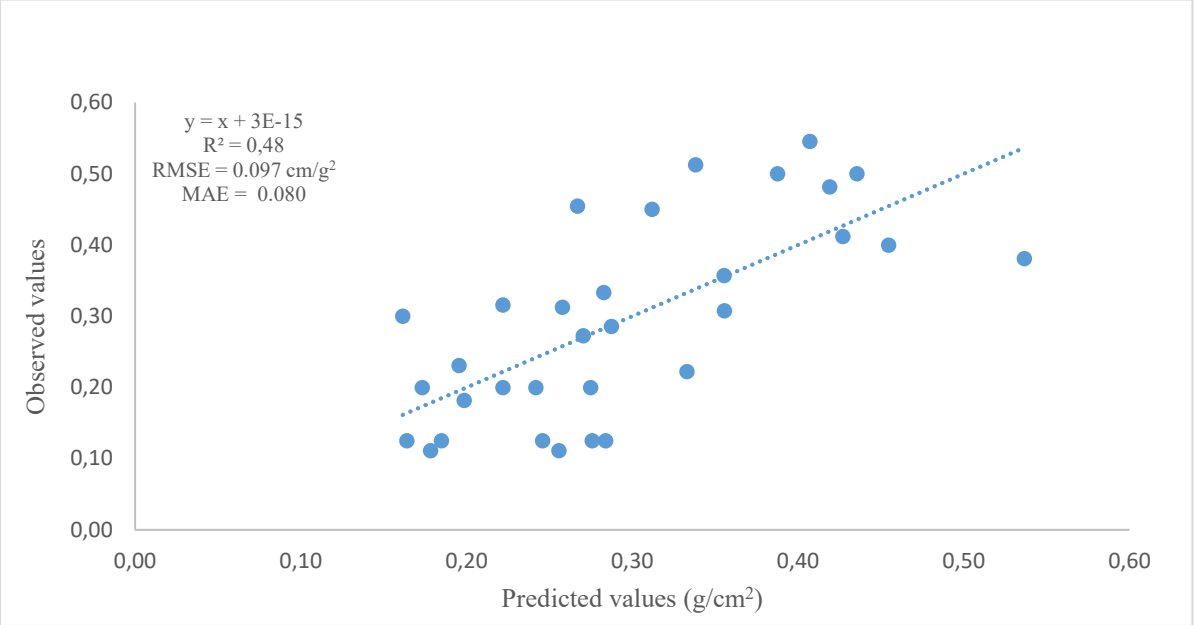

Figure 3.2 Red edge derived indices regression model for natural vegetation leaf water content estimation containing 7 different vegetation indices and 32 sample points for verification.

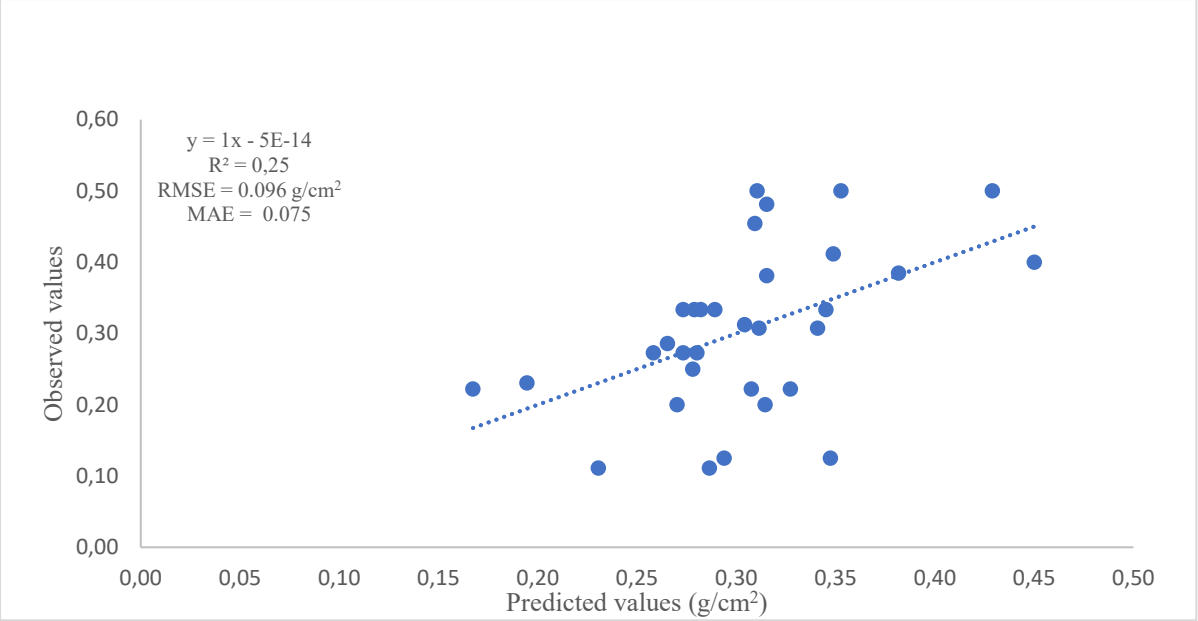

Figure 3.3. Moisture related indices regression model for natural vegetation leaf water content estimation containing 11 different vegetation indices and 32 sample points for verification.

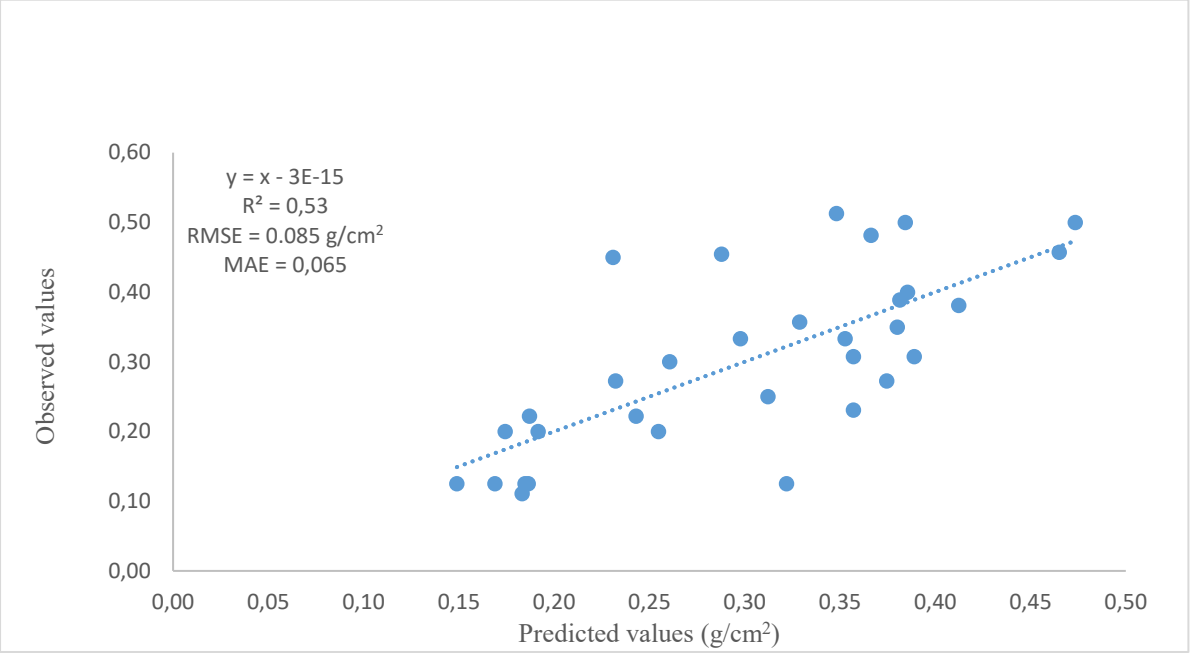

Figure 3.4 Combined indices regression model for natural vegetation leaf water content estimation containing 11 different vegetation indices and 32 sample points for verification.

3.4.2 Mapping the vegetation moisture content using selected vegetation indices and data from Sentinel-2 imagery

For this study, ordinary Kriging was used to create an interpolation map of vegetation leaf water content in the study area. Kriging is a geostatistical interpolation with multistep technique that considers both the distance and the degree of variation between known points when estimating the unknown points (Paramasivam and Venkatramanan, 2019). In Kriging, interpolated values are modelled by a Gaussian process that is governed by prior covariance and it is used to forecast geographic area. This method of interpolation was considered for this study to gain a general overview of how vegetation leaf moisture content is distributed across the entire catchment and compare the results obtained from the models for accuracy since sampled points are not spread throughout the study area.

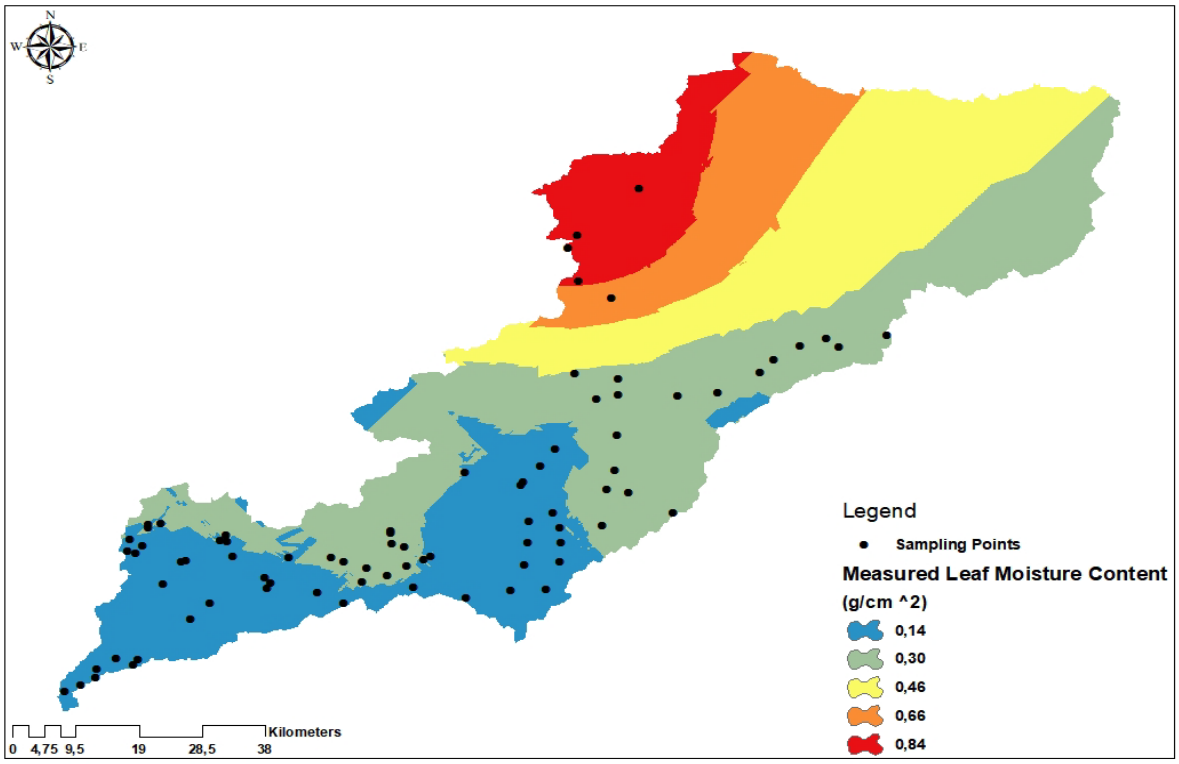

Figure 3.5 Interpolation map of sampling points

This study used sentinel-2 imagery and 11 vegetation indices for estimating vegetation water content to produce thematic maps which show how vegetation moisture is distributed across LRC. Sentinel-2 imagery was available for the entire catchment; however, vegetation indices are only used to estimate vegetation water content for area covered with natural vegetation. Vegetation moisture varies across the study area as estimated on thematic map below. Areas dominated with needle leaves vegetation and where vegetation is very sparsely distributed also shows low resemblance of vegetation moisture content across the study areas. Also, areas with high rainfall such as areas found along the mountain

range, riparian vegetation, and vegetation in, and nearby wetlands tend to have higher moisture content as most of the vegetation indices-based maps are showing. Remote estimations of vegetation water content are relatively consistent with traditional field data results.

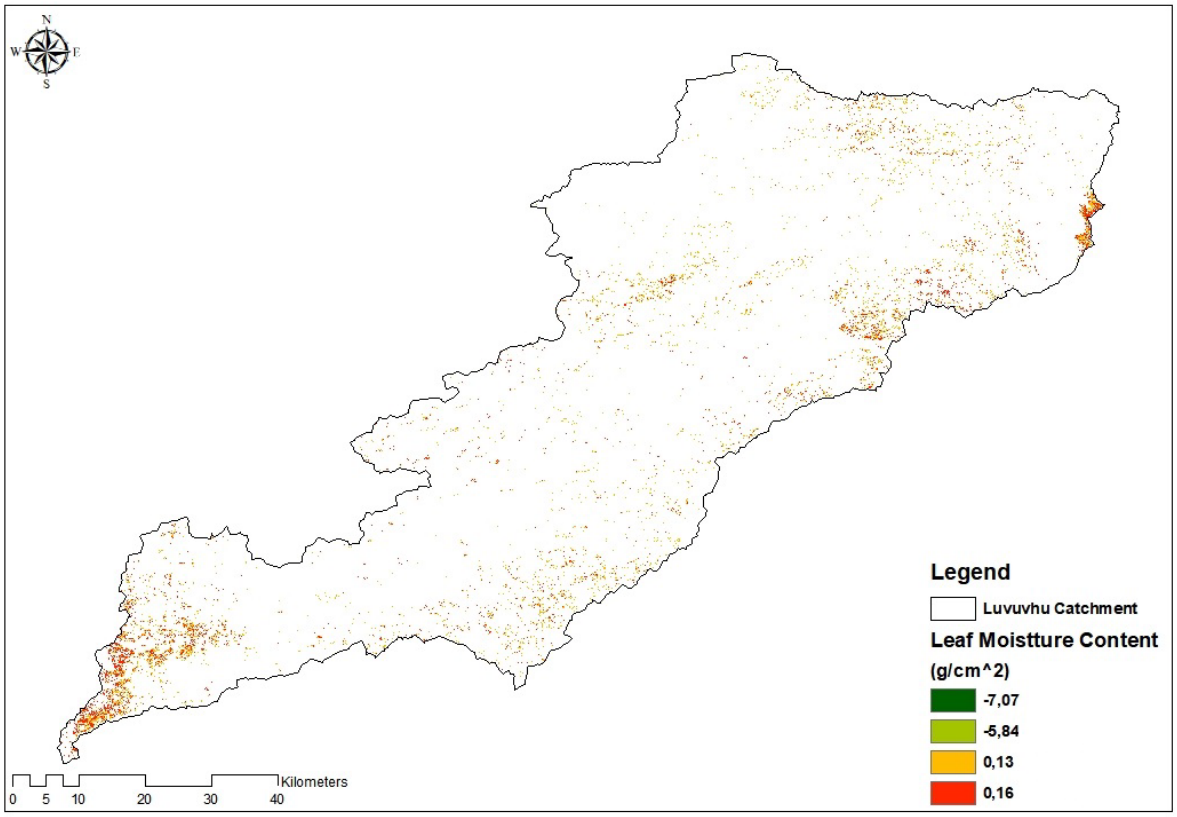

Figure 3.6 Vegetation moisture content distribution map in the study area based on Sentinel-2 data and 12 indices.

3.5 Discussion

The aim of this study was to estimate natural vegetation leaf moisture content from Sentinel-2 data using regression models and various vegetation indices. This study also compared the performance of red-edge band spectral indices vs moisture based spectral indices in estimating leaf water content of natural vegetation. At the end, leaf water content was mapped through the best model. The study tested three groups of vegetation indices (red edge-based indices, moisture related indices, and combined indices) for vegetation leaf water content through stepwise regression in R, vegetation indices that were not fit for the model were eliminated in both models and the final model of combined indices was made of 11 vegetation indices of which their coefficients were used to produce thematic maps showing distribution of vegetation moisture content in the study area. The verification accuracy of the red edge-

based indices model produced an accuracy of R^2 = 0.48, RMSE = 0.097 g/cm^2, MAE = 0.080%, moisture related indices model produced an accuracy of R^2 = 0.25, RMSE = 0.097 g/cm^2, MAE = 0.075%, and the model containing both red edge-based and moisture related produced an accuracy of R^2 = 0.54, RMSE = 0.085g/cm^2, MAE = 0.065%.

The findings of study showed that bands such as the red edge, NIR, and SWIR of the Sentinel-2 satellite are extremely sensitive to the leaf water content, this suggested that vegetation water content indices can be well-established using Sentinel-2 data. However, Zhang and Zhou (2015) indicated that vegetation indices are likely to detect other vegetation parameters and somehow exclude spectral water information, and in turn, there are vegetation indices which are only sensitive to spectral water information and exclude other vegetation parameters. To sustain the level suitable for vegetation basic functions, leaf water content per unit leaf area mostly fluctuates in response to severe water stress, at the same time, remote estimation of vegetation leaf water content is influenced by leaf structure and dry mass (Cecato et al., 2001).

There is a vast variation in vegetation water content across the catchment which is influenced by a number of factors including plant species, growing conditions, phenological stages and climatic variation (Gao et al., 2015). Natural vegetation across the study area also varies greatly ranging from dense forest along the mountains, needle-leaved plants as well as broadleaved vegetation, all these plants have different leaf surface area depending on their respective species. The types of leaves and the nature of ecosystems where these plants are found also determine the level of moisture content, for example *Ficus sycamore* have broadleaves and are common where there are wetlands, this has a great influence in the vegetation leaf moisture content of this particular plant species. Physiological indicators that are commonly used to assess plant water conditions mainly include stomatal conductance (Zhou et al., 2007), leaf water potential (Dzikiti et al., 2010), canopy water content (CWC) (Cecato et al., 2002), leaf equivalent water thickness (EWT) (Ustin et al., 1998), live fuel moisture content (LFMC) (Wang et al., 2013), and relative water content (RWC) (Hirano and Maki, 2018).

Vegetation water stress has been assessed using leaf water status and CWC as an indicator (Dzikiti et al., 2010) and is determined not only by vegetation water status or CWC but can also be observed on plant's growth and development stages (Cecato et al., 2002). Signs that can be observed to reveal that plants are responding to low moisture content include opening of plant canopy, curling, de-colouring, as well as shrinking of leaves (Niijland et al., 2014). When a plant is undergoing the water stress phase, it can use photo-protection strategies to avoid malfunctioning such as decrease of the photosynthetic potential of the plant (Lichtenthaler, 1996). Should the water stress conditions persist, the plant's green pigment (chlorophyll) decreases which affects the leaf absorbance and reflectance. A wide-scale mapping of leaf water content of natural vegetation is crucial for monitoring vegetation health and environmental flows such as evapotranspiration.

Vegetation indices-based thematic map that was established using (RedEdgeNDVI2, RedEdgeNDVI3, NMDI1, Red_Model, NDII3, SWIR3, NDWI2 and NDWI3, SR1, SR2, SR3) shows the distribution of natural vegetation moisture content in the study area. Thematic maps show that the study area only has small proportion wherein there is relatively high vegetation moisture content whereas the larger proportion of the study area shows lower vegetation moisture content. The south-eastern part of the catchment receives relatively high rainfall, which is influenced by the mountain range, and is responsible for healthier vegetation with higher vegetation moisture content compared to other areas that recorded lower amounts. The north-eastern part of the catchment also recorded significant vegetation water content; these are the areas that are not dominated by human settlement.

3.6 Conclusion

This study explored the feasibility of using Sentinel-2 imagery and different spectral indices from both narrow and broadband that are directly and indirectly sensitive to vegetation moisture content to estimate vegetation leaf water content of natural vegetation across the LRC. The study tested three groups of vegetation indices (red edge-based indices, moisture related indices, and combined indices) for vegetation leaf water content through stepwise regression in R, vegetation indices that were not fit for the model were eliminated in both models and the final model of combined indices was made of 11 vegetation indices of which their coefficients were used to produce thematic maps showing distribution of vegetation moisture content in the study area. The verification accuracy of the red edge-based indices model produced an accuracy of R^2 = 0.48, RMSE = 0.097 g/cm^2, MAE = 0.080%, moisture related indices model produced an accuracy of R^2 = 0.25, RMSE = 0.097 g/cm^2, MAE = 0.075%, and the model containing both red edge-based and moisture related produced an accuracy of R^2 = 0.54, RMSE = 0.085g/cm^2, MAE = 0.065%. This paper established that vegetation moisture content varies vastly across the study area, this is also influenced by the diversity of vegetation species that are dominant within that area. Based on the results of this study, it is also concluded that data obtained from the Sentinel-2 satellite can be used efficiently with the right vegetation water content indices to estimate vegetation leaf water content at a large scale. This is crucial to monitor drought, water stress and vegetation health in general. However, vegetation water content on its own, cannot be used to determine vegetation health, other factors that can be assessed to include chlorophyll, leaf area index (LAI) as well as nutrients such as nitrogen.

CHAPTER FOUR: MAPPING PLANT NITROGEN CONCENTRATION WITHIN LUVUVHU CATCHMENT AREA USING SENTINEL-2 IMAGERY

Abstract

Plant nitrogen estimation using real-time and non-convection methods is very crucial for ecosystem management. This study aimed at estimating plant N concentration of indigenous vegetation in Luvuvhu River Catchment (LRC) using both fields and remotely sensed data from Sentinel-2 imagery. The study used three different categories of spectral indices to fulfil its objectives. Red edge-based, nitrogen related, and combined spectral indices based on Sentinel-2 data were subjected to stepwise regression on R studio software to determine which category of spectral indices is more efficient in estimating plant nitrogen concentration. Results have shown that combined spectral indices performed better with R^2 = 0,59, RMSE = 0,47% and MAE = 0,38%, followed by nitrogen related spectral indices with R^2 = 0,44, RMSE = 0.65% and MAE = 0,48%, and the last category is red edge-based spectral indices with R^2 = 0,35, RMSE = 0.81% and MAE = 0,65%. The coefficients of the best performing model obtained from stepwise regression were used to compute multiple linear regression on QGIS to produce a map showing the concentration of plant nitrogen across the study area. Plant N varies with plant species and, the thematic map created show how plant N varies across the study area. The combined spectral indices for plant nitrogen concentration and mapping have proved to be efficient compared to narrowband and broadband indices alone in this study.

Keywords: Nitrogen, Sentinel-2, Spectral indices, broadband, narrowband

4.1. Introduction

Nitrogen (N) is a main regulator of several leaf physiological processes, such as photosynthesis, respiration, and transpiration (Reich et al., 2006), and it correlates well with chlorophyll (Chl)content, light use efficiency (LUT), and net primary production (Jiang et al., 2021). N is the principal component which restrains productivity of various terrestrial ecosystems (Richards et al., 2012). This is influenced by the fact that N is a well-known resource that limits plants' productivity and growth (Ustin, 2013). Spatial patterns of N at leaf level help us to understand the part that terrestrial ecosystems play in the larger Earth system since they are connected to fluctuations of carbon, water, and energy (Ollinger et al., 2008). Canopy N is also associated with the capacity of vegetation to hold atmospheric N deposition (Lindsay et al., 2012), which has increased together with atmospheric carbon dioxide (CO_2) over the years as a result of increased use of fossil fuel and production of artificial fertilizer using harmful chemicals (Galloway et al., 2008).

As the main nutrient that limits plants' growth, plant N availability, the way it fluctuates in ecosystems, and how it responds to global change will have long term significant impacts on C sequestration in various ecosystems (Luo et al., 2004). Photosynthetic C fixation and plant productivity are highly determined by leaf N concentration (Hungate et al., 2003). Several studies, mainly those that are carried out in greenhouses and chambers, have indicated that high temperatures can result in increased or reduced concentration of leaf N of trees (Hobbie et al., 2001; Luomala et al., 2003) and grasses in arctic or alpine tundra (Grogan & Chapin, 2000). Leaf N concentration of different plant function groups responds differently to increased temperatures even when they are within the same ecosystem (Arft et al., 1999). For instance, a study by Read and Morgan (1996) concluded that concentration of leaf N dropped in *Bouteloua fracilis* (C4 grass) but increased in *Pascopyrum smithii* (C3 grass) when temperature was increased. The way different plant functional groups respond to rising temperatures can lead to changes in community structure of plants, and plant N uptake (Lilley et al., 2001). Therefore, it is crucial to understand how plant N responds to heat stress so that we can predict ecosystem C and N cycling in future climatic scenarios (Lindsay et al., 2012). The distribution of plant N varies across the landscape due to many variables.

Plant N concentration among plants found in natural ecosystems differs by over 32% (Hobbie et al., 2005) and this varies with topographic gradients and cycling of nutrients, among species (Craine et al., 2009), and in response to manipulations of resource obtainability for experimental purposes (Amundson et al., 2003). Plant N may also be affected by other factors such as land-use history, changes in CO2 concentration, acid deposition, and limitation of another nutrient element supply (Goodale and Aber, 2001; Hallett and Hornbeck, 1997). Overall, leaf N can be used as a measure to generalize patterns of N cycling, globally (Lindsay et al., 2012) as well as a vital indicator to assess changes in N cycling that

might accompany anthropogenic influence on ecosystems such as rising atmospheric CO_2 (Hurber et al., 2011). Estimations of N at leaf level and canopy nitrogen concentration of vegetation allow for a better understanding of ecosystem functioning and biochemical processes (Lee and Nguyeni, 2005).

Traditionally, chemical analysis has been used to obtain canopy and foliar N (Serrano et al., 2002). This approach is accurate, but destructive, time-consuming, and costly (Sáez-Plaza et al., 2013). Thus, make it impractical to measure canopy and leaf N for a large area of forests consisting of different vegetation types using the chemical analysis method. To our advantage, remote sensing has turned things around, such assessments and assessments can be carried out a low cost, and within a very short space of time across large spatial scales (Walshe et al., 2020). Remote sensing has been used for various applications in vegetation monitoring such as land cover change detection, species classification, land cover estimation, and defoliation (Walshe et al., 2020). Leaf nitrogen has been determined in forests (Singh et al., 2015), grassland and crop ecosystems using remote sensing techniques over the years (Yao et al., 2015).

Airborne and spaceborne serve as exceptional tools for temporal and spatial monitoring of leaf nitrogen since they provide continuous information in manifold spectral and directional settings (Ustin et al., 2004; Cohen and Goward, 2004). A growing number of hyperspectral imagery reports have been exceptional when it comes to leaf and canopy N prediction for various plants community (Wang and Wei, 2016). However, hyperspectral data are often affected by high dimensionality and are relatively costly to acquire. On the other hand, multispectral data such as Sentinel-2 and field spectroscopy can be used primary data sources since they are relatively cheaper and easily accessible (Chemura et al., 2018). Research on multiple layer radiative transfer models (MRTM) have shown that the vertical differences in leaf characteristics have a significant influence on canopy reflectance and affect retrieval of canopy traits especially on canopies that have lower leaf cover (Luo et al, 2013). Remote sensing of plant N beyond the leaf scale has been the derivation of presentative samples from a heterogeneous canopy (He and Mui, 2010). Leaf trait contents are distributed differently across vegetation canopies along vertical canopy profile of different species which makes it complex to estimate them (Tawanda et al., 2018). Other factors such canopy structure, mask of the strong water absorption (Dash and Curran, 2004), viewing geometry and background make it a challenge to retrieve N at the canopy level (Grogan & Chapin, 2000). Plants mostly show higher nutrient content in the upper canopy and on leaves that are receiving direct or increased solar radiation (Weerasinghe et al., 2014). Spectral alteration such as using first/second derivatives and log transformation of reflectance, water removal, continuum removal, and wavelet analysis are approaches that are used to enhanced N retrieval (Zhao et al., 2013).

Retrieval of many vegetation parameters such as plant N, leaf Chl, and others are dominated by empirical techniques such as spectral indices (Gitelson et al., 2003), traditional regression techniques such as stepwise multiple linear regression and partial least square regression, to a number of machine

learning approaches such as support vector regression (SVM), neural network and many more (Zhao et al., 2013). Spectral indices are one of the simplest and frequently utilized methods to estimate leaf biochemical contents such as N, Chl and vegetation leaf water content (Gitelson et al., 2003; Wang et al., 2018). N in leaf cells mostly occurs in proteins and chlorophylls (Kokaly et al., 2009). Plant N and Chl correlate well across various plant species (Homolova et al., 2013), therefore, spectral indices formulated for Chl have been employed as a means of N estimation (Le Maire et al., 2008). This study aimed to map plant N concentration using different categories of spectral indices and stepwise multiple linear regression in the Luvuvhu River Catchment.

4.2. Materials and methods

4.2.1 Description of the study area

The Luvuvhu River Catchment is located in the northeastern region of Limpopo province, South Africa as shown in 4.1. The catchment is situated between the latitudes 22^0 17' 33'' S and 23^0 17' 57'' S and longitudes 29^0 49' 46'' E and 31^0 23' 32'' E. The Luvuvhu Catchment Area covers an area of approximately 331 602, 447 hectares with an elevation in the catchment ranging between 200 to 1,700 m resulting in shallow storage dams that are exposed to excess evaporation due to large water surfaces (Odiyo et al., 2012). The catchment is also characterized by topographic features such as the Soutpansberg mountain range in the eastern side of the catchment. This topographic feature rises to a height of approximately 1 700 m above mean sea level prior to reaching the low-lying surface of the Limpopo River Valley (Kundu et al., 2013). The landscape in other parts of the catchment has a mean ridge height of about 800 - 1 200 m while some places within the catchment whereas other parts of the catchment reach a peak above 1 500 m (Singo et al., 2021; Kundu et al., 2013).

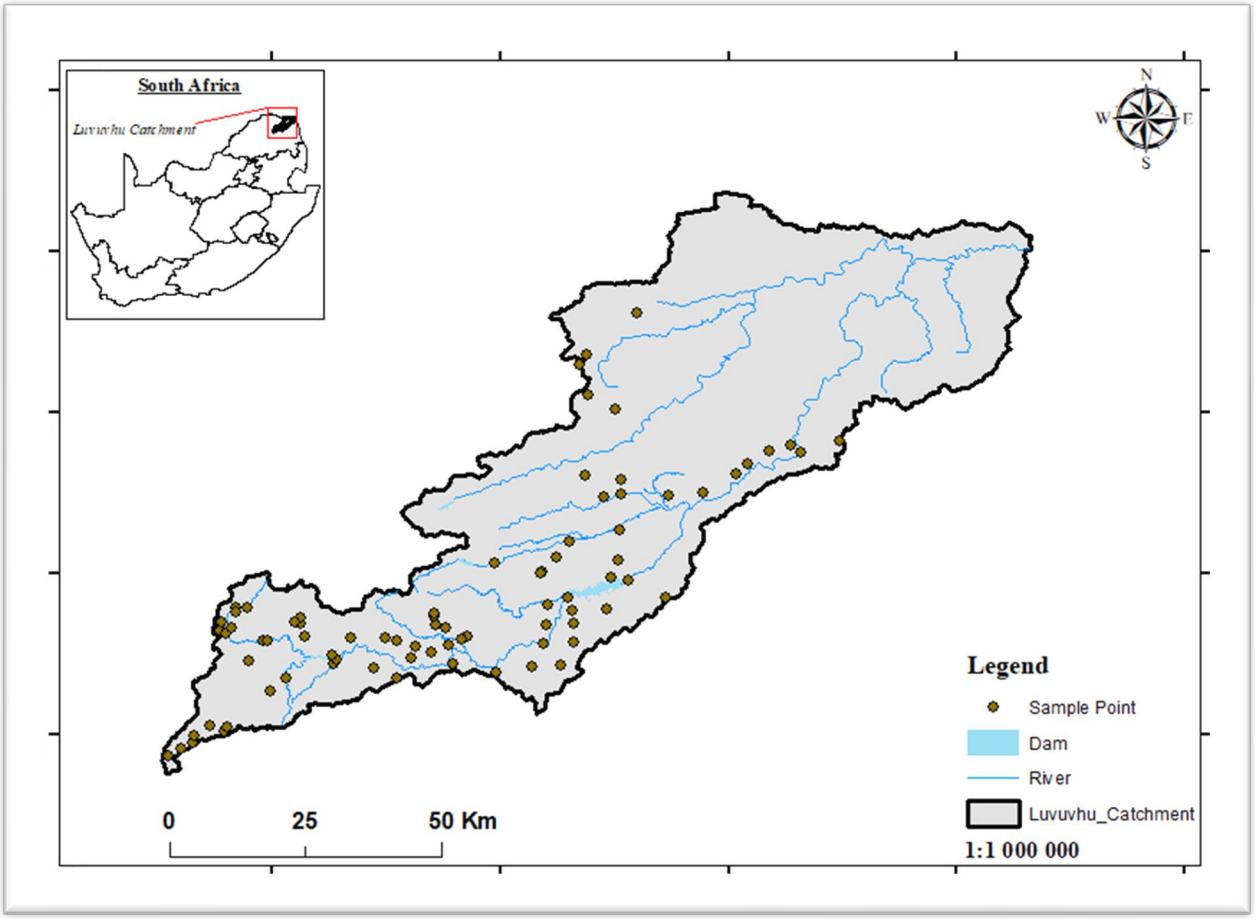

Figure 4.1 Map showing the study area

Precipitation in some parts of the catchment is influenced by orographic uplift due to east-west orientation of Soutpansberg mountain range where the western movement of moisture from the Indian Ocean results into 1 200 mm to 1 500 mm/year in the forested mountain headwaters (Shongwe, 2007). Semi-arid forest and bushland receive only receive 200 mm to 600 mm/year as the terrain drops across the study area. Extreme topographic diversity and altitude changes over short distances within the Soutpansberg result in dramatic climatic variance within the LRC (Volenzo and Odiyo, 2018). Luvuvhu River Catchment is characterized by subtropical climate with distinct wet during November to March, and little rainfall from April to October during winter with little precipitation. High temperatures in the study area influence the gradual increase in evaporation rates ranging between 1 400 mm and 1 900 mm/year (Nethononda, 2018).

4.2.2 Field data collection

Fieldwork was conducted from the 2nd of December 2021 to the 11th of December 2021 using simple random sampling. The study region had both broadleaf and needle leaf plant species and their distribution varied across the study area. To incorporate various plant species and canopy structures, dominating species within the sampled point was the one considered for this study. However, other plant species around the sampled points were also taken into consideration to supplement plant data collected. A total of 85 sampling points was generated and spread out within the study area with at least 2 km between the points to minimize pixel overlapping on satellite imagery. Data were randomly split into 60% training ($n = 49$) and 40% validation ($n = 33$) data sets. This reasonable discrepancy between the output values and the validation set will improve the credibility of the model while a large discrepancy may invalidate the model. Standard Garmin eTrex 10 Handheld GPS with the maximum spatial accuracy of approximately of 3 meters was used to record coordinates at the center of each plot. At each sampled point, depending on its heterogeneity, one dominating overstory plant species was selected for sampling. Each sample was composed of five leaflets taken from the sunlit branches of an individual trees. Wet weight of the leaves was measured in the field using Digital Portable Kitchen Scale of accuracy of approximately 0.1g. Leaf samples were then stored in coded brown paper bags which were folded to avoid leaves drying out. Wet leaf samples were placed in the oven for 24 hours. After 24 hours when the leaves have dried out, dry weight of the leaves was measured to obtain dry mass of the leaves. The oven dried samples of leaf N content (expressed in percentage) were sent to the laboratory for nitrogen analysis.

4.2.3 Image acquisition and pre-processing

Satellite images from Sentinel-2 were downloaded from (https://scihub.copernicus.eu/) between 02nd December and 09th December 2021 for image classification. In 2015 and 2017, a pair of Sentinel-2 satellites was launched. The launch of Sentinel-2A in 2015 and Sentinel-2B in 2017 has improved the remote monitoring of land surfaces and assessment of vegetation variables (Gitelson et al., 2014). Sentinel-2 provides data at an unprecedented spatial and temporal resolution (Frampton et al., 2013). Both Sentinel-2A and Sentinel-2B satellites have Multi- Spectral Imager (MSI) with a swath width of 290 km and offers remotely sensed data in 13 spectral bands from the visible and near infrared region to the shortwave infrared region, of which four bands are at 10 m, six bands at 20 m and the remaining three bands at 60 m spatial resolution (Xie et al., 2019; Richter et al., 2019).

Table 4.1 List of sentinel-2 bands (Herman et al., 2018)

Band	Description	Wavelength (µ/m)	Resolution (m)
B1	Coastal aerosol	0.443	60
B2	Blue	0.490	10
B3	Green	0.560	10
B4	Red	0.665	10
B5	Vegetation Red Edge	0.705	20
B6	Vegetation Red Edge	0.740	20
B7	Vegetation Red Edge	0.783	20
B8	NIR (near infrared)	0.842	10
B8A	Narrow NIR	0.865	20
B9	SIWR (shortwave infrared)	0.945	60
B10	SIWR (shortwave infrared) – cirrus	1.375	60
B11	SIWR	1.610	20
B12	SIWR	2.190	20

4.3 Derivation of spectral variables

The first activity with regard to the mapping of plant N across the study areas was to resample Sentinel-2 image strips to 30 m spatial resolution, then mosaic them to a single image. The regression model from stepwise regression was used to compute multiple linear regression (equation) using raster calculator on QGIS which was then applied to the masked image and resulted in the map showing plant N concentration across Luvuvhu River Catchment. This study used 27 vegetation indices that were listed in the literature (Baret, 2016; Kemenova et al., 2017). Selected optical indices based of Sentinel-2 sensor are developed from visible NIR, and red-edge part of the spectrum. Study also explored chlorophyll-related spectral indices that use the red-edge part of the spectrum, and since chlorophyll serves as a proxy to nitrogen, such spectral indices can be explored for indirect nitrogen estimation in

the forest, which has yielded good results in many ecosystems such as grassland and for agricultural crops (Clevers and Gitelson, 2013). Vegetation indices were calculated using formulas on Table 4.2.

Table 4.2 Summary of selected optical narrowband spectral indices used in this study based on Sentinel-2.

Vegetation index	Formula	Reference
Simple ratio2 (SR2)	$SR2 = \frac{B07}{B04}$	Jordan, 1969
Simple ratio3 (SR3)	$SR3 = \frac{B07}{B06}$	
Simple ratio4 (SR4)	$SR4 = \frac{B07}{B05}$	
Normalised difference index (NDI)	$NDI = \frac{B05 - B04}{B05 + B04}$	Delegiole et al., 2011
Chlorophyll index green with B07	$Clg7 = \left(\frac{B07}{B05}\right) - 1$	Gitelson, 2006
Chlorophyll index red edge with B07 (Clre7)	$Clre7 = \left(\frac{B07}{B05}\right) - 1$	Gitelson, 2003
MERIS terrestrial chlorophyll index (MTCI)	$MTCI = \frac{B06 - B05}{B05 - B04}$	Dash and Curran et al., 2004
green Normalised difference vegetation index (gNDVI)	$gNDVI1 = \frac{B06 - B03}{B06 + B03}$	Gitelson et al., 1996
Normalised difference red edge (NDRE)	$NDRE = \frac{B06 - B05}{B06 + B05}$	Sims and Gamon, 2002
	$NDRE1 = \frac{B07 - B05}{B07 + B05}$	
Red_Model	$Red\_Model = B08 - B06$	Xue et al., 2004
Enhanced difference red edge vegetation index ($NDVI_{Red\ edge}$)	$NDVI1 = \frac{B08 - B05}{B08 + B05}$	Han et al., 2019

$$NDVI2 = \frac{B08 - B06}{B08 + B06}$$

Table 4.3 Summary of selected optical broadband spectral indices used in this study based on Sentinel-2.

Vegetation index	Formula	Reference
Difference vegetation index (DVI)	$\mathrm{DVI} = \mathrm{B08} - \mathrm{B04}$	Richardson and Wiegard, 1977
Optimised Soil Adjusted Vegetation Index (OSAVI)	$\mathrm{OSAVI} = \frac{(1 + 0{,}16)(\mathrm{B08} - \mathrm{B04})}{\mathrm{B08} + \mathrm{B04} + 0{,}16}$	Rondeaux and Steve, 1996
(GIPVI)	$\mathrm{GIPVI} = \frac{\mathrm{B08}}{\mathrm{B08} + \mathrm{B03}}$	Dimitrov et al., 2019
Normalised difference vegetation index (NDVI)	$\mathrm{NDVI} = \frac{\mathrm{B03} - \mathrm{B08}}{\mathrm{B03} + \mathrm{B08}}$	DeFries et al., 1995
Moisture stress index (MSI)	$\mathrm{MSI1} = \frac{\mathrm{B10}}{\mathrm{B08}}$ $\mathrm{MSI2} = \frac{\mathrm{B11}}{\mathrm{B08}}$ $\mathrm{MSI3} = \frac{\mathrm{B12}}{\mathrm{B08}}$	Meng et al., 2016
Ratio Vegetation Index (RVI)	$\mathrm{RVI} = \frac{\mathrm{B08}}{\mathrm{B04}}$	Jordan, 1969
Shortwave infrared ratio (SWIR)	$\mathrm{SWIR1} = \frac{\mathrm{B10}}{\mathrm{B11}}$ $\mathrm{SWIR2} = \frac{\mathrm{B10}}{\mathrm{B12}}$ $\mathrm{SWIR3} = \frac{\mathrm{B11}}{\mathrm{B12}}$	Vanhellemont and Ruddick, 2015
Enhanced difference infrared index (NDII)	$\mathrm{NDII1} = \frac{\mathrm{B10} - \mathrm{B04}}{\mathrm{B10} + \mathrm{B04}}$	Wang et al., 2015

$$\text{NDII2} = \frac{\text{B11} - \text{B04}}{\text{B11} + \text{B04}}$$

$$\text{NDII3} = \frac{\text{B12} - \text{B04}}{\text{B12} + \text{B04}}$$

4.3.1 Model calibration

For this study, n = 82 samples were collected from the field and dataset was randomly split into 60% (n = 49) training data and 40% (n = 33) calibration data in R studio software. Training data set was used to train the model for plant nitrogen concentration estimation in R studio software. The study used stepwise multiple linear regression for each data set to determine variables that are significant and insignificant for the final model. Variables that were not significant for the respective models were eliminated, and models remained with variables that were significant.

4.3.2 Model validation

Validation data set (n = 33) was used to assess the validity of the model. Three data sets that were calibrated using stepwise multiple linear regression were validated by comparing observed values and predicted values from the validation data set. The coefficient of determination (R^2), root mean square error (RMSE), and mean absolute error (MAE) were used to describe and compute the relationship between observed and predicted plant nitrogen, and the three metrics can be expressed as follows:

$$\text{RMSE} = \sqrt{\frac{\Sigma_{t=1}^{T}(x_t - y_t)^2}{T}} \quad (5)$$

$$\text{MAE} = \frac{\Sigma_{i=1}^{n}|y_i - x_i|}{n} \quad (6)$$

Where xi and yi are the measured and predicted plant nitrogen, x is the mean of measured plant nitrogen, and n is the total number of samples.

4.4 Results

4.4.1 Plant species from the sampled point

Table 4.4 Sampled indigenous species with important statistical information

Species	Plant nitrogen (%)			
	Min	Max	Mean	Range
Ficus sur	1.19	2.21	1.68	1.02
Combretum erythrophyll	1.45	2.38	1.94	0.93
Albizia adianthipholia	1.8	3.67	2.58	1.87
Acacia mellifera	2.01	3.07	2.55	1.06
Celtis africana	1.3	2.44	1.74	1.14
Acacia siberiana	1.28	3.3	2.49	2.02
Bridellia micrantha	0.8	1.76	1.37	0.96
Acacia tortilis	1.65	3.01	2.17	1.36
Schlerocrya birea	0.8	4.45	1.59	3.65
Dichrostackys cinerea	2.32	4.45	3.28	2.13
Combretum mole	1.09	3.27	2.22	2.18
Ficus sycamore	1.28	2.75	1.75	1.47
Terminalla sericea	1.22	2.79	0.35	1.57
Other	1.07	3.26	2.32	2.19

n = 82

4.4.2 Stepwise regression results

Stepwise regression was repeated for narrowband spectral indices, broadband spectral indices, and combined bands spectral indices where insignificant variables were eliminated from the models. Combined spectral indices have produced higher correlation between observed and predicted values of plant nitrogen with $R^2 = 0,59$, followed by broadband with $R^2 = 0,44$ and the narrowband indices with $R^2 = 0,35$.

Table 4.5 significant variables resulting from stepwise logistic regression analysis

	Source	Estimate	Std. Error	t-value	Pr(>|t|)

Narrowband indices	Intercept	4.840	4.673	1.036	0.311
	SR1	-0.010	1.391	-0.073	0.943
	SR4	-2.489	3.685	-0.675	0.506
	NDRE1	1.466	21.605	0.068	0.946
	NDI	-6.122	30.267	-0.202	0.841
	gNDVI1	5.478	12.586	0.435	0.667
	Red_Model	2.044	6.401	0.319	0.752
	Red EdgeNDVI	5.677	26.300	0.2016	0.831
	gNDVI	-6.502	12.527	-0.519	0.609
Broadband indices	Intercept	2.421e+00	3.036e+00	0.797	0.43241
	OSAVI	-2.032e+05	6.625e+04	-3.067	0.00499 **
	MSI1	-9.921e+02	2.776e+02	-3.574	0.00140 **
	MSI3	6.409e+00	2.896e+00	2.213	0.03588 *
	NDVI	2.357e+05	7.684e+04	3.067	0.00499 **
	NDII3	-8.660e+00	3.849e+00	-2.250	0.03314 *
Combined indices	Intercept	-22.637	10.067	-2.249	0.035962 *
	SR2	-2.411	1.196	-2.016	0.057397
	SR3	17.933	8.790	2.040	0.054749
	NDRE	48.791	25.020	1.950	0.065319
	NDI	39.727	26.055	1.525	0.142992
	Red_Model	-3.499	1.323	-2.646	0.015503 *
	RedEdgeNDVI2	-47.209	22.850	-2.066	0.052022
	MSI2	-6.903	2.749	-2.511	0.020718 *
	SWIR1	361.274	174.804	2.067	0.051951
	SWIR3	20.141	5.029	4.005	0.00695 ***
	NDII2	-61.308	-3.729	4-3.729	0.001324 **
	NDII3	68.576	4.037	4.037	0.000646 ***

Note: *** Model significant at the probability level 0.001 ($p < 0.001$); **Model significant at the 0.01 probability level ($p < 0.01$); * Model significant at the 0.05 probability level ($p < 0.05$).

Results showed that from this model, spectral indices from the rededge were the most insignificant indices with all of them producing results at $p>0.05$. From this model, the most significant spectral indices come from the broadband part of the spectrum with OSAVI, MSI1 and NDVI having $p<0.05$, however, more than 60% of broadband spectral indices have shown negative relationship with regard to plant nitrogen concentration in the study area. OSAVI, MSI1 and NDII3 have showed significant negative relationship with NDVI and MSI3 showing positive relation with regard to plant nitrogen

concentration. About 40% of spectral indices selected from combined spectral indices model have shown to be significant with $p < 0.05$, with SWIR3 and NDII3 being most significant at $p<0.001$ and positive relationship with regard to plant nitrogen concentration.

4.4.3 Performance of vegetation indices in mapping plant nitrogen

Figure shows the results of indigenous plant nitrogen concentration models which were constructed based on Sentinel-2 data. These models randomly selected 49 training points to train the model and used 33 as verification points, and the narrowband model produced an accuracy of $R^2 = 0.35$, RMSE = 0.81%and MAE = 0.65, broadband model produced an accuracy of $R^2 = 0.44$, RMSE = 0.65% and MAE = 0.48, and the model containing both narrowband and broadband produced an accuracy of $R^2 = 0.59$, RMSE = 0.47% and MAE = 0.35%. Based on these results, the study has selected the model with both narrowband and broadband indices to estimate plant nitrogen across the study area.

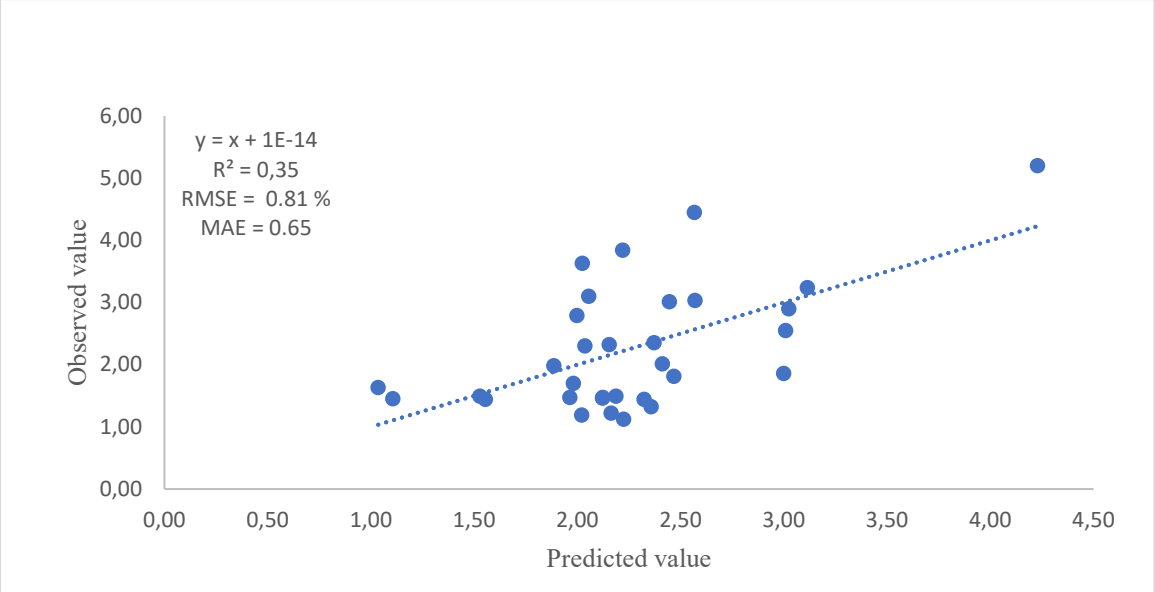

Figure 4.2 Relationship between observed and predicted values of plant nitrogen using selected rededge indices from stepwise regression and 33 validation points

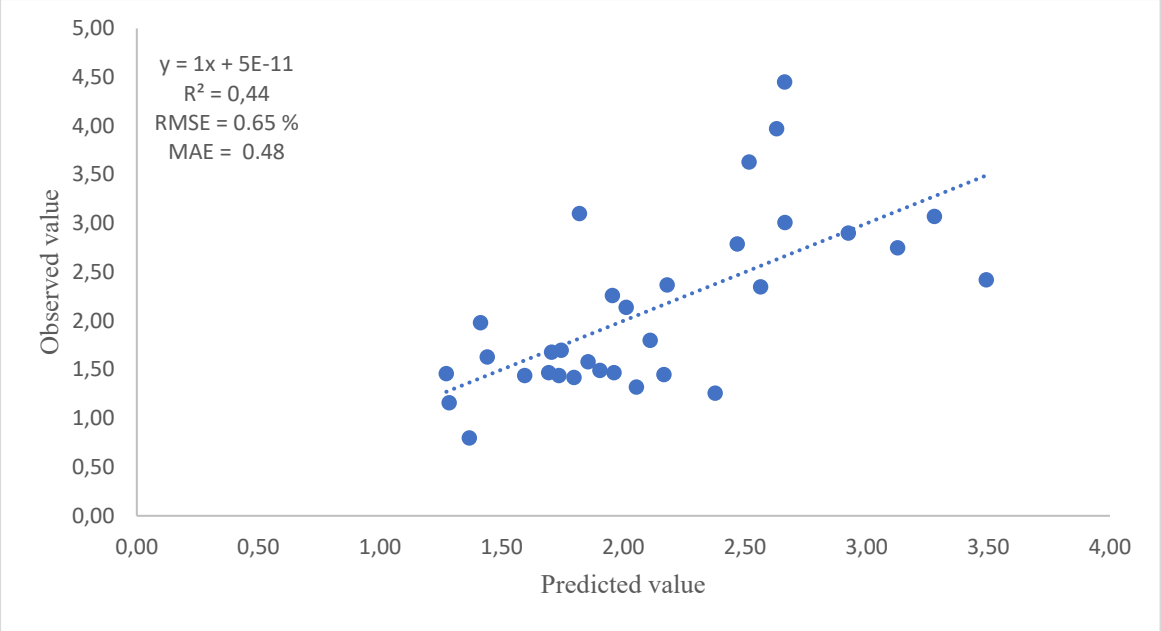

Figure 4.3 Relationship between observed and predicted values of plant nitrogen using selected nitrogen related indices from stepwise regression and 33 validation points

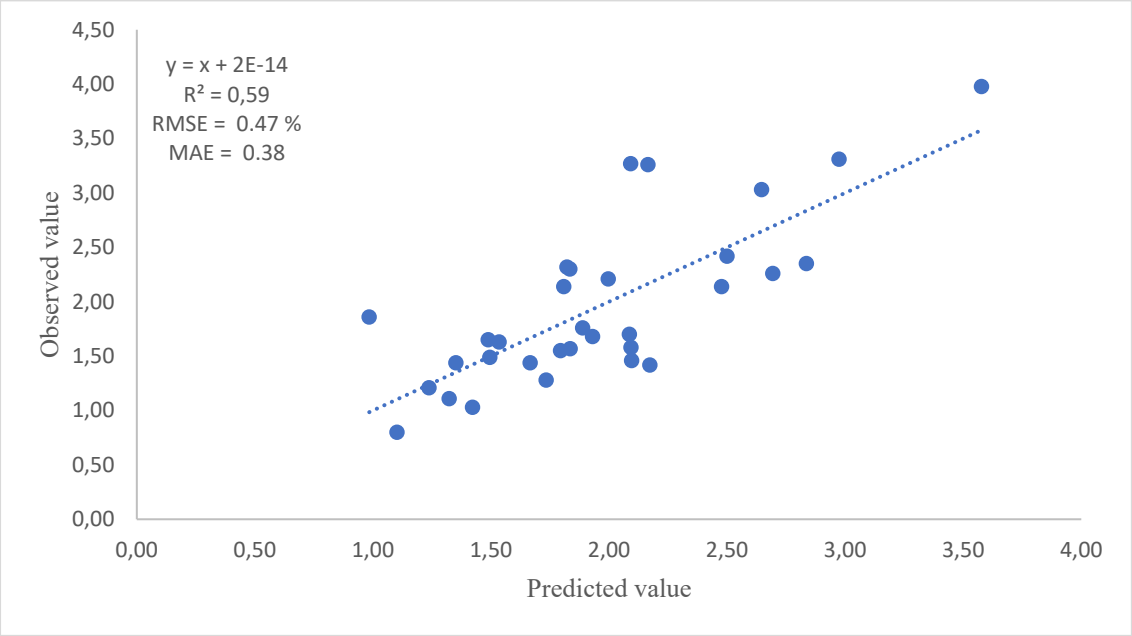

Figure 4.4 Relationship between observed and predicted values of plant nitrogen using selected combined bands indices from stepwise regression and 33 validation points.

4.4.4. Kriging Mapping of plant N in LRC

This study used ordinary Kriging to create the interpolation of plant N in Luvuvhu Catchment Area. Kriging is a geostatistical interpolation with multistep technique that considers both the distance and the degree of variation between known points when estimating the unknown points (Paramasivam and Venkatramanan, 2019). In Kriging, interpolated values are modelled by a Gaussian process governed by prior covariance, and it is used to forecast geographic area. This method of interpolation was considered for this study to gain a general overview of how plant N concentration is like across the entire catchment since sampled points are not spread throughout the study area. Data obtained from the interpolation map helps to improve the accuracy of the study since it gives general overview of plant N concentration.

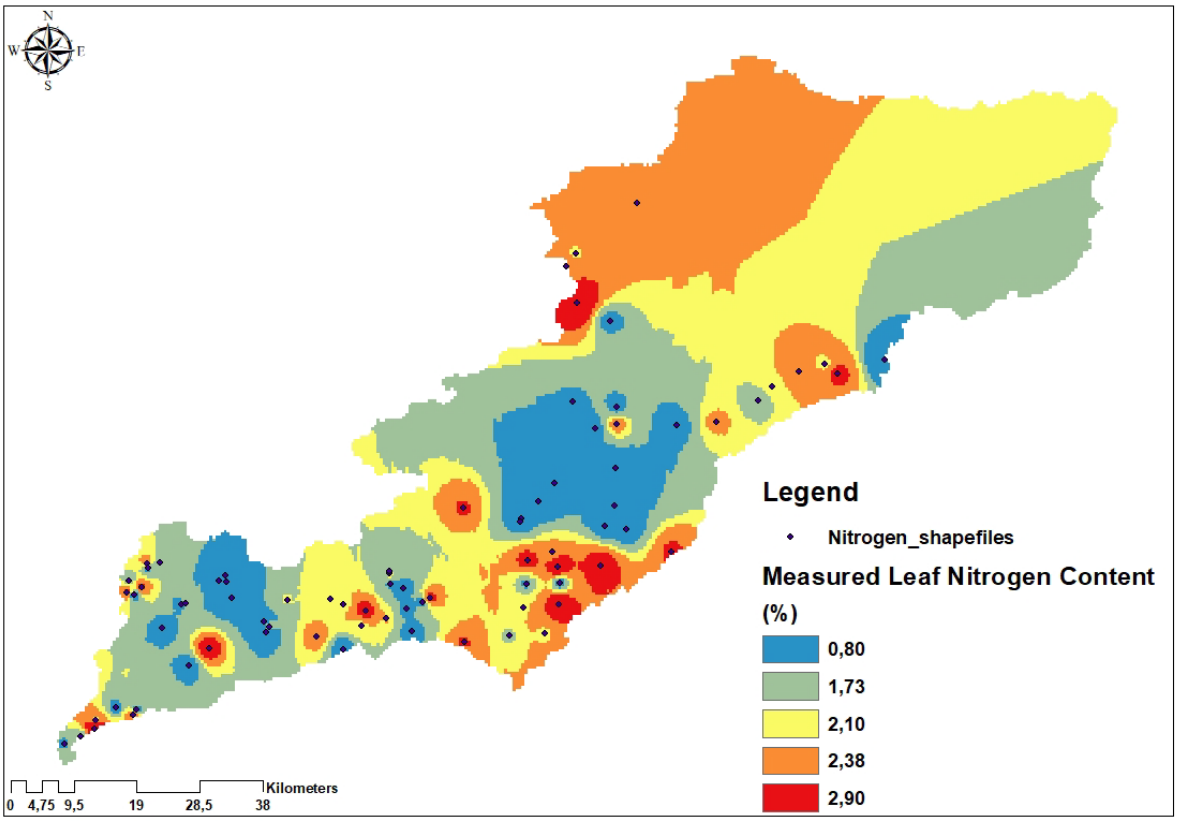

Figure 4.5 Interpolation map of sampling points

4.4.5 Plant N mapping using multiple linear regression and vegetation indices

The spatial distribution of plant N correlates well with the distribution of various plants species across the catchment, this was observed during field visits.

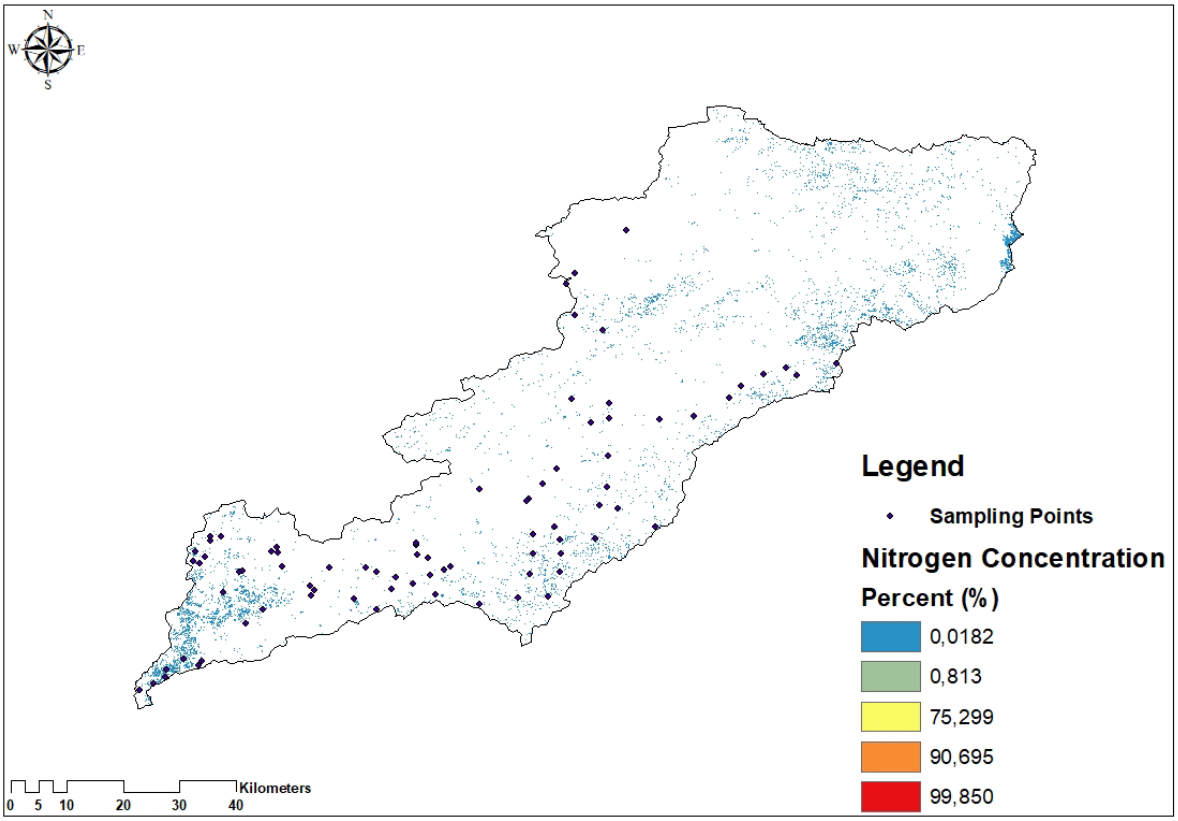

Figure 4.6 Plant nitrogen concentration distribution map in the study area based on Sentinel-2 data and 11 indices.

4.5 Discussion

The aim of this study was to estimate and map plant nitrogen concentration of indigenous vegetation in the Luvuvhu River Catchment in Limpopo province using Sentine-2 data. Remote sensing makes it feasible to monitor plant nitrogen concentration at a large scale effectively at low cost. However, remote sensing mostly obtains spectral reflectance of the canopy of vegetation which requires the need to understand spectral traits of vegetation to be mapped. This allows for the establishment of the relationship between physiological, ecological variables, and spectral reflectance which will allow rapid nitrogen estimation and vegetation health monitoring (Vigneau et al., 2011; Osbome et al., 2011). Spectral reflectance of vegetation is influenced by many factors which result in changes in spectral

reflectance across the study area (Liu at al., 2019). Therefore, this presents a challenge to come up with spectral indices which are simple and applicable for plant N estimation.

In this study, three groups of spectral indices linked to the biochemical and physical properties of vegetation such as nitrogen, structure, and chlorophyll were used with Sentinel-2 imagery to estimate canopy foliar nitrogen in the study area. Three models were built for plant N concentration in this study, namely, rededge, nitrogen based, and combined spectral indices to explore the relationship between predicted and observed nitrogen values for plant nitrogen concentration estimation. Spectral indices constructed from the combination of bands (rededge and nitrogen based) in Sentinel-2 data have the potential to extract vegetation properties and be utilised for a wide range of application such as plant nitrogen, chlorophyll, and water content estimation (Li et al., 2014; Hunt et al., 2013). A combination of spectral regression models which are suitable for plant N estimation are very useful for vegetation health monitoring. Stepwise regression was used to determine the category of spectral indices with better performance when it comes to predicting plant nitrogen.

For this study, regression model of combined spectral indices was used since it showed higher correlation between the observed and predicted values of plant N which presents reference for the plant N monitoring using spectral indices in the subtropical environment. Comparatively, combination of broadband and narrowband spectral indices performed better for this study with $R^2 = 0,59$, followed by broadband spectral indices with $R^2 = 0,44$ and finally narrowband spectral indices with $R^2 = 0,35$. Variation of plant nitrogen concentration is well explained by functional and species composition in the study area. This is dependable looking into studies from various ecosystems, such as temperate, tropical, boreal, and Mediterranean ecosystems (Asner et al., 2008; Mathis et al., 2021; Asner et al., 2009).

Sentinel-2 allows the construction of chlorophyll-related spectral indices using the red-edge part of the spectrum, and since chlorophyll serves as a proxy to nitrogen, such spectral indices can be explored for indirect nitrogen estimation in the forest, which has yielded good results in many ecosystems such as grassland and for agricultural crops (Clevers and Gitelson, 2013). However, spectral indices also have many factors that mostly affect them and are usually affected by many factors and show various characteristics (Zheng et al., 2018). For vegetation parameters estimations, some of spectral indices have excessive capability for soil noise reduction (Rondeaux, 1996), while others are very useful by avoiding at saturation for vegetation spectra (Jordan, 1969). In cases where the ecosystem is nitrogen-rich, the correlation between chlorophyll and nitrogen becomes weak (Schemmer et al., 2013). Therefore, it is very crucial to be considerate when choosing spectral indices that are related to chlorophyll for nitrogen estimation, and also to consider the features that are sensitive to nitrogen when selecting spectral indices to estimate plant nitrogen (Osco et al., 2020; Zheng et al., 2018). NIR serves as a principal constituent for various spectral indices (Rondeaux, 1996). However, in practice, the red

edge is one of the most utilized spectral features for vegetation health evaluation (Vigneau et al., 2011; Osbome, 2002).

4.6 Conclusion

This study compared the performance of three groups of spectral indices which are mostly related to nitrogen, chlorophyll, and structural properties, derived from Sentinel-2 imagery to estimate the concentration of plant nitrogen in a subtropical environment of South Africa. Plant nitrogen varies greatly across the study area depending on species composition. Results from stepwise regression showed that showed that plant nitrogen can be estimated using different groups of indices with acceptable accuracy in the subtropical environment. Comparatively, combination of nitrogen based and rededge spectral indices performed better for this study with R^2 = 0,59, followed by nitrogen based spectral indices with R^2 = 0,44 and finally rededge spectral indices with R^2 = 0,35. Most of the structural related indices could estimate nitrogen at a moderate to good accuracy, due to the functional link between canopy structure and nitrogen resulting from functional type and species differences.

CHAPTER 5: CONCLUSIONS AND SYNTHESIS

5.1 Introduction

Over the last decades, accurate mapping, and monitoring of vegetation cover in the world, and especially in South Africa have been challenging, probably because of the complex structure of its canopy. Vegetation cover mapping using optical remote sensing is very common, and NDVI is the most widely used approach (deFries et al., 1995). However, NDVI on its own could not distinguish between natural vegetation and croplands since croplands were giving similar NDVI values to natural vegetation. This requires more robust classifiers, and their performance should also be independent of site characteristics. That led to the use of maximum likelihood classifier to assist distinguishing between croplands and indigenous vegetation. The study also used different spectral indices and stepwise multiple linear regression to estimate and map leaf water content and plant nitrogen concentration.

This study aimed to map indigenous vegetation health in the Luvuvhu River Catchment using Sentinel-2 data. To achieve this main objective, the study had the following specific objectives:

v. Map the area covered by vegetation in Luvuvhu Catchment Area, and
vi. Distinguish between the area covered with indigenous vegetation and croplands.
vii. Mapping of vegetation leaf water content using Sentinel-2 data
viii. Mapping of the plant nitrogen concentration through Sentinel-2 data

5.2 To map the area covered by vegetation in Luvuvhu Catchment Area and distinguish between the area covered with indigenous vegetation and croplands.

The first objective of this study was to map areas covered with vegetation across the catchment, then distinguish between croplands and indigenous vegetation. This study used NDVI with threshold of < 2 to map areas covered with vegetation. A vegetation map of the study area was used to distinguish between croplands and indigenous vegetation using maximum likelihood classifier with overall accuracy of 98,41 and KAPPA hat of 0,949. It is also noted with great concern that there is a lot of natural vegetation disturbance or clearing in the study area. Vegetation is cleared for a number of reasons such as fuelwood, land occupation, agricultural expansion and many more.

5.3 Mapping of vegetation leaf water content using Sentinel-2 data

One of the objectives of this study was to estimate and map water content across the study area. This was done by selecting spectral indices that are related to water content estimation. Selected indices were grouped into three categories (moisture based, rededge, and combined spectral indices), and stepwise regression was performed for each of them using training data. Study concluded that combined spectral indices performed better with R^2 = 0,53, RMSE = 0,085g/cm and MAE = 0,065%, compared to narrowband indices with R^2 = 0,48, RMSE = 0,097 g/cm and MAE = 0,080%, and broadband indices with R^2 = 0,25, RMSE = 0,096 g/cm and MAE = 0,075%. Mapping of vegetation leaf water content was done using multiple linear regression in QGIS and a produced thematic map showing how vegetation leaf water content is distributed across the study area. The thematic map indicates that there is vast variation in terms of vegetation leaf water content across the study area wherein the mountain range, southwestern and parts of north western part of the catchment have higher vegetation leaf moisture content. The north-eastern parts of the catchment have relatively low vegetation leaf water content.

5.4 Mapping of the plant nitrogen concentration through Sentinel-2 data

The methodology used in chapter 3 was adopted for chapter 4 of this study. Stepwise linear regression was used on narrowband, broadband, and combined indices in R studio software using training dataset. With the use of stepwise regression, spectral indices that were not fit for the models were eliminated. The study compared the final models for each category of spectral indices and established that the model for combined spectral indices performed better (R = 0,59, RMSE = 0,47% and MAE = 0,38%) and was selected for plant N mapping using multiple linear regression in QGIS. It is also established that plant leaf concentration is unevenly distributed across the study area.

5.5 Conclusion

The main aim of this study was to evaluate the health of indigenous vegetation in Luvuvhu River Catchment using Sentinel-2 imagery. This study has shown that Sentinel-2 data can be used to estimate and map biophysical and biochemical variables of vegetation. Based on the findings of this study, it can be concluded that:

(i) Sentinel-2 can be useful in vegetation cover mapping using NDVI. The same images from Sentinel-2 were used to distinguish between croplands and indigenous vegetation using maximum likelihood classifier with an overall accuracy of 98.41% and KAPPA hat of 0,949.

(ii) The combined spectral indices used to estimate vegetation leaf water content have produced better accuracy compared to other models with R^2 = 0.53, RMSE = 0.085 g/cm and MAE = 0.065%, followed by narrowband indices with R^2 = 0.48, RMSE = 0.097g/cm and MAE = 0.080%, and lastly, the broadband indices with R^2 = 0.25, RMSE = 0.096g/cm and MAE = 0.075%. Indices used for this chapter were selected based on their relation to leaf water content in other studies.

(ii) The use of Sentinel-2 imagery, together with spectral indices related to biophysical and biochemical vegetation parameters have proven to be effective for plant N concentration at a landscape scale. Model with combined indices have outperformed other models with R^2 = 0,59, RMSE = 0,47% and MAE = 0,38%.

5.6 Limitations and recommendations

Several limitations exist in this thesis in both chapters 3 and 4. The first limitation is the distribution of the sample points throughout the entire field. Sample points were often weighted towards the accessible side of the field. The issue with this is the enormous size of the study field. Evenly distributing the sample points throughout the entire field was not realistic in terms of labour and accessibility. Most parts of the study area were privately owned land, and often there were no personnel to grant permission to access the property. A suggestion for future research for this limitation is by having multiple teams retrieving the data in different sections of the field simultaneously. However, this would require more fieldwork members and a multiple set of equipment.

Recommendations

Insights on other explanatory variables could be included in future models that capture the prediction of canopy nitrogen. Other spatial field information, such as LAI, drainage and soil information could be used in future models along with spectral VIs. This information can give a better idea on the contributions of nitrogen content that occur below the canopy and could possibly give another direction into analysing plant nitrogen stress.

REFERENCES

Adhikari, D., Reshi, Z., Datta, B.K., Samant, S.S., Chettri, A., Upadhaya, K., Shah, M.A., Singh, P.P., Tiwary, R., Majumdar, K. and Pradhan, A., 2018. Inventory and characterization of new populations through ecological niche modelling improve threat assessment. Curr Sci, 114(3), pp.519-531.

Adjognon, G.S., Rivera-Ballesteros, A. and van Soest, D., 2019. Satellite-based tree cover mapping for forest conservation in the drylands of Sub Saharan Africa (SSA): Application to Burkina Faso gazetted forests. *Development engineering*, *4*, p.100039.

Amundson, R., Austin, A.T., Schuur, E.A., Yoo, K., Matzek, V., Kendall, C., Uebersax, A., Brenner, D. and Baisden, W.T., 2003. Global patterns of the isotopic composition of soil and plant nitrogen. *Global biogeochemical cycles*, *17*(1).

Arft, A.M., Walker, M.D., Gurevitch, J.E.T.A., Alatalo, J.M., Bret-Harte, M.S., Dale, M., Diemer, M., Gugerli, F., Henry, G.H.R., Jones, M.H. and Hollister, R.D., 1999. Responses of tundra plants to experimental warming: meta-analysis of the international tundra experiment. *Ecological monographs*, *69*(4), pp.491-511.

Asner, G.P., Knapp, D.E., Kennedy-Bowdoin, T., Jones, M.O., Martin, R.E., Boardman, J. and Hughes, R.F., 2008. Invasive species detection in Hawaiian rainforests using airborne imaging spectroscopy and LiDAR. *Remote sensing of Environment*, *112*(5), pp.1942-1955.

Asner, G.P., Rudel, T.K., Aide, T.M., Defries, R. and Emerson, R., 2009. A contemporary assessment of change in humid tropical forests. *Conservation Biology*, *23*(6), pp.1386-1395.

BassiriRad, H., Constable, J.V., Lussenhop, J., Kimball, B.A., Norby, R.J., Oechel, W.C., Reich, P.B., Schlesinger, W.H., Zitzer, S., Sehtiya, H.L. and Silim, S., 2003. Widespread foliage δ15N depletion under elevated CO2: inferences for the nitrogen cycle. *Global Change Biology*, *9*(11), pp.1582-1590.

Batten, G.D., 1998. Plant analysis using near infrared reflectance spectroscopy: the potential and the limitations. *Australian Journal of Experimental Agriculture*, *38*(7), pp.697-706.

Boegh, E., Soegaard, H., Broge, N., Hasager, C.B., Jensen, N.O., Schelde, K. and Thomsen, A., 2002. Airborne multispectral data for quantifying leaf area index, nitrogen concentration, and photosynthetic efficiency in agriculture. *Remote sensing of Environment*, *81*(2-3), pp.179-193.

Brooks, C.P., Holmes, C., Kramer, K., Barnett, B. and Keitt, T.H., 2009. The role of demography and markets in determining deforestation rates near Ranomafana National Park, Madagascar. *PloS one*, *4*(6), p.e5783.

Brooks, T.M., Wright, S.J. and Sheil, D., 2009. Evaluating the success of conservation actions in safeguarding tropical forest biodiversity. *Conservation Biology*, *23*(6), pp.1448-1457.

Bullock, E.L., Woodcock, C.E. and Olofsson, P., 2020. Monitoring tropical forest degradation using spectral unmixing and Landsat time series analysis. Remote sensing of Environment, 238, p.110968.

Bullock, E.L., Woodcock, C.E. and Olofsson, P., 2020. Monitoring tropical forest degradation using spectral unmixing and Landsat time series analysis. *Remote sensing of Environment*, *238*, p.110968.

Byrd, K.B., O'Connell, J.L., Di Tommaso, S. and Kelly, M., 2014. Evaluation of sensor types and environmental controls on mapping biomass of coastal marsh emergent vegetation. *Remote Sensing of Environment*, *149*, pp.166-180.

Cassman, K.G., Dobermann, A. and Walters, D.T., 2002. Agroecosystems, nitrogen-use efficiency, and nitrogen management. AMBIO: A Journal of the Human Environment, 31(2), pp.132-140.

Ceccato, P., Flasse, S., Tarantola, S., Jacquemoud, S. and Grégoire, J.M., 2001. Detecting vegetation leaf water content using reflectance in the optical domain. *Remote sensing of environment*, *77*(1), pp.22-33.

Ceccato, P., Flasse, S., Tarantola, S., Jacquemoud, S. and Grégoire, J.M., 2001. Detecting vegetation leaf water content using reflectance in the optical domain. *Remote sensing of environment*, *77*(1), pp.22-33.

Chang, Y., Yan, L., Wu, T. and Zhong, S., 2016. Remote sensing image stripe noise removal: From image decomposition perspective. *IEEE Transactions on Geoscience and Remote Sensing*, *54*(12), pp.7018-7031.

Chapin, F.S., Pickett, S.T., Power, M.E., Jackson, R.B., Carter, D.M. and Duke, C., 2011. Earth stewardship: a strategy for social–ecological transformation to reverse planetary degradation. *Journal of Environmental Studies and Sciences*, *1*(1), pp.44-53.

Chastain, R., Housman, I., Goldstein, J., Finco, M. and Tenneson, K., 2019. Empirical cross sensor comparison of Sentinel-2A and 2B MSI, Landsat-8 OLI, and Landsat-7 ETM+ top of atmosphere spectral characteristics over the conterminous United States. *Remote sensing of environment*, *221*, pp.274-285.

Chemura, A., Mutanga, O., Odindi, J. and Kutywayo, D., 2018. Mapping spatial variability of foliar nitrogen in coffee (Coffea arabica L.) plantations with multispectral Sentinel-2 MSI data. *ISPRS Journal of Photogrammetry and Remote Sensing*, *138*, pp.1-11.

Chen, G., Li, S., Knibbs, L.D., Hamm, N.A., Cao, W., Li, T., Guo, J., Ren, H., Abramson, M.J. and Guo, Y., 2018. A machine learning method to estimate PM2. 5 concentrations across China with remote sensing, meteorological and land use information. Science of the Total Environment, 636, pp.52-60.

Cheng, G., Zhou, P. and Han, J., 2016. Learning rotation-invariant convolutional neural networks for object detection in VHR optical remote sensing images. *IEEE Transactions on Geoscience and Remote Sensing*, *54*(12), pp.7405-7415.

Cheng, Y.B., Zarco-Tejada, P.J., Riaño, D., Rueda, C.A. and Ustin, S.L., 2006. Estimating vegetation water content with hyperspectral data for different canopy scenarios: Relationships between AVIRIS and MODIS indexes. *Remote Sensing of Environment*, *105*(4), pp.354-366.

Clerici, N., Valbuena Calderón, C.A. and Posada, J.M., 2017. Fusion of Sentinel-1A and Sentinel-2A data for land cover mapping: a case study in the lower Magdalena region, Colombia. Journal of Maps, 13(2), pp.718-726.

Clevers, J.G. and Gitelson, A.A., 2013. Remote estimation of crop and grass chlorophyll and nitrogen content using red-edge bands on Sentinel-2 and-3. *International Journal of Applied Earth Observation and Geoinformation*, *23*, pp.344-351.

Cohen, W.B. and Goward, S.N., 2004. Landsat's role in ecological applications of remote sensing. *Bioscience*, *54*(6), pp.535-545.

Congalton, R.G. and Green, K., 2019. Assessing the accuracy of remotely sensed data: principles and practices. CRC press.

Cord, A.F., Klein, D. and Dech, S., 2010. Remote sensing time series for modeling invasive species distribution: a case study of Tamarix spp. in the US and Mexico.

Cowling, S.A., Cox, P.M., Jones, C.D., Maslin, M.A., Peros, M. and Spall, S.A., 2008. Simulated glacial and interglacial vegetation across Africa: implications for species phylogenies and trans-African migration of plants and animals. *Global Change Biology*, *14*(4), pp.827-840.

Cox, P.M., Betts, R.A., Jones, C.D., Spall, S.A. and Totterdell, I.J., 2000. Acceleration of global warming due to carbon-cycle feedbacks in a coupled climate model. *Nature*, *408*(6809), pp.184-187.

Craine, J.M., Elmore, A.J., Aidar, M.P., Bustamante, M., Dawson, T.E., Hobbie, E.A., Kahmen, A., Mack, M.C., McLauchlan, K.K., Michelsen, A. and Nardoto, G.B., 2009. Global patterns of foliar nitrogen isotopes and their relationships with climate, mycorrhizal fungi, foliar nutrient concentrations, and nitrogen availability. *New Phytologist*, *183*(4), pp.980-992.

Croft, H., Chen, J.M. and Zhang, Y., 2014. The applicability of empirical vegetation indices for determining leaf chlorophyll content over different leaf and canopy structures. *Ecological Complexity*, *17*, pp.119-130.

Dagada, K., 2017. Influence of climate change on flood and drought cycles and implications on rainy season characteristics in Luvuvhu River Catchment (Doctoral dissertation).

Dagada, K., 2017. *Influence of climate change on flood and drought cycles and implications on rainy season characteristics in Luvuvhu River Catchment* (Doctoral dissertation).

Danson, F.M. and Bowyer, P., 2004. Estimating live fuel moisture content from remotely sensed reflectance. *Remote Sensing of Environment*, *92*(3), pp.309-321.

Darvishzadeh, R., Skidmore, A., Schlerf, M. and Atzberger, C., 2008. Inversion of a radiative transfer model for estimating vegetation LAI and chlorophyll in a heterogeneous grassland. *Remote sensing of environment*, *112*(5), pp.2592-2604.

Dash, J. and Curran, P.J., 2004. The MERIS terrestrial chlorophyll index.

Davies, S.L., Turner, N.C., Palta, J.A., Siddique, K.H.M. and Plummer, J.A., 2000. Remobilisation of carbon and nitrogen supports seed filling in chickpea subjected to water deficit. Australian Journal of Agricultural Research, 51(7), pp.855-866.

De Koning, F., Aguiñaga, M., Bravo, M., Chiu, M., Lascano, M., Lozada, T. and Suarez, L., 2011. Bridging the gap between forest conservation and poverty alleviation: the Ecuadorian Socio Bosque program. *Environmental Science & Policy*, *14*(5), pp.531-542.

DeFries, R., Hansen, M. and Townshend, J., 1995. Global discrimination of land cover types from metrics derived from AVHRR pathfinder data. *Remote sensing of environment*, *54*(3), pp.209-222.

DeFries, R., Hansen, M. and Townshend, J., 1995. Global discrimination of land cover types from metrics derived from AVHRR pathfinder data. *Remote sensing of environment*, *54*(3), pp.209-222.

Dimitrov, P., Kamenova, I., Roumenina, E., Filchev, L., Ilieva, I., Jelev, G., Gikov, A., Banov, M., Krasteva, V., Kolchakov, V. and Kercheva, M., 2019. Estimation of biophysical and biochemical variables of winter wheat through Sentinel-2 vegetation indices. *Bulg. J. Agric. Sci*, *25*, pp.819-832.

Dong, J., Crow, W.T., Tobin, K.J., Cosh, M.H., Bosch, D.D., Starks, P.J., Seyfried, M. and Collins, C.H., 2020. Comparison of microwave remote sensing and land surface modeling for surface soil moisture climatology estimation. *Remote Sensing of Environment*, *242*, p.111756.

Dong, J., Metternicht, G., Hostert, P., Fensholt, R. and Chowdhury, R.R., 2019. Remote sensing and geospatial technologies in support of a normative land system science: Status and prospects. *Current Opinion in Environmental Sustainability*, *38*, pp.44-52.

Du, Y., Zhang, Y., Ling, F., Wang, Q., Li, W. and Li, X., 2016. Water bodies' mapping from Sentinel-2 imagery with modified normalized difference water index at 10-m spatial resolution produced by sharpening the SWIR band. *Remote Sensing*, *8*(4), p.354.

Dzikiti, S., Verreynne, J.S., Stuckens, J., Strever, A., Verstraeten, W.W., Swennen, R. and Coppin, P., 2010. Determining the water status of Satsuma mandarin trees [Citrus Unshiu Marcovitch] using spectral indices and by combining hyperspectral and physiological data. *Agricultural and Forest Meteorology*, *150*(3), pp.369-379.

Easterday, K., Kislik, C., Dawson, T.E., Hogan, S. and Kelly, M., 2019. Remotely sensed water limitation in vegetation: insights from an experiment with unmanned aerial vehicles (UAVs). *Remote Sensing*, *11*(16), p.1853.

Estel, S., Kuemmerle, T., Levers, C., Baumann, M. and Hostert, P., 2016. Mapping cropland-use intensity across Europe using MODIS NDVI time series. *Environmental Research Letters*, *11*(2), p.024015.

Evans, J.R., 1989. Photosynthesis and nitrogen relationships in leaves of C 3 plants. Oecologia, 78(1), pp.9-19.

Fan, J., Defourny, P., Dong, Q., Zhang, X., De Vroey, M., Bellemans, N., Xu, Q., Li, Q., Zhang, L. and Gao, H., 2020. Sent2Agri System Based Crop Type Mapping in Yellow River Irrigation Area. *Journal of Geodesy and Geoinformation Science*, *3*(4), p.110.

Fan, J.W., Wang, K., Harris, W., Zhong, H.P., Hu, Z.M., Han, B., Zhang, W.Y. and Wang, J.B., 2009. Allocation of vegetation biomass across a climate-related gradient in the grasslands of Inner Mongolia. *Journal of Arid Environments*, *73*(4-5), pp.521-528.

Fern, R.R., Foxley, E.A., Bruno, A. and Morrison, M.L., 2018. Suitability of NDVI and OSAVI as estimators of green biomass and coverage in a semi-arid rangeland. *Ecological Indicators*, *94*, pp.16-21.

Filazzola, A., Mahdiyan, O., Shuvo, A., Ewins, C., Moslenko, L., Sadid, T., Blagrave, K., Imrit, M.A., Gray, D.K., Quinlan, R. and O'Reilly, C.M., 2020. A database of chlorophyll and water chemistry in freshwater lakes. *Scientific Data*, *7*(1), pp.1-10.

Foley, S., Rivard, B., Sanchez-Azofeifa, G.A. and Calvo, J., 2006. Foliar spectral properties following leaf clipping and implications for handling techniques. *Remote Sensing of Environment*, *103*(3), pp.265-275.

Fourty, T., Baret, F., Jacquemoud, S., Schmuck, G. and Verdebout, J., 1996. Leaf optical properties with explicit description of its biochemical composition: direct and inverse problems. Remote sensing of Environment, 56(2), pp.104-117.

Fourty, T.H. and Baret, F., 1998. On spectral estimates of fresh leaf biochemistry. International Journal of Remote Sensing, 19(7), pp.1283-1297.

Frampton, W.J., Dash, J., Watmough, G. and Milton, E.J., 2013. Evaluating the capabilities of Sentinel-2 for quantitative estimation of biophysical variables in vegetation. ISPRS journal of photogrammetry and remote sensing, 82, pp.83-92.

Frampton, W.J., Dash, J., Watmough, G. and Milton, E.J., 2013. Evaluating the capabilities of Sentinel-2 for quantitative estimation of biophysical variables in vegetation. *ISPRS journal of photogrammetry and remote sensing*, *82*, pp.83-92.

Galloway, J., Raghuram, N. and Abrol, Y.P., 2008. A perspective on reactive nitrogen in a global, Asian and Indian context. *Current Science*, pp.1375-1381.

Gao, B.C., 1996. NDWI—A normalized difference water index for remote sensing of vegetation liquid water from space. *Remote sensing of environment*, *58*(3), pp.257-266.

Gao, X., Zhuang, S., Jin, J. and Cao, P., 2015. Bound water content and pore size distribution in swollen cell walls determined by NMR technology. *BioResources*, *10*(4), pp.8208-8224.

Gaulton, R., Danson, F.M., Ramirez, F.A. and Gunawan, O., 2013. The potential of dual-wavelength laser scanning for estimating vegetation moisture content. *Remote Sensing of Environment*, *132*, pp.32-39.

Gitelson, A. and Merzlyak, M.N., 1994. Quantitative estimation of chlorophyll-a using reflectance spectra: Experiments with autumn chestnut and maple leaves. *Journal of Photochemistry and Photobiology B: Biology*, *22*(3), pp.247-252.

Gitelson, A., Karnieli, A., Goldman, N., Yacobi, Y.Z. and Mayo, M., 1996. Chlorophyll estimation in the Southeastern Mediterranean using CZCS images: adaptation of an algorithm and its validation. *Journal of Marine Systems*, *9*(3-4), pp.283-290.

Gitelson, A.A., Gritz, Y. and Merzlyak, M.N., 2003. Relationships between leaf chlorophyll content and spectral reflectance and algorithms for non-destructive chlorophyll assessment in higher plant leaves. *Journal of plant physiology*, *160*(3), pp.271-282.

Gitelson, A.A., Peng, Y., Arkebauer, T.J. and Schepers, J., 2014. Relationships between gross primary production, green LAI, and canopy chlorophyll content in maize: Implications for remote sensing of primary production. Remote Sensing of Environment, 144, pp.65-72.

Gitelson, A.A., Peng, Y., Arkebauer, T.J. and Schepers, J., 2014. Relationships between gross primary production, green LAI, and canopy chlorophyll content in maize: Implications for remote sensing of primary production. *Remote Sensing of Environment*, *144*, pp.65-72.

Goodale, C.L. and Aber, J.D., 2001. The long-term effects of land-use history on nitrogen cycling in northern hardwood forests. *Ecological Applications*, *11*(1), pp.253-267.

Griscom, H.R., Miller, S.N., Gyedu-Ababio, T. and Sivanpillai, R., 2010. Mapping land cover change of the Luvuvhu catchment, South Africa for environmental modelling. GeoJournal, 75(2), pp.163-173.

Griscom, H.R., Miller, S.N., Gyedu-Ababio, T. and Sivanpillai, R., 2010. Mapping land cover change of the Luvuvhu catchment, South Africa for environmental modelling. *GeoJournal*, *75*(2), pp.163-173.

Grogan, P. and Chapin, F.S., 2000. Nitrogen limitation of production in a Californianannual grassland: The contribution of arbuscularmycorrhizae. *Biogeochemistry*, *49*(1), pp.37-51.

Guanter, L., Kaufmann, H., Segl, K., Foerster, S., Rogass, C., Chabrillat, S., Kuester, T., Hollstein, A., Rossner, G., Chlebek, C. and Straif, C., 2015. The EnMAP spaceborne imaging spectroscopy mission for earth observation. *Remote Sensing*, *7*(7), pp.8830-8857.

Hackman, K.O., Gong, P. and Wang, J., 2017. New land-cover maps of Ghana for 2015 using Landsat 8 and three popular classifiers for biodiversity assessment. International Journal of Remote Sensing, 38(14), pp.4008-4021.

Hackman, K.O., Gong, P. and Wang, J., 2017. New land-cover maps of Ghana for 2015 using Landsat 8 and three popular classifiers for biodiversity assessment. *International Journal of Remote Sensing*, *38*(14), pp.4008-4021.

Hallett, R.A. and Hornbeck, J.W., 1997. Foliar and soil nutrient relationships in red oak and white pine forests. *Canadian Journal of Forest Research*, *27*(8), pp.1233-1244.

Han, L., Yang, G., Dai, H., Xu, B., Yang, H., Feng, H., Li, Z. and Yang, X., 2019. Modeling maize above-ground biomass based on machine learning approaches using UAV remote-sensing data. *Plant methods*, *15*(1), pp.1-19.

Hansen, M.C. and Loveland, T.R., 2012. A review of large area monitoring of land cover change using Landsat data. *Remote sensing of Environment*, *122*, pp.66-74.

He, B., Cai, Y., Ran, W. and Jiang, H., 2014. Spatial and seasonal variations of soil salinity following vegetation restoration in coastal saline land in eastern China. *Catena*, *118*, pp.147-153.

He, Y. and Mui, A., 2010. Scaling up semi-arid grassland biochemical content from the leaf to the canopy level: Challenges and opportunities. *Sensors*, *10*(12), pp.11072-11087.

Heimann, M. and Reichstein, M., 2008. Terrestrial ecosystem carbon dynamics and climate feedbacks. Nature, 451(7176), pp.289-292.

Herman, M.R., Nejadhashemi, A.P., Abouali, M., Hernandez-Suarez, J.S., Daneshvar, F., Zhang, Z., Anderson, M.C., Sadeghi, A.M., Hain, C.R. and Sharifi, A., 2018. Evaluating the role of evapotranspiration remote sensing data in improving hydrological modeling predictability. *Journal of Hydrology*, *556*, pp.39-49.

Herrmann, I., Pimstein, A., Karnieli, A., Cohen, Y., Alchanatis, V. and Bonfil, D.J., 2011. LAI assessment of wheat and potato crops by VENμS and Sentinel-2 bands. Remote Sensing of Environment, 115(8), pp.2141-2151.

Hikosaka, K., Anten, N.P., Borjigidai, A., Kamiyama, C., Sakai, H., Hasegawa, T., Oikawa, S., Iio, A., Watanabe, M., Koike, T. and Nishina, K., 2016. A meta-analysis of leaf nitrogen distribution within plant canopies. *Annals of Botany*, *118*(2), pp.239-247.

Hirano, K. and Maki, M., 2018. Imminent nowcasting for severe rainfall using vertically integrated liquid water content derived from X-band polarimetric radar. *Journal of the Meteorological Society of Japan. Ser. II*.

Hobbie, E.A. and Colpaert, J.V., 2003. Nitrogen availability and colonization by mycorrhizal fungi correlate with nitrogen isotope patterns in plants. *New Phytologist*, *157*(1), pp.115-126.

Hobbie, E.A., Jumpponen, A. and Trappe, J., 2005. Foliar and fungal 15 N: 14 N ratios reflect development of mycorrhizae and nitrogen supply during primary succession: testing analytical models. *Oecologia*, *146*(2), pp.258-268.

Hoffmann, A.M., Noga, G. and Hunsche, M., 2015. Fluorescence indices for monitoring the ripening of tomatoes in pre-and postharvest phases. *Scientia Horticulturae*, *191*, pp.74-81.

Homolova, L., Malenovský, Z., Clevers, J.G., García-Santos, G. and Schaepman, M.E., 2013. Review of optical-based remote sensing for plant trait mapping. *Ecological Complexity*, *15*, pp.1-16.

Hope, G., Kershaw, A.P., van der Kaars, S., Xiangjun, S., Liew, P.M., Heusser, L.E., Takahara, H., McGlone, M., Miyoshi, N. and Moss, P.T., 2004. History of vegetation and habitat change in the Austral-Asian region. *Quaternary International*, *118*, pp.103-126.

Hope, R.A., Jewitt, G.P.W. and Gowing, J.W., 2004. Linking the hydrological cycle and rural livelihoods: A case study in the Luvuvhu catchment, South Africa. Physics and Chemistry of the Earth, Parts A/B/C, 29(15-18), pp.1209-1217.

Houborg, R. and McCabe, M.F., 2018. A hybrid training approach for leaf area index estimation via Cubist and random forests machine-learning. *ISPRS Journal of Photogrammetry and Remote Sensing*, *135*, pp.173-188.

Huber, S.A., Balz, A., Abert, M. and Pronk, W., 2011. Characterisation of aquatic humic and non-humic matter with size-exclusion chromatography–organic carbon detection–organic nitrogen detection (LC-OCD-OND). *Water research*, *45*(2), pp.879-885.

Hudson, I. and Ramm, R., 1987. Lincoln weed control in cereals and pasture.

Hudson, P.J., Cattadori, I.M., Boag, B. and Dobson, A.P., 2006. Climate disruption and parasite–host dynamics: patterns and processes associated with warming and the frequency of extreme climatic events. Journal of helminthology, 80(2), pp.175-182.

Hungate, B.A., Dukes, J.S., Shaw, M.R., Luo, Y. and Field, C.B., 2003. Nitrogen and climate change. *Science*, *302*(5650), pp.1512-1513.

Hunt, E.R., Horneck, D.A., Spinelli, C.B., Turner, R.W., Bruce, A.E., Gadler, D.J., Brungardt, J.J. and Hamm, P.B., 2018. Monitoring nitrogen status of potatoes using small unmanned aerial vehicles. *Precision agriculture*, *19*(2), pp.314-333.

Idso, S.B., Reginato, R.J., Jackson, R.D. and Pinter, J.P., 1981. Measuring yield-reducing plant water potential depressions in wheat by infrared thermometry. *Irrigation Science*, *2*(4), pp.205-212.

Immitzer, M., Vuolo, F. and Atzberger, C., 2016. First experience with Sentinel-2 data for crop and tree species classifications in central Europe. Remote sensing, 8(3), p.166.

Immitzer, M., Vuolo, F. and Atzberger, C., 2016. First experience with Sentinel-2 data for crop and tree species classifications in central Europe. *Remote sensing*, *8*(3), p.166.

Jensen, A.M., Hardy, T., McKee, M. and Chen, Y., 2011, July. Using a multispectral autonomous unmanned aerial remote sensing platform (AggieAir) for riparian and wetlands applications. In *2011 IEEE International Geoscience and Remote Sensing Symposium* (pp. 3413-3416). IEEE.

Jiang, L., Kogan, F.N., Guo, W., Tarpley, J.D., Mitchell, K.E., Ek, M.B., Tian, Y., Zheng, W., Zou, C.Z. and Ramsay, B.H., 2010. Real-time weekly global green vegetation fraction derived from advanced very high resolution radiometer-based NOAA operational global vegetation index (GVI) system. *Journal of Geophysical Research: Atmospheres*, *115*(D11).

Jiao, W., Wang, L. and McCabe, M.F., 2021. Multi-sensor remote sensing for drought characterization: current status, opportunities and a roadmap for the future. *Remote Sensing of Environment*, *256*, p.112313.

Jordan, C.F., 1969. Derivation of leaf-area index from quality of light on the forest floor. *Ecology*, *50*(4), pp.663-666.

Jucker, T., Caspersen, J., Chave, J., Antin, C., Barbier, N., Bongers, F., Dalponte, M., van Ewijk, K.Y., Forrester, D.I., Haeni, M. and Higgins, S.I., 2017. Allometric equations for integrating remote sensing imagery into forest monitoring programmes. *Global change biology*, *23*(1), pp.177-190.

Knight, J.F., Lunetta, R.S., Ediriwickrema, J. and Khorram, S., 2006. Regional scale land cover characterization using MODIS-NDVI 250 m multi-temporal imagery: A phenology-based approach. *GIScience & Remote Sensing*, *43*(1), pp.1-23.

Kodani, E., Awaya, Y., Tanaka, K. and Matsumura, N., 2002. Seasonal patterns of canopy structure, biochemistry, and spectral reflectance in a broad-leaved deciduous Fagus crenata canopy. Forest Ecology and Management, 167(1-3), pp.233-249.

Kokaly, R.F., Asner, G.P., Ollinger, S.V., Martin, M.E. and Wessman, C.A., 2009. Characterizing canopy biochemistry from imaging spectroscopy and its application to ecosystem studies. Remote sensing of environment, 113, pp. S78-S91.

Kokaly, R.F., Asner, G.P., Ollinger, S.V., Martin, M.E. and Wessman, C.A., 2009. Characterizing canopy biochemistry from imaging spectroscopy and its application to ecosystem studies. *Remote sensing of environment*, *113*, pp.S78-S91.

Kooistra, L., Clevers, J.G.P.W., Beza, E., van Vliet, P., van den Borne, J. and van der Velde, W., 2012, April. Opportunities for Sentinel-2 in an integrated sensor approach to support decision making in precision agriculture. In *First Sentinel-2 Preparatory Symposium* (Vol. 707, p. 9).

Kumar, D. and Shekhar, S., 2015. Statistical analysis of land surface temperature–vegetation indexes relationship through thermal remote sensing. Ecotoxicology and environmental safety, 121, pp.39-44.

Kumar, N., Chu, A. and Foster, A., 2008. Remote sensing of ambient particles in Delhi and its environs: estimation and validation. International Journal of Remote Sensing, 29(12), pp.3383-3405.

Kundu, P.M., Mathivha, F.I. and Nkuna, T.R., 2015. *The Use of GIS and Remote Sensing Techniques to Evaluate the Impact of Land Use and Land Cover Change on the Hydrology of Luvuvhu River Catchment in Limpopo Province: Report to the Water Research Commission* (p. 15). Pretoria, South Africa: Water Research Commission.

Lamarque, J.F., Kiehl, J.T., Brasseur, G.P., Butler, T., Cameron-Smith, P., Collins, W.D., Collins, W.J., Granier, C., Hauglustaine, D., Hess, P.G. and Holland, E.A., 2005. Assessing future nitrogen deposition and carbon cycle feedback using a multimodel approach: Analysis of nitrogen deposition. Journal of Geophysical Research: Atmospheres, 110(D19).

Lambert, M.J., Waldner, F. and Defourny, P., 2016. Cropland mapping over Sahelian and Sudanian agrosystems: A knowledge-based approach using PROBA-V time series at 100-m. *Remote Sensing*, *8*(3), p.232.

Landis, J.R. and Koch, G.G., 1977. The measurement of observer agreement for categorical data. biometrics, pp.159-174.

Le Maire, G., François, C., Soudani, K., Berveiller, D., Pontailler, J.Y., Bréda, N., Genet, H., Davi, H. and Dufrêne, E., 2008. Calibration and validation of hyperspectral indices for the estimation of broadleaved forest leaf chlorophyll content, leaf mass per area, leaf area index and leaf canopy biomass. *Remote sensing of environment*, *112*(10), pp.3846-3864.

Lee, B.W. and Nguyen, T.A., 2005. SPATIAL YIELD VARIABILITY AND SITE-SPECIFIC NITROGEN PRESCRIPTION FOR THE IMPROVED YIELD AND GRAIN QUALITY OF RICE.

In *Proceedings of the Korean Society of Crop Science Conference* (pp. 57-74). The Korean Society of Crop Science.

Lemaire, G., Wilkins, R. and Hodgson, J., 2005. Challenges for grassland science: managing research priorities. *Agriculture, ecosystems & environment*, *108*(2), pp.99-108.

Lepine, L.C., Ollinger, S.V., Ouimette, A.P. and Martin, M.E., 2016. Examining spectral reflectance features related to foliar nitrogen in forests: Implications for broad-scale nitrogen mapping. Remote Sensing of Environment, 173, pp.174-186.

Li, F., Miao, Y., Feng, G., Yuan, F., Yue, S., Gao, X., Liu, Y., Liu, B., Ustin, S.L. and Chen, X., 2014. Improving estimation of summer maize nitrogen status with red edge-based spectral vegetation indices. *Field Crops Research*, *157*, pp.111-123.

Lichtenthaler, H.K., 1996. Vegetation stress: an introduction to the stress concept in plants. *Journal of plant physiology*, *148*(1-2), pp.4-14.

Lilley, J.M., Bolger, T.P., Peoples, M.B. and Gifford, R.M., 2001. Nutritive value and the nitrogen dynamics of Trifolium subterraneum and Phalaris aquatica under warmer, high CO2 conditions. *New Phytologist*, *150*(2), pp.385-395.

Luo, S., Wang, C., Li, G. and Xi, X., 2013. Retrieving leaf area index using ICESat/GLAS full-waveform data. *Remote sensing letters*, *4*(8), pp.745-753.

Luo, Y., Su, B.O., Currie, W.S., Dukes, J.S., Finzi, A., Hartwig, U., Hungate, B., McMurtrie, R.E., Oren, R.A.M., Parton, W.J. and Pataki, D.E., 2004. Progressive nitrogen limitation of ecosystem responses to rising atmospheric carbon dioxide. *Bioscience*, *54*(8), pp.731-739.

Luomala, E.M., Laitinen, K., Kellomäki, S. and Vapaavuori, E., 2003. Variable photosynthetic acclimation in consecutive cohorts of Scots pine needles during 3 years of growth at elevated CO2 and elevated temperature. *Plant, Cell & Environment*, *26*(5), pp.645-660.

Lynch, K., Jackson, D.W. and Cooper, J.A.G., 2008. Aeolian fetch distance and secondary airflow effects: the influence of micro-scale variables on meso-scale foredune development. *Earth Surface Processes and Landforms: The Journal of the British Geomorphological Research Group*, *33*(7), pp.991-1005.

Mathis, C.L., McNeil Jr, D.J., Lee, M.R., Grozinger, C.M., King, D.I., Otto, C.R. and Larkin, J.L., 2021. Pollinator communities vary with vegetation structure and time since management within regenerating timber harvests of the Central Appalachian Mountains. *Forest Ecology and Management*, *496*, p.119373.

Mazibuko, S.M., Mukwada, G. and Moeletsi, M.E., 2021. Assessing the frequency of drought/flood severity in the Luvuvhu River catchment, Limpopo Province, South Africa. Water SA, 47(2), pp.172-184.

Meentemeyer, R.K., Rank, N.E., Anacker, B.L., Rizzo, D.M. and Cushman, J.H., 2008. Influence of land-cover change on the spread of an invasive forest pathogen. *Ecological Applications*, *18*(1), pp.159-171.

Meng, J., Li, S., Wang, W., Liu, Q., Xie, S. and Ma, W., 2016. Mapping forest health using spectral and textural information extracted from spot-5 satellite images. *Remote Sensing*, *8*(9), p.719.

Mishra, R., Singh, E., Kumar, A. and Kumar, S., 2021. Application of remote sensing for assessment of change in vegetation cover and the subsequent impact on climatic variables. *Environmental Science and Pollution Research*, *28*(31), pp.41675-41687.

Nare, L., Odiyo, J.O., Francis, J. and Potgieter, N., 2011. Framework for effective community participation in water quality management in Luvuvhu Catchment of South Africa. Physics and Chemistry of the Earth, Parts A/B/C, 36(14-15), pp.1063-1070.

Nare, L., Odiyo, J.O., Francis, J. and Potgieter, N., 2011. Framework for effective community participation in water quality management in Luvuvhu Catchment of South Africa. Physics and Chemistry of the Earth, Parts A/B/C, 36(14-15), pp.1063-1070.

Nethononda, V.G., 2018. Determination of irrigation water quality of surface and groundwater in Luvuvhu catchment in Limpopo, South Africa (Doctoral dissertation, University of Zululand).

Nethononda, V.G., 2018. *Determination of irrigation water quality of surface and groundwater in Luvuvhu catchment in Limpopo, South Africa* (Doctoral dissertation, University of Zululand).

Nijland, W., De Jong, R., De Jong, S.M., Wulder, M.A., Bater, C.W. and Coops, N.C., 2014. Monitoring plant condition and phenology using infrared sensitive consumer grade digital cameras. *Agricultural and Forest Meteorology*, *184*, pp.98-106.

Nouri, H., Beecham, S., Anderson, S. and Nagler, P., 2014. High spatial resolution WorldView-2 imagery for mapping NDVI and its relationship to temporal urban landscape evapotranspiration factors. *Remote sensing*, *6*(1), pp.580-602.

Novelli, F., Spiegel, H., Sandén, T. and Vuolo, F., 2019. Assimilation of sentinel-2 leaf area index data into a physically-based crop growth model for yield estimation. *Agronomy*, *9*(5), p.255.

Nzabarinda, V., Bao, A., Xu, W., Uwamahoro, S., Udahogora, M., Umwali, E.D., Nyirarwasa, A. and Umuhoza, J., 2021. A spatial and temporal assessment of vegetation greening and precipitation changes for monitoring vegetation dynamics in climate zones over Africa. *ISPRS International Journal of Geo-Information*, *10*(3), p.129.

Odiyo, J.O., Chimuka, L., Mamali, M.A. and Fatoki, O.S., 2012. Trophic status of Vondo and Albasini Dams; impacts on aquatic ecosystems and drinking water. *International Journal of Environmental Science and Technology*, *9*(2), pp.203-218.

Odiyo, J.O., Phangisa, J.I. and Makungo, R., 2012. Rainfall–runoff modelling for estimating Latonyanda River flow contributions to Luvuvhu River downstream of Albasini Dam. Physics and Chemistry of the Earth, Parts A/B/C, 50, pp.5-13.

Ollinger, S.V. and Smith, M.L., 2005. Net primary production and canopy nitrogen in a temperate forest landscape: an analysis using imaging spectroscopy, modeling and field data. Ecosystems, 8(7), pp.760-778.

Ollinger, S.V., Richardson, A.D., Martin, M.E., Hollinger, D.Y., Frolking, S.E., Reich, P.B., Plourde, L.C., Katul, G.G., Munger, J.W., Oren, R. and Smith, M.L., 2008. Canopy nitrogen, carbon assimilation, and albedo in temperate and boreal forests: Functional relations and potential climate feedbacks. Proceedings of the National Academy of Sciences, 105(49), pp.19336-19341.

Ollinger, S.V., Richardson, A.D., Martin, M.E., Hollinger, D.Y., Frolking, S.E., Reich, P.B., Plourde, L.C., Katul, G.G., Munger, J.W., Oren, R. and Smith, M.L., 2008. Canopy nitrogen, carbon assimilation, and albedo in temperate and boreal forests: Functional relations and potential climate feedbacks. *Proceedings of the National Academy of Sciences*, *105*(49), pp.19336-19341.

Olsen, J.L., Stisen, S., Proud, S.R. and Fensholt, R., 2015. Evaluating EO-based canopy water stress from seasonally detrended NDVI and SIWSI with modeled evapotranspiration in the Senegal River Basin. *Remote Sensing of Environment*, *159*, pp.57-69.

Osbome, R.W., Bar-Shalom, Y. and Willett, P., 2011, July. Track-to-track association with augmented state. In *14th International Conference on Information Fusion* (pp. 1-8). IEEE.

Oumar, Z. and Mutanga, O., 2013. Using WorldView-2 bands and indices to predict bronze bug (Thaumastocoris peregrinus) damage in plantation forests. International Journal of Remote Sensing, 34(6), pp.2236-2249.

Paramasivam, C.R. and Venkatramanan, S., 2019. An introduction to various spatial analysis techniques. *GIS and geostatistical techniques for groundwater science*, pp.23-30.

Perry, E.M., Bluml, M., Goodwin, I., Cornwall, D. and Swarts, N.D., 2014, August. Remote sensing of N deficiencies in apple and pear orchards. In XXIX International Horticultural Congress on Horticulture: Sustaining Lives, Livelihoods and Landscapes (IHC2014): 1130 (pp. 575-580).

Pesaresi, M., Corbane, C., Julea, A., Florczyk, A.J., Syrris, V. and Soille, P., 2016. Assessment of the added-value of Sentinel-2 for detecting built-up areas. Remote Sensing, 8(4), p.299.

Pfeifer, M., Gonsamo, A., Disney, M., Pellikka, P. and Marchant, R., 2012. Leaf area index for biomes of the Eastern Arc Mountains: Landsat and SPOT observations along precipitation and altitude gradients. Remote Sensing of Environment, 118, pp.103-115.

Phiri, D., Simwanda, M., Salekin, S., Nyirenda, V.R., Murayama, Y. and Ranagalage, M., 2020. Sentinel-2 data for land cover/use mapping: A review. *Remote Sensing*, *12*(14), p.2291.

Ramoelo, A. and Cho, M.A., 2018. Explaining leaf nitrogen distribution in a semi-arid environment predicted on Sentinel-2 imagery using a field spectroscopy derived model. *Remote Sensing*, *10*(2), p.269.

Ramoelo, A., Dzikiti, S., Van Deventer, H., Maherry, A., Cho, M.A. and Gush, M., 2015. Potential to monitor plant stress using remote sensing tools. Journal of Arid Environments, 113, pp.134-144.

Read, J.J. and Morgan, J.A., 1996. Growth and Partitioning inPascopyrum smithii (C3) andBouteloua gracilis (C4) as Influenced by Carbon Dioxide and Temperature. *Annals of Botany*, *77*(5), pp.487-496.

Reich, P.B., Hobbie, S.E., Lee, T., Ellsworth, D.S., West, J.B., Tilman, D., Knops, J.M., Naeem, S. and Trost, J., 2006. Nitrogen limitation constrains sustainability of ecosystem response to CO 2. Nature, 440(7086), pp.922-925.

Reich, P.B., Hobbie, S.E., Lee, T., Ellsworth, D.S., West, J.B., Tilman, D., Knops, J.M., Naeem, S. and Trost, J., 2006. Nitrogen limitation constrains sustainability of ecosystem response to CO2. *Nature*, *440*(7086), pp.922-925.

Richards, A.E., Brackin, R., Lindsay, D.A.J. and Schmidt, S., 2012. Effect of fire and tree-grass patches on soil nitrogen in Australian tropical savannas. *Austral Ecology*, *37*(6), pp.668-677.

Richardson, L.L. and LeDrew, E.F. eds., 2006. Remote sensing of aquatic coastal ecosystem processes (p. 324). Dordrecht: Springer.

Richter, A., Ng, K.T.W. and Karimi, N., 2019. A data driven technique applying GIS, and remote sensing to rank locations for waste disposal site expansion. Resources, Conservation and Recycling, 149, pp.352-362.

Richter, A., Ng, K.T.W. and Karimi, N., 2019. A data driven technique applying GIS, and remote sensing to rank locations for waste disposal site expansion. *Resources, Conservation and Recycling*, *149*, pp.352-362.

Rodriguez-Galiano, V.F., Ghimire, B., Pardo-Iguzquiza, E., Chica-Olmo, M. and Congalton, R.G., 2012. Incorporating the downscaled Landsat TM thermal band in land-cover classification using random forest. *Photogrammetric Engineering & Remote Sensing*, *78*(2), pp.129-137.

Roumenina, E., Jelev, G., Dimitrov, P., Filchev, L., Kamenova, I., Gikov, A., Banov, M. and Veneta, K., 2020. Qualitative Evaluation and Within-Field Mapping of Winter Wheat Crop Condition Using Multispectral Remote Sensing Data. *Bulgarian Journal of Agricultural Science*, *26*(6), pp.1129-1142.

Sáez Plaza, P., 2013. NavasM J. Wybrainiec S, et al. An overview of the Kjeldahl method on nitrogen determination. Part II. Sampling preparation, working scale, instrumental finish, and quality control. *Critical Reviews in Analytical Chemistry*, *43*(4), pp.224-272.

Sáez-Plaza, P., Navas, M.J., Wybraniec, S., Michałowski, T. and Asuero, A.G., 2013. An overview of the Kjeldahl method of nitrogen determination. Part II. Sample preparation, working scale, instrumental finish, and quality control. Critical Reviews in Analytical Chemistry, 43(4), pp.224-272.

Schlemmer, M., Gitelson, A., Schepers, J., Ferguson, R., Peng, Y., Shanahan, J. and Rundquist, D., 2013. Remote estimation of nitrogen and chlorophyll contents in maize at leaf and canopy levels. International Journal of Applied Earth Observation and Geoinformation, 25, pp.47-54.

Schlemmer, M., Gitelson, A., Schepers, J., Ferguson, R., Peng, Y., Shanahan, J. and Rundquist, D., 2013. Remote estimation of nitrogen and chlorophyll contents in maize at leaf and canopy levels. *International Journal of Applied Earth Observation and Geoinformation*, *25*, pp.47-54.

Schneider-Binder, E., 2017. Habitats with Large Bitter Cress (L.) in the Spring Area of Nera River (Semenic Mountains, Romania). *Transylvanian Review of Systematical and Ecological Research*, *19*(1), pp.19-28.

Schulz, D., Yin, H., Tischbein, B., Verleysdonk, S., Adamou, R. and Kumar, N., 2021. Land use mapping using Sentinel-1 and Sentinel-2 time series in a heterogeneous landscape in Niger, Sahel. *ISPRS Journal of Photogrammetry and Remote Sensing*, *178*, pp.97-111.

Sedano, F., Lisboa, S.N., Sahajpal, R., Duncanson, L., Ribeiro, N., Sitoe, A., Hurtt, G. and Tucker, C.J., 2021. The connection between forest degradation and urban energy demand in sub-Saharan Africa: A characterization based on high-resolution remote sensing data. *Environmental Research Letters*, *16*(6), p.064020.

Serrano, L., Filella, I. and Penuelas, J., 2000. Remote sensing of biomass and yield of winter wheat under different nitrogen supplies. *Crop science*, *40*(3), pp.723-731.

Serrano, L., Penuelas, J. and Ustin, S.L., 2002. Remote sensing of nitrogen and lignin in Mediterranean vegetation from AVIRIS data: Decomposing biochemical from structural signals. Remote sensing of Environment, 81(2-3), pp.355-364.

Serrano, L., Penuelas, J. and Ustin, S.L., 2002. Remote sensing of nitrogen and lignin in Mediterranean vegetation from AVIRIS data: Decomposing biochemical from structural signals. Remote sensing of Environment, 81(2-3), pp.355-364.

Serrano, L., Penuelas, J. and Ustin, S.L., 2002. Remote sensing of nitrogen and lignin in Mediterranean vegetation from AVIRIS data: Decomposing biochemical from structural signals. *Remote sensing of Environment*, *81*(2-3), pp.355-364.

Shongwe, L.B., 2007. The implications of transfrontier conservation areas: a comparative policy analysis study of sustainable development in South Africa between the great Limpopo transfrontier conservation area and Lubombo transfrontier resource area (Doctoral dissertation, University of Pretoria).

Shongwe, L.B., 2007. *The implications of transfrontier conservation areas: a comparative policy analysis study of sustainable development in South Africa between the great Limpopo transfrontier conservation area and Lubombo transfrontier resource area* (Doctoral dissertation, University of Pretoria).

Sibanda, M., Dube, T., Bangamwabo, V.M., Mutanga, O., Shoko, C. and Gumindoga, W., 2016. Understanding the spatial distribution of elephant (Loxodonta africana) poaching incidences in the mid-Zambezi Valley, Zimbabwe using Geographic Information Systems and remote sensing. Geocarto International, 31(9), pp.1006-1018.

Sims, D.A. and Gamon, J.A., 2002. Relationships between leaf pigment content and spectral reflectance across a wide range of species, leaf structures and developmental stages. *Remote sensing of environment*, *81*(2-3), pp.337-354.

Singo, L.R., Kundu, P.M. and Odiyo, J.O., 2016. Impact of land use change on surface runoff and stream discharges in Luvuvhu River Catchment.

Singo, L.R., Kundu, P.M., Odiyo, J.O., Mathivha, F.I. and Nkuna, T.R., 2012. Flood frequency analysis of annual maximum stream flows for Luvuvhu River Catchment, Limpopo Province, South Africa.

Singo, L.R., Kundu, P.M., Odiyo, J.O., Mathivha, F.I. and Nkuna, T.R., 2012. Flood frequency analysis of annual maximum stream flows for Luvuvhu River Catchment, Limpopo Province, South Africa.

Socolow, R.H., 1999. Nitrogen management and the future of food: lessons from the management of energy and carbon. Proceedings of the National Academy of Sciences, 96(11), pp.6001-6008.

Talukdar, S., Singha, P., Mahato, S., Pal, S., Liou, Y.A. and Rahman, A., 2020. Land-use land-cover classification by machine learning classifiers for satellite observations—a review. Remote Sensing, 12(7), p.1135.

Talukdar, S., Singha, P., Mahato, S., Pal, S., Liou, Y.A. and Rahman, A., 2020. Land-use land-cover classification by machine learning classifiers for satellite observations—A review. *Remote Sensing*, *12*(7), p.1135.

Templer, P.H., Pinder, R.W. and Goodale, C.L., 2012. Effects of nitrogen deposition on greenhouse-gas fluxes for forests and grasslands of North America. Frontiers in Ecology and the Environment, 10(10), pp.547-553.

Trisakti, B., 2014. Pendugaan Laju Erosi Tanah Menggunakan Data Satelit Landsat dan SPOT (Soil Erosion Rate Estimation Using Landsat and SPOT). Jurnal Penginderaan Jauh dan Pengolahan Data Citra Digital, 11(2).

Turner, D., Clarke, K., Lewis, M. and Ostendorf, B., 2013, December. Using NDVI dynamics as an indicator of native vegetation management in a heterogeneous and highly fragmented landscape. In *20th International Congress on Modelling and Simulation, Adelaide, South Australia*.

Ustin, S.L., Roberts, D.A., Gamon, J.A., Asner, G.P. and Green, R.O., 2004. Using imaging spectroscopy to study ecosystem processes and properties. *BioScience*, *54*(6), pp.523-534.

Ustin, S.L., Roberts, D.A., Pinzon, J., Jacquemoud, S., Gardner, M., Scheer, G., Castaneda, C.M. and Palacios-Orueta, A., 1998. Estimating canopy water content of chaparral shrubs using optical methods. *Remote Sensing of Environment*, *65*(3), pp.280-291.

Vanhellemont, Q. and Ruddick, K., 2015. Advantages of high quality SWIR bands for ocean colour processing: Examples from Landsat-8. *Remote Sensing of Environment*, *161*, pp.89-106.

Vigneau, N., Ecarnot, M., Rabatel, G. and Roumet, P., 2011. Potential of field hyperspectral imaging as a non destructive method to assess leaf nitrogen content in Wheat. *Field Crops Research*, *122*(1), pp.25-31.

Viña, A. and Gitelson, A.A., 2005. New developments in the remote estimation of the fraction of absorbed photosynthetically active radiation in crops. *Geophysical Research Letters*, *32*(17).

Virnodkar, S.S., Pachghare, V.K., Patil, V.C. and Jha, S.K., 2020. Remote sensing and machine learning for crop water stress determination in various crops: a critical review. *Precision Agriculture*, *21*(5), pp.1121-1155.

Volenzo, T.E. and Odiyo, J., 2018. Ecological public health and participatory planning and assessment dilemmas: the case of water resources management. International journal of environmental research and public health, 15(8), p.1635.

Volenzo, T.E. and Odiyo, J., 2018. Ecological public health and participatory planning and assessment dilemmas: the case of water resources management. *International Journal of Environmental Research and Public Health*, *15*(8), p.1635.

Walshe, D., McInerney, D., Van De Kerchove, R., Goyens, C., Balaji, P. and Byrne, K.A., 2020. Detecting nutrient deficiency in spruce forests using multispectral satellite imagery. *International Journal of Applied Earth Observation and Geoinformation*, *86*, p.101975.

Wang, G., Wei, Y., Qiao, S., Lin, P. and Chen, Y., 2018. *Generalized inverses: theory and computations* (Vol. 53). Singapore: Springer.

Wang, L. and Qu, J.J., 2007. NMDI: A normalized multi-band drought index for monitoring soil and vegetation moisture with satellite remote sensing. *Geophysical Research Letters*, *34*(20).

Wang, L. and Wei, Y., 2016. Revised normalized difference nitrogen index (NDNI) for estimating canopy nitrogen concentration in wetlands. *Optik*, *127*(19), pp.7676-7688.

Wang, S., Baig, M.H.A., Zhang, L., Jiang, H., Ji, Y., Zhao, H. and Tian, J., 2015. A simple enhanced water index (EWI) for percent surface water estimation using Landsat data. *IEEE Journal of Selected Topics in Applied Earth Observations and Remote Sensing*, *8*(1), pp.90-97.

Wang, X., Zhang, F. and Johnson, V.C., 2018. New methods for improving the remote sensing estimation of soil organic matter content (SOMC) in the Ebinur Lake Wetland National Nature Reserve (ELWNNR) in northwest China. *Remote sensing of environment*, *218*, pp.104-118.

Wang, Y. and Liu, Z., 2013. Vertical distribution and influencing factors of soil water content within 21-m profile on the Chinese Loess Plateau. *Geoderma*, *193*, pp.300-310.

Wang, Z., Wang, T., Darvishzadeh, R., Skidmore, A.K., Jones, S., Suarez, L., Woodgate, W., Heiden, U., Heurich, M. and Hearne, J., 2016. Vegetation indices for mapping canopy foliar nitrogen in a mixed temperate forest. Remote sensing, 8(6), p.491.

Weerasinghe, L.K., Creek, D., Crous, K.Y., Xiang, S., Liddell, M.J., Turnbull, M.H. and Atkin, O.K., 2014. Canopy position affects the relationships between leaf respiration and associated traits in a tropical rainforest in Far North Queensland. *Tree physiology*, *34*(6), pp.564-584.

Xie, Q., Dash, J., Huete, A., Jiang, A., Yin, G., Ding, Y., Peng, D., Hall, C.C., Brown, L., Shi, Y. and Ye, H., 2019. Retrieval of crop biophysical parameters from Sentinel-2 remote sensing imagery. International Journal of Applied Earth Observation and Geoinformation, 80, pp.187-195.

Xie, Q., Dash, J., Huete, A., Jiang, A., Yin, G., Ding, Y., Peng, D., Hall, C.C., Brown, L., Shi, Y. and Ye, H., 2019. Retrieval of crop biophysical parameters from Sentinel-2 remote sensing imagery. *International Journal of Applied Earth Observation and Geoinformation*, *80*, pp.187-195.

Xie, Y., Sha, Z. and Yu, M., 2008. Remote sensing imagery in vegetation mapping: a review. *Journal of plant ecology*, *1*(1), pp.9-23.

Xiong, J., Thenkabail, P.S., Tilton, J.C., Gumma, M.K., Teluguntla, P., Oliphant, A., Congalton, R.G., Yadav, K. and Gorelick, N., 2017. Nominal 30-m cropland extent map of continental Africa by integrating pixel-based and object-based algorithms using Sentinel-2 and Landsat-8 data on Google Earth Engine. Remote Sensing, 9(10), p.1065.

Xu, Y., Du, B., Zhang, L., Cerra, D., Pato, M., Carmona, E., Prasad, S., Yokoya, N., Hänsch, R. and Le Saux, B., 2019. Advanced multi-sensor optical remote sensing for urban land use and land cover classification: Outcome of the 2018 IEEE GRSS data fusion contest. *IEEE Journal of Selected Topics in Applied Earth Observations and Remote Sensing*, *12*(6), pp.1709-1724.

Yao, Y., Zhu, J.G. and Lu, Q.G., 2015. Experimental study on nitrogen transformation in combustion of pulverized semi-coke preheated in a circulating fluidized bed. *Energy & Fuels*, *29*(6), pp.3985-3991.

Yesuph, A.Y. and Dagnew, A.B., 2019. Land use/cover spatiotemporal dynamics, driving forces and implications at the Beshillo catchment of the Blue Nile Basin, North Eastern Highlands of Ethiopia. Environmental Systems Research, 8(1), pp.1-30.

Yesuph, A.Y. and Dagnew, A.B., 2019. Land use/cover spatiotemporal dynamics, driving forces and implications at the Beshillo catchment of the Blue Nile Basin, North Eastern Highlands of Ethiopia. *Environmental Systems Research*, *8*(1), pp.1-30.

Zarco-Tejada, P.J., Miller, J.R., Noland, T.L., Mohammed, G.H. and Sampson, P.H., 2001. Scaling-up and model inversion methods with narrowband optical indices for chlorophyll content estimation in closed forest canopies with hyperspectral data. IEEE Transactions on Geoscience and Remote Sensing, 39(7), pp.1491-1507.

Zhang, C., Chen, K., Liu, Y., Kovacs, J.M., Flores-Verdugo, F. and de Santiago, F.J.F., 2012. Spectral response to varying levels of leaf pigments collected from a degraded mangrove forest. *Journal of applied remote sensing*, *6*(1), p.063501.

Zhang, F. and Zhou, G., 2019. Estimation of vegetation water content using hyperspectral vegetation indices: A comparison of crop water indicators in response to water stress treatments for summer maize. *BMC ecology*, *19*(1), pp.1-12.

Zhang, J., 2010. Multi-source remote sensing data fusion: status and trends. International Journal of Image and Data Fusion, 1(1), pp.5-26

Zhang, M., Zhao, C., Shao, Q., Yang, Z., Zhang, X., Xu, X. and Hassan, M., 2019. Determination of water content in corn stover silage using near-infrared spectroscopy. *International Journal of Agricultural and Biological Engineering*, *12*(6), pp.143-148.

Zhang, R., Jia, M., Wang, Z., Zhou, Y., Wen, X., Tan, Y. and Cheng, L., 2021. A comparison of Gaofen-2 and Sentinel-2 imagery for mapping mangrove forests using object-oriented analysis and random forest. *IEEE Journal of Selected Topics in Applied Earth Observations and Remote Sensing*, *14*, pp.4185-4193.

Zhang, X., Chen, S., Sun, H., Wang, Y. and Shao, L., 2010. Water use efficiency and associated traits in winter wheat cultivars in the North China Plain. *Agricultural Water Management*, *97*(8), pp.1117-1125.

Zhao, K., Valle, D., Popescu, S., Zhang, X. and Mallick, B., 2013. Hyperspectral remote sensing of plant biochemistry using Bayesian model averaging with variable and band selection. *Remote Sensing of Environment*, *132*, pp.102-119.

Zhou, M. and Memelink, J., 2016. Jasmonate-responsive transcription factors regulating plant secondary metabolism. *Biotechnology advances*, *34*(4), pp.441-449.

Zhou, S., Duursma, R.A., Medlyn, B.E., Kelly, J.W. and Prentice, I.C., 2013. How should we model plant responses to drought? An analysis of stomatal and non-stomatal responses to water stress. *Agricultural and Forest Meteorology*, *182*, pp.204-214.

Zhou, Y., Zhang, Z., Rao, J. and Chen, B., 2022. Predicting and mapping soil magnetic susceptibility in an agro-pastoral transitional zone: Influencing factors and implications. *Soil and Tillage Research*, *219*, p.105352.

Zhu, M.D., Zhang, M., Gao, D.J., Zhou, K., Tang, S.J., Zhou, B. and Lv, Y.M., 2020. Rice OsHSFA3 gene improves drought tolerance by modulating polyamine biosynthesis depending on abscisic acid and ROS levels. *International journal of molecular sciences*, *21*(5), p.1857.